Quantifying the contribution of surface runoff to karst-related flooding between Le Roy and Caledonia, NY

G.W.H. Simons and B.R. Voortman
June 2009
Supervisor UU: Dr. M. van der Perk
Supervisor SUNY Brockport: P. L. Richards (Ph.D.)

Universiteit Utrecht
Department of Physical Geography
Faculty of Geosciences
Utrecht University

The College at BROCKPORT
STATE UNIVERSITY OF NEW YORK
Department of the Earth Sciences
SUNY College at Brockport
Brockport, NY, USA

Abstract

Karst-related flooding occurs in several depressions between Le Roy and Caledonia, NY, USA. The timing of these flood events suggests that a regional groundwater phenomenon contributes to the flood volumes, in addition to contributions by surface water and subsurface quickflow. To gain better understanding of the proportions of these components, two watersheds near Le Roy (Britt Road and Quinlan Road) were studied in detail. A rainfall-runoff model was constructed in the PCRaster language to quantify the portion of flood volume originating from surface runoff for two different flood events. For an event in October 2006, runoff explained the entire flood volume in the Quinlan Road watershed. For an event at the end of November 2006, the contribution of surface runoff to the flood volume was about 49% and 46% for the Britt Road and Quinlan Road watershed, respectively. The remaining part of the flood volume must have been derived from subsurface quick flow or groundwater. In these model simulations swampy areas and the flood zone were assumed to be impermeable, simulating the presence of a high water table. Without this assumption all the surface water entering the flood zone would infiltrate into the subsurface. From a sensitivity analysis it was found that microtopography storage is an influential parameter in runoff generation in these watersheds.

These findings suggest that high groundwater levels are the main driving force behind the floodings. Without a groundwater level close to the land surface in the Britt Road watershed or groundwater mounding at the sinkholes in the Quinlan Road watershed, no flooding would occur. However, to accurately quantify the quickflow and groundwater components contributing to the floodings, additional research needs to be performed at the actual time of flooding.

Acknowledgements

We are grateful to Dr. Whitney Autin who made it possible for us to come to Brockport. He initiated the exchange of MSc.-students between the SUNY College of Brockport and Utrecht University and managed practical issues regarding the exchange, including transport. Furthermore we had a very pleasant stay in New York State because of the interesting excursions and delightful barbeques Whitney organized. His colleague Paul Richards supervised our project and provided us with the necessary tools and the knowledge to successfully perform this research. Paul, thank you for your support. We would also like to thank our supervisor at Utrecht University, dr. Marcel van der Perk, who advised us about setting up our research, the processing of our field data, and the writing of our thesis. For financial support, we would like to thank the K.F. Hein foundation, the Molengraaff funding agency and Utrecht University.

Steffie Paardekooper and Joël Sprangers, two fellow Msc.-students at Utrecht University, accompanied us during our field work and performed a geological study in the area. Steffie and Joel, thank you for the pleasant atmosphere and getting our minds off water and soil from time to time. Peter Veronesi and Zen were so kind to have us as their guests for the duration of the project. Pete, we are very thankful for your hospitality, your practical help in building the field equipment, and the interesting talks at the campfire.

Contents

List of tables

List of figures

1. Introduction

1.1 Background and problem definition

Karst-related flooding is observed in areas around the world, with magnitudes and dynamics varying with the climatological, (hydro)geological and geomorphological characteristics of the region. The strong and complex interaction between surface water and groundwater in karst areas increases their susceptibility to floods. Large volumes of surface water can rapidly penetrate into the subsurface through solutional pathways and sinkholes, which usually serve as the storm drains of a karst terrain. Three distinct classes of karst-related flooding are distinguished by Zhou (2006), based on the dominant processes that lead to flooding. Firstly, limitations in the drainage capacity of the sinkhole may lead to problems in transferring all of the storm runoff to the subsurface (r*echarge-related sinkhole flooding*). This is often the case in watersheds where the generation of surface runoff is enhanced by the presence of human construction, or where the sinkhole throat is plugged by eroded material or disposed waste, (Zhou, 2006). Secondly, flooding can occur when the in-coming flow rate exceeds the conveyance capacity of the conduits in the karst aquifer (*flow-related flooding*). This concept can be expanded with *contact flooding*, which refers to the rise of the water table in the contact zone of distinctly different geological units. Thirdly, flooding can occur when groundwater discharge is reduced due to an increase in water levels at discharge points (*discharge-related flooding).* This could, for example, be caused by damming of the surface water to which the groundwater discharges.

So far, research has focused on some of the most hazardous examples of flash flooding in karst areas (eg. Maréchal *et al*., 2008; Bonacci *et al*., 2006). Most of these documented flood sites are located in semi-arid areas, where surface runoff coming from bare, impermeable soils is found to be the dominant factor causing the flood event (Bonacci *et al*., 2006). Flood sites are located downhill, where the surface runoff generated during a high-intensity precipitation or snowmelt event is quickly transported via steep slopes. However, karst-related flooding may also occur under substantial different conditions, as illustrated by the erratic flooding of depressions in the Onondaga formation, a karstic limestone in the western part of New York State (USA) (figure 1.1). Slopes in the individual watersheds in this area are gentle, and climate conditions are humid (Peel *et al.,* 2007). High intensity rain events in summer do not coincide with flood events, while lower intensity rain events in autumn, winter or early spring lead to flooding. Surface floods in the area are not just confined to locations adjacent to sinkholes or fields in direct contact with rivers or streams. Flooding is also occurring in fields without direct contact with a source of water visible at the surface. The timing and location of these flood events suggests that generation of surface runoff is not the only cause of flooding. This is supported by an undergraduate study by Rhinehart (2005) who showed that surface runoff only accounted for 10% of the flood volume during a flood event in November 2005 of the local Quinlan Road watershed. However, this study was largely simplified and used a curve number method to estimate surface runoff and rough assumptions regarding the flood volume and the size of the watershed. Based on these findings it is hypothesized that a regional groundwater phenomenon contributes to the flood volumes, in addition to contributions by surface water and subsurface quickflow. This is uncommon as sinkholes are supposed to form only in areas of groundwater recharge.

The societal consequences of single flood events are incomparable with more hazardous events in mountainous areas. Still, flood events are a nuisance to local residents and the numerous floodings in the area lead to garden and basement flooding and damage to crop fields and a golf

course. Besides the relevance for local residents the flood events are in particular notable for displaying characteristics regarded as uncommon for flooding in karst areas. A better understanding of the hydrologic system causing the floods could lead to new insights in processes leading to karst-related flooding.

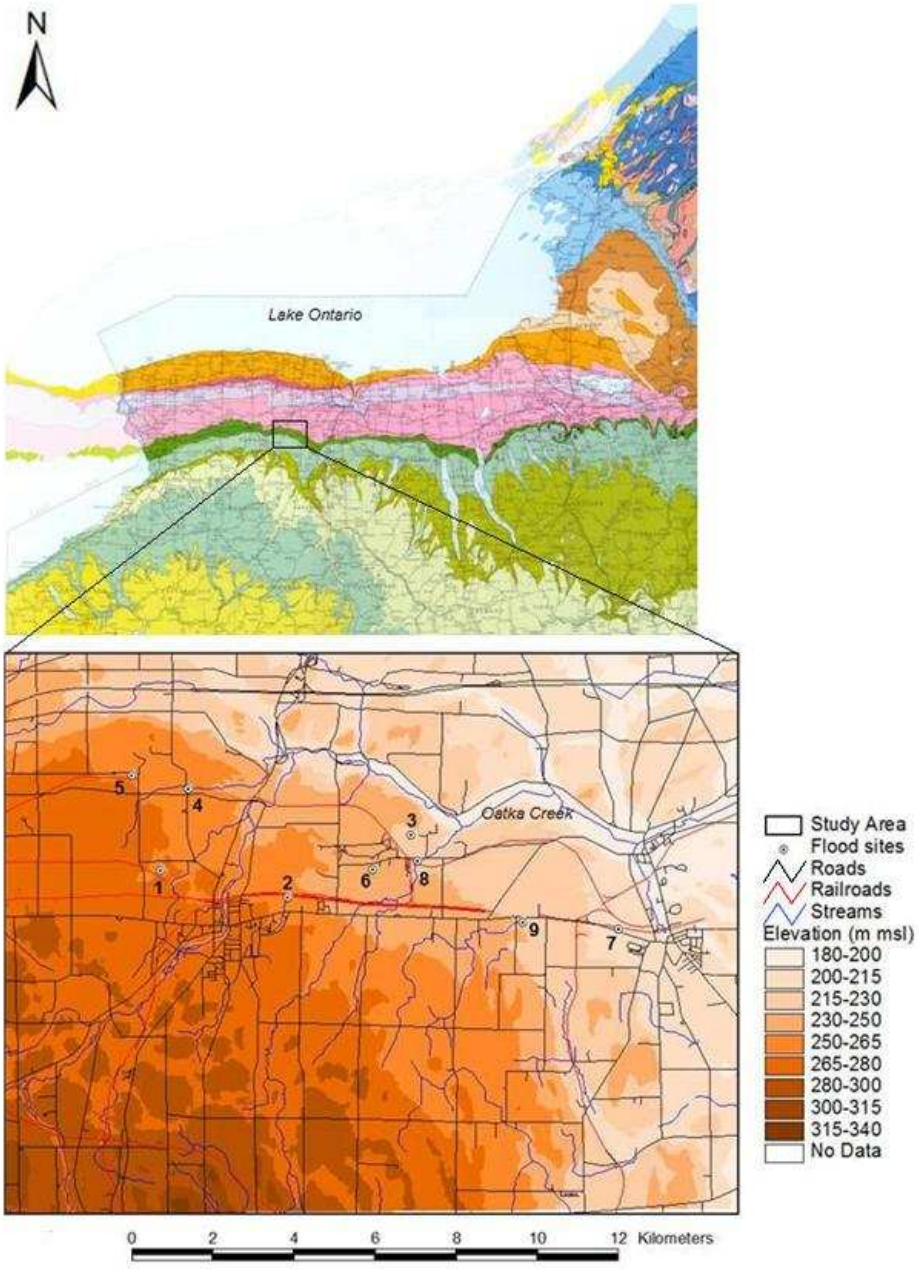

Figure 1.1 *Geological map of western New York and an elevation map of the study area. On the geological map, the Onondaga Formation is visible as a dark green band, laterally stretching across the state. On the elevation map, the numbers represent sites where periodical flooding occurs. Quinlan road and Britt road are marked with numbers 1 and 5 respectively. The valley of Oatka Creek to the north marKs the base of the Onondaga Formation.*

1.2 Research objectives

This research focuses on floodings observed in two local watersheds located in the Onondaga formation in western New York State, namely the Britt Road and Quinlan Road watersheds. This study aims:

- To quantify, for both watersheds, the portion of the flood volume that is generated as surface runoff in the watershed.
- To understand the reaction of the watersheds to heavy rainfall events, and investigate how they differ in terms of runoff generation.

A similar procedure was followed for both watersheds. By modeling surface runoff generation from precipitation during selected events known for flooding, the volume of runoff contributing to the body of water at the flood site was estimated. For this study a rainfall-runoff model was constructed. The performance of a rainfall-runoff model is dependent on the accuracy of model input parameters, the model structure and physical processes included in the model. A secondary aim of this study is:

- To find out the relative sensitivity of the model to the different parameters.

1.3 Thesis Outline

The characteristics of the study area are of special interest as previous studies focused on flood events occurring under substantial different conditions. Therefore this thesis continues with a description of the study area in chapter 2. The structure of the rainfall-runoff model and physical processes taken into account determined the applied methods. Therefore, the structure of the rainfall-runoff model and the choices made in parameterization of the different physical processes involved is explained in chapter 3 and is followed by an explanation of the applied methods in chapter 4. Chapter 4 deals with the origin of the data used in this study, as well as the statistical processes leading up to the definitive model input. Furthermore, the methods with respect to the calculation of the total flood volumes, the selection of flood events for simulation, and the statistical processing of the model output is clarified in this chapter. The results of the procedures explained in chapter 4 are presented in chapter 5, for model input as well as model output. The findings of this study are discussed in chapter 6, with special attention for the implications of the modeling results. Chapter 7 summarizes the main conclusions of this study and provides recommendations for future research.

2. Study area

The study area is located in New York State, between the villages of Le Roy and Caledonia. Small flood sites are spread around the study area, each with their own local watershed. Two of the local watersheds around the town of Le Roy that are known for flooding are studied in detail for this thesis. These watersheds are referred to as the Britt Road watershed (743200, 4766400, NAD 1983, UTM) and the Quinlan Road watershed (743800, 4764000, NAD 1983, UTM), named after the roads alongside which they are located. Their locations are marked in Figure 1.1 and displayed in more detail in Figure 2.1. Floods in the Quinlan Road watershed occur at two sinkholes, where surface water collected by two streams discharge into the subsurface. Floods in the Britt Road watershed occur at an agricultural field without a visible source of water at the surface.

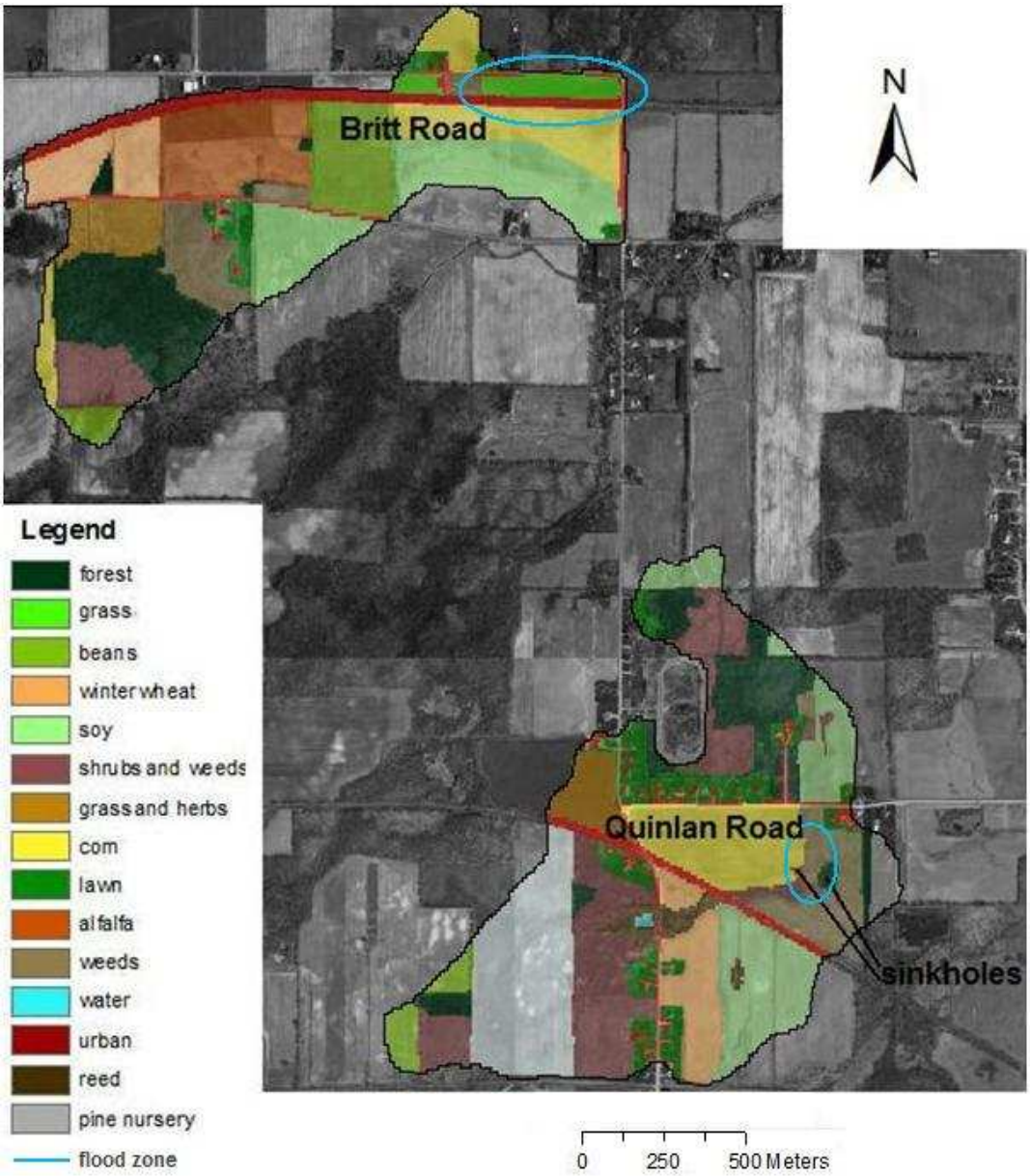

Fig 2.1 *Aerial photograph of the Britt Road and Quinlan Road watersheds. The sinkhole locations near Quinlan Road are marked, and the different types of land use in the watersheds are indicated with colours.*

The proximity of the two watersheds (approximately 1 km) causes them to be similar in properties. There is little spatial variation in soil grain size in both watersheds, with soil textures ranging from silt loam to very fine sandy loam (appendix A.5 and A.6). Soils on top of the Onondaga Formation are thin and immature. This is a result of erosion during glacial retreat of the Laurentide Ice Sheet during the late Wisconsin (9000 y BP), when glacial meltwater eroded much of the unconsolidated sediment in the area (Fairchild, 1909). Land management is mostly agricultural, with some fallow lands (now covered with weeds or shrubs) and forest patches present (see Figure 2.1 and appendix A.3 and A.4). Notable anthropogenic constructions include roads, housing and an abandoned, heightened railroad track crossing each of the watersheds. Ditches and tile drainage systems regulate the hydrology of the agricultural fields. Slopes in the area are gentle (see appendix A.1 and A.2 for detailed elevation information).

According to the revised Köppen-Geiger classification (Peel et. al, 2007) climate conditions in Western New York are humid and continental. It should, however, be noted that there is strong modification from the Great Lakes. Winters are characterized by enhanced snowfall due to lake effect processes, and average temperatures of below 0 ^{o}C are recorded at the Batavia climate station (FRD, 1998). Winter usually lasts from mid-November to early April. Summers are classified as hot and humid with an average rainfall of 9.7 cm in August, and average temperatures exceeding 22^{o}C in the hottest month (July). Transitional seasons are short.

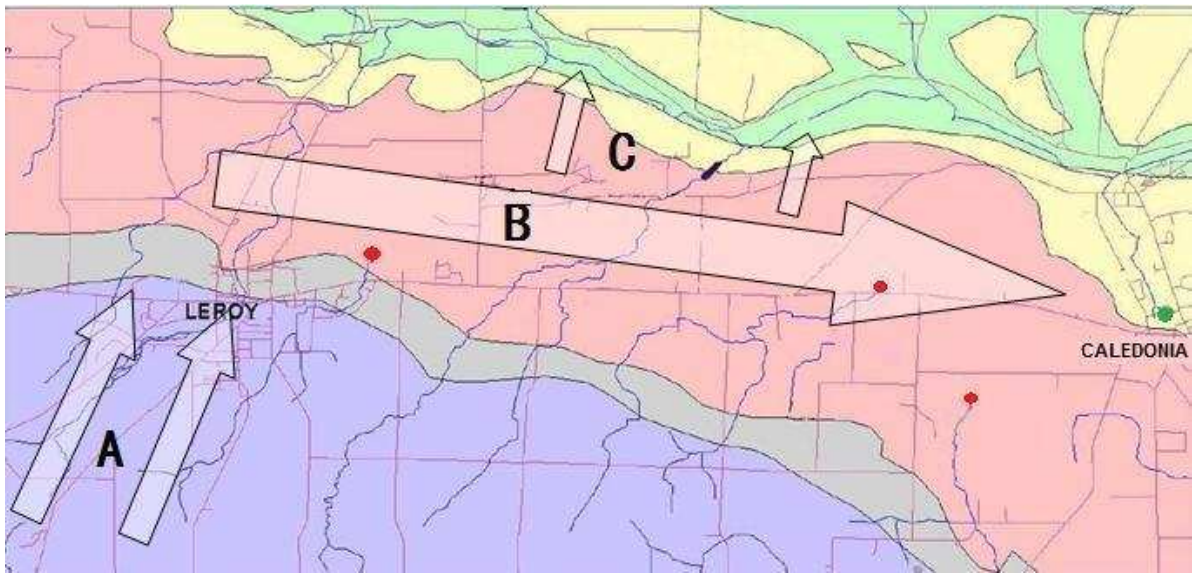

Figure 2.2) *Hypothesized hydrological system in the study area. The termination of surface streams is displayed by red dots, the green dot indicates the location of the Caledonia springs. The Onondaga Formation is coloured pink (Richards, 2007)*

Previous research has provided some insight into the hydrogeology of the study area. Dynamic changes in groundwater level (over 2.5 m) have been observed in periods as short as three days. (Dunn En. Co., 1992). Unpublished transducer data from Richards and Rhinehart (2006) show a rise of water tables in winter and spring to the base of the soil zone, or even ground surface level. The fast rise of water tables is probably associated with the karstic properties of the aquifer and the regional hydrogeology. The karstic Onondaga formation is positioned at the base of the Glaciated Allegheny Plateau which lies to the south and mostly consists of shale bedrock. Richards (2007) hypothesized that there is shallow groundwater flow northward from the Allegheny Plateau, on top of an

impermeable shale layer acting as an aquitard (A in Figure 2.2). Once this groundwater reaches the Onondaga Formation it is deflected eastward through fractures (B), as observed by Dunn en. Co. (1992). The karstic fractures mostly trend north, north east and east and dominate the permeability of the otherwise largely impermeable limestone unit (Richards, 2007). The fractures can reach widths of up to 10 cm (Fronk, 1991). Apart from groundwater flow, several northward flowing surface streams are intersected by the Onondaga Formation as well. Between Le Roy and Caledonia, with the exception of one tributary (Mud Creek), all streams terminate in the contact zone, discharging their water into the Onondaga Formation via sinkholes (red dots). The groundwater is then transported to the point of discharge at the springs near Caledonia (green dot), possibly losing some of its water through northward seepage into Oatka Creek (C). Both the unsaturated zone and soil zone in the area are thin, meaning that only a small amount of water can be stored. This characteristic, in combination with the highland recharge areas to the south and a piezometric surface that is close to ground surface level, causes the area to be especially vulnerable to flooding. The observed floods occur at sites where this groundwater phenomenon coincides with drainage water from surface tributaries (the stream termination sites), surface runoff and/or snow melt.

3. Model Description

A rainfall-runoff model was constructed to model surface runoff generation in the Britt Road and Quinlan Road watershed. The rainfall-runoff model is a dynamic distributed model, capable of simulating runoff during single storm events for small watersheds. The model is based on the runoff component of the European Soil Erosion Model (EUROSEM) (Morgan *et al*., 1995) and simulates interception by vegetation cover, and infiltration including the effect of rock fragments and depression storage. The model makes use of the kinematic wave approximation to rout the excess water downstream. The model simulates quick flow generated by surface runoff and does not include other quick flow components, although most agricultural field are equipped with tile drains. This supply of subsurface water is impossible to quantify in this study and therefore neglected. Model output includes the total amount of runoff, the storm hydrograph and an animation of the discharge during the storm event. The entire model script can be found in appendix D.

The model was constructed in the high level computer language of PCRaster (PCRaster 2008, Van Dreusen 1995, Wesseling *et al.* 1996), because of its flexibility and power in environmental modeling. Processes were modeled on a grid with a cell size of 10 by 10 meter. The model runs with timesteps of 10 seconds, which enables the inclusion of runoff as input to the infiltration model. Longer timesteps, larger than the travel time of runoff through a raster cell, would make it possible for runoff to skip a few raster cells before infiltrating or filling up the depression storage in other areas. Equations used to describe the physical processes are only applicable for instantaneous conditions and cannot be applied to averaged conditions without loss of accuracy. Applying them to conditions averaged over 10 seconds is thus more acceptable than averaged over one minute or one hour.

For every simulated event, a series of Monte Carlo simulations was performed for each watershed. The number of timesteps for which the model was run was based on the curve of the cumulative volume of runoff generated by a preliminary model run of the event, which becomes constant (maximum change in volume of 0.1 m^3 in 100 timesteps) at a given point in time.

This chapter gives an overview of the physical processes included in the runoff model, how they were parameterized in the model, and a description of the model structure.

3.1 Rainfall Interception

Rainfall input to the model is in the form of a time series providing a depth [L] for each timestep during an event. Precipitation is the first input into the model and is divided into two parts, namely that falling either on open ground or passing through gaps in the canopy and reaching the soil surface as direct throughfall, and the part striking the vegetation cover. This division is based on the simple relationship:

$$IC = R * COV \tag{3.1}$$

where *IC* = the depth of rainfall intercepted by the vegetation (m/timestep), *R* = rain (m/timestep) and *COV* = the fraction of the surface covered with vegetation (m^2/m^2). The intercepted water (*IC*) is stored on leaves and branches. This prevents an initial portion of the precipitation to reach the soil surface. This interception store can be considered as a depth which has to be filled before rain is allowed to pass the vegetation canopy to the ground, as in the American Kinematic Runoff and Erosion Model (*KINEROS*) (Woolhiser, 1990). A more dynamic approach is more appropriate since

precipitation is able to pass from the canopy to the ground at the same time as the interception store is filled. This dynamic approach is applied in the EUROSEM model and was adopted in the runoff model. The depth of the interception store was modelled as a function of the cumulative rainfall, using the exponential relationship proposed by Merriam (1973):

$$IC_{store} = IC_{\max}(1 - e^{-R_{cum}/IC_{\max}}) \tag{3.2}$$

where IC_{store} = the content of the interception store (m), IC_{max} = is the maximum interception store and R_{cum} = the cumulative rainfall (m). In this study, IC_{max} is defined as the maximum amount of water left on the canopy at the end of a precipitation event under zero evaporation conditions, and after drip has stopped (Breuer *et al*., 2003).

3.2 Infiltration

Water that reaches the soil surface as throughfall or direct rain is available for infiltration. There is a wide variety of infiltration models available, which are physically based, semi-empirical, or empirical. The well-known KINEROS and EUROSEM runoff models use the Smith and Parlange (1978) infiltration model. Mishra *et al*. (2003) evaluated the performance of fourteen popular infiltration models and concluded that this infiltration model performs well on loamy soils which are abundantly present in both watersheds. Therefore, we chose this infiltration model for this study. The Smith and Parlange (1978) infiltration model calculates the infiltration capacity as function of the cumulative infiltration since the start of the event:

$$F_c = Ks\frac{e^{F_{cum}/B}}{e^{F_{cum}/B} - 1} \tag{3.3}$$

where *Fc* = the maximum rate at which water enters the soil, known as the infiltration capacity (m/T), *Ks* = the effective saturated hydraulic conductivity (m/T), F_{cum} = the cumulative infiltration since the start of the event (m) and *B* = an integral capillary and saturation deficit parameter (m). Thus, *Fc* approaches *Ks* for an infinite value of F_{cum}. The term *B* can be seen as an indication of the suction force that the soil is able to exert on the water. It is obtained from:

$$B = G(\theta_s - \theta_i) \tag{3.4}$$

where *G* = the net effective capillary drive (m), ϑ_s = the saturated soil water content (m^3/m^3) and ϑ_i = the initial soil water content (m^3/m^3). The term *G* is a conductivity-weighted integral of the capillary head of the soil, defined as:

$$G = \frac{1}{Ks}\int_{-\infty}^{0} K(\Psi)d\Psi \tag{3.5}$$

where ψ = the soil matric potential (m) and $K(\psi)$ = a hydraulic conductivity function. *G* is conceptually equivalent to a value of effective capillary head.

Rock fragments reduce the total soil moisture storage capacity ($\vartheta_s - \vartheta_i$) and, therefore, the term B should be modified using the relationship (Woolhiser *et al*. 1990):

$$B_{roc} = B(1 - ROC) \tag{3.6}$$

where B_{roc} is modified for rock fragments (m) and *ROC* is the volumetric rock content of the soil (m^3/m^3). Rock fragments affect infiltration in a second way. Rocks which are embedded in a surface seal reduce infiltration, whereas rocks which sit on the surface or are surrounded by macropores (eg. as a result of tillage) protect the soil structure and enhance the infiltration rate. The positive effect of rock fragments on *Ks* is sometimes outweighed by the effects of tillage, and therefore adjusting the saturated conductivity for rock fragments can be inappropriate (Morgan *et al*. 1995). In this study, a possible enhancement of hydraulic conductivity by the presence of rock fragments was neglected due to this uncertainty.

3.3 Depression storage

In most hydrological studies the amount of water stored on the land surface in local depressions caused by surface roughness and microtopography is neglected because the basis for modeling depression storage is extremely limited. Especially the depression storage of agricultural fields is difficult to model because the depression storage is assumed to be dynamic within storm events due to soil erosion and deposition (Onstad *et al*., 1984; Potter, 1990; and Darboux and Huang, 2005). The depression storage of vegetated areas with a dense vegetation cover is more static, as the soil suffers less from soil erosion (Richards *et al*., 2008). Despite the difficulties in quantifying microtopography storage, the parameter was included in this study because of the substantial influence it can have on runoff generation in the model, the storage capacity of surface microtopography is subtracted from the excess precipitation that could potentially cause surface runoff, since this storage capacity has to be satisfied fully before any overland flow can occur. Depression storage values in the model are based on the relation between slope and depression storage, as further explained in paragraph 4.3.3.

3.4 Routing

Runoff routing was simulated over a local drain direction network according to the kinematic wave equation, in combination with Manning's equation. The kinematic wave model assumes negligible acceleration and pressure terms in the momentum equation and only considers the friction term. The slope of the water surface is assumed to be equal to the slope of the water bottom surface. Miller (1984) summarizes several criteria to determine when the kinematic wave approximation is applicable, but there is no single universal criterion for making this decision. The kinematic wave is frequently used because of its simplicity in comparison with other alternatives, such as the dynamic wave approximation. The kinematic wave model is defined by the following two equations. Units given are those used by the *kinematic* function of PCRaster:

$$q = \frac{\partial Q}{\partial x} + \frac{\partial A}{\partial t} \tag{3.7}$$

where Q = flow (m^3/s), x = distance in flow direction (m), A = the cross sectional area of flow (m^2), t = time (s) and q = the lateral inflow ($m^3/s/m$). Equation of momentum:

$$S_0 = S_f \tag{3.8}$$

where S_0 = the gravity force term and S_f = the friction force term. Manning's equation relates flow velocity to hydraulic radius, friction slope and Manning's roughness coefficient by the following equation:

$$V = \frac{(R^{2/3} S_f^{1/2})}{n} \tag{3.9}$$

where V = the flow velocity (m/s), R = the hydraulic radius (m), S_f = the friction slope (m/m) and n = Manning's roughness coefficient (-).

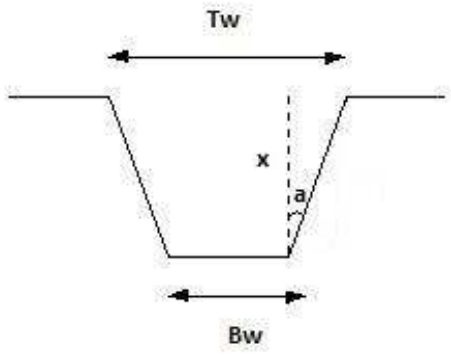

Figure 3.1 *Channel characteristics: top width (Tw), bottom width (Bw), channel depth (x) and slope angle (a).*

The combination of equations 3.7, 3.8 and 3.9 leads to a detailed routing scheme. The hydraulic radius in Manning's equation is defined as the cross-sectional area of flow divided by the wetted perimeter, and is thus a measure for the efficiency of flow. For sheet flow, the wetted perimeter is represented by the cell width of a grid cell, resulting in a very low hydraulic radius equal to the water depth. Sheet flow was assumed for all raster cells, with the exception of ditches and streams. Water that enters a stream or ditch is modeled as channel flow. Channels are assumed to have a wetted perimeter of a trapezoidal shape. The hydraulic radius is then dependent on the water depth, bottom width and the slope angle of the channel (see Figure 3.1).

3.5 Model structure

The interaction between different model components is presented in Figure 3.2. After the subtraction of rainfall interception, the net precipitation is used as input to the infiltration model. If the net rainfall intensity exceeds the infiltration capacity of the soil, the infiltration model will generate excess precipitation (potential Hortonian runoff). The excess precipitation will only become runoff when the depression storage is satisfied. The model only generates saturated overland flow in areas that are assumed impermeable at the start of the simulated event, by assigning a saturated conductivity value of 0. The excess water that becomes runoff is transported over a local drain direction network to the flood zone. In the course of its travel time, runoff can infiltrate in areas where the infiltration capacity is not exceeded or it can fill up the depression storage of areas where it is not completely filled. All of the water that is on the land surface is available for infiltration. This means that the input of the infiltration model is the net rainfall, ponding water that is on the land surface as depression storage and runoff originating from upstream cells. The infiltration capacity of streams and ditches is assumed to be zero, meaning that all water entering a stream or ditch is routed downstream to the flood zone without any loss of water.

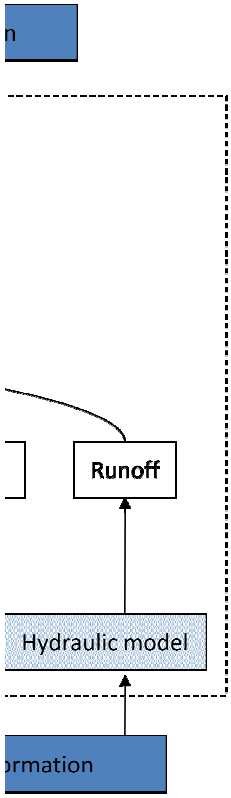

4. Methods

4.1 Selection of rainfall events for simulation

A set of flood events needs to be selected for model simulation. To this end, data ranging from June 2006 to August 2008 was available from a pressure transducer placed in the western Quinlan Road sinkhole. Flood events for both watersheds are identified from these records, under the assumption that when the Quinlan Road sinkhole overflows, flooding also occurs along Britt Road. This assumption is most likely to be valid for the highest peaks in sinkhole water level, which are therefore preferred for modeling. The transducer data were combined with precipitation and snow depth data to determine which flood events are suitable for modeling (appendix B.3). An excerpt of these data series is presented in Figure 4.1. Precipitation data were obtained from a tipping bucket station located in the Quinlan Road watershed. The main advantage of these data is the small temporal resolution in which precipitation is registered, which allows rainfall events to be simulated in timesteps suitable for runoff modeling (as explained in paragraph 3.5). Also, its location in the Quinlan Road watershed makes it a reliable source of precipitation data for both watersheds. Temperature and snow depth data are only available on a day-to-day scale. These data are obtained from the NOAA climate station in Pavilion, which is situated approximately 15 km south of the two watersheds. Peaks in the transducer data that are preceded by a peak in rainfall, rather than a decline in snow thickness, are regarded as suitable events for runoff modeling. Modeling of snowmelt is very difficult due to variations in snow density, the coarse temporal resolution of the data, variations in sunlight exposure, uncertainties regarding the frozen state of the soil and uncertainties regarding the degree of saturation of the soil during snowmelt conditions.

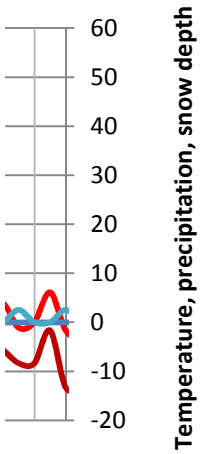

(mm)

er 20, 2006 and "2",

Two flood events that occurred on October 20, 2006 (1) and November 30, 2006 (2) were chosen for simulation. Both events show an apparent correlation with a peak in precipitation, and no indication of snowmelt prior to the flooding of the sinkhole (Figure 4.1). The two selected events differ strongly in terms of the shape of their precipitation curve (Figure 4.2). Event 2 has a slow build-up towards a sharp peak of high rainfall intensity, whereas for event 1 the volume of precipitation is more evenly distributed through time. This difference is interesting to investigate because of the impact it may have on the importance of some of the model parameters. For example, the *B* parameter could be expected to be of more influence on the model output for a more intense rainfall event.

Two different scenarios are run for each watershed (Table 4.1). This is due to uncertainties regarding the saturation of certain parts of the watersheds. In scenario *1b* and *2b*, the major part of

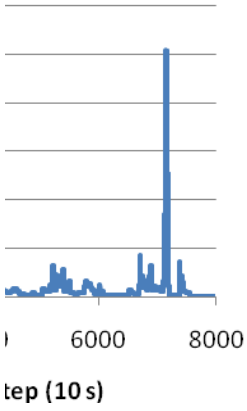

30, 2006).

Table 4.1 *Flood scenarios selected for simulation.*

Flood event	Scenario	Comments
October 20, 2006	*1a*	*Infiltration in all area's according to measured Ks*
	1b	*Britt Road: impermeability assumed in forest and on flood site* *Quinlan Road: impermeability assumed in forest and near lake*
November 30, 2006	*2a*	*Infiltration in all area's according to measured Ks*
	2b	*Britt Road: impermeability assumed in forest and on flood site* *Quinlan Road: impermeability assumed in forest and near lake*

the forest in the south of Britt Road and the reported flood site in the watershed are assumed impermeable due to saturation. The first assumption is based on eyewitness reports and field observations in the forest, where marks on the trees indicate frequent ponding (Figure 4.3). For the Quinlan Road watershed, part of the northern forest and the area around the Keeney Road lake are assumed saturated in these scenarios for similar reasons. Near the lake, swamp conditions are even observed in late summer. The low-lying flood site at Britt Road is assumed saturated to simulate a water table intersecting the ground surface. The exact outline of the saturated areas in the *1b* and *2b* scenarios can be found in appendices A.11 and A.12.

Figure 4.3 *Marks on the lower tree stems in the Britt Road forest, indicating frequent ponding in the area.*

4.2 Flood volume calculation

4.2.1 Britt Road

To compute the flood volume corresponding with a certain event, information on the extent of the flood and detailed elevation data of the flood site are necessary. No exact flood outline is known for any of the simulated events. The extent of the Britt Road floodings corresponding with the highest peaks in sinkhole water level data is assumed to be equal to the extent of a flood event that occurred on February 19, 2009. The outline of this event was accurately determined by means of a GPS (see Figure 4.4). Some ponding occurred outside of the watershed, but this was neglected in the computations. Detailed elevation data of the flood site was collected by surveying the area with a semi-total station. This survey data is the basis for a Triangular Irregular Network (TIN), which was used in computing the flood volume. Using the ArcGIS software package, the volume of the TIN was calculated. The elevation of the February 2009 flood outline was taken as the water height. The calculated flood volume can be found in Table 5.5.

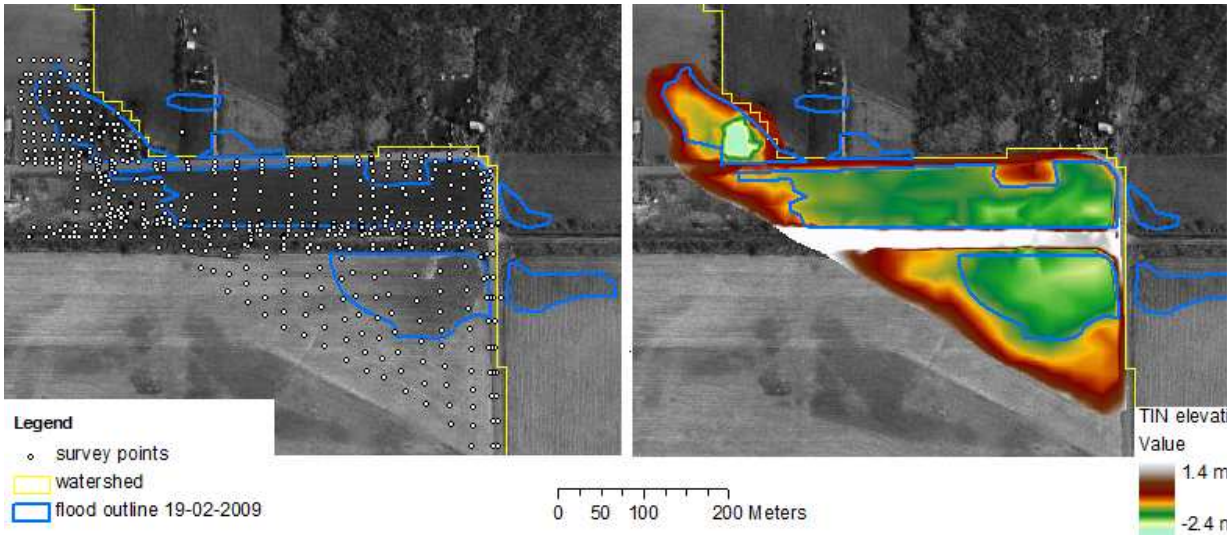

Figure 4.4 *Flood outline of the February 19, 2009 event in the Britt Road watershed, with the survey points(l) and the resulting TIN (r).*

4.2.2 Quinlan Road

For the Quinlan Road watershed, aerial photographs are available that were taken during a flood event in 2005 (Figure 4.6a). The picture gives information on the flood extent at the moment it was captured and displays drying features associated with the maximum extent of the flood. The aerial photograph shows a height within the flood zone and a lighter coloring of the southern part of the flood zone which is related to a shallow water depth (Figure 4.6a). The morphology of the flood zone suggests that the sinkholes are located at a fault which explains the height difference between the southern and northern part of the flood zone. This is supported by the color of the soil when the area is not flooded (Figure 4.5). Moist darker soils are found in depressions and dry light soils are found on heights. The sinkholes are located in the contact zone between dark and light soil (Figure 4.5). A fault is a common feature for sinkholes to form because it is a location with a high infiltration capacity.

Rhinehart (2005) calculated the theoretical volume of flood water that could come from the Quinlan Road watershed using the Soil Conservation Service (SCS) curve number method, and

compared it to an estimation of the total flood volume of a certain event. The flood volume estimation by Rhinehart (2005) was primarily based on survey data of the western sinkhole, excluding information captured by the aerial photograph. By linking the extent of the flood event captured on the aerial photograph to the survey data an extra contour line can be implemented in the interpolation of the DEM of the flood zone. Figure 4.6a shows in red contour lines that were created by linking survey data to the flood extent visible on the aerial photograph. From the contour lines a large scale DEM was created by the Topo to Raster interpolation method of the ArcGIS software package. A second small-scale DEM of the western sinkhole was created by an Inverse Distance Weighted (IDW) interpolation of the survey data. A rough estimate of the topography of the flood zone was obtained by combining these DEMs.

For the Quinlan Road watershed, the flood volume was calculated based on water depth rather than the flood extent (which is the applied method for the Britt Road watershed). Water depth is registered by the pressure transducer located at the bottom of the western sinkhole (appendix B.3).

Figure 4.5 *Photograph of the flood zone in the Quinlan road watershed. The blue arrows show the locations of the sinkholes. Darker colouring of the soil indicates higher soil moisture content and is related to local depressions (source: Miscrosoft Windows Live Maps).*

Figure 4.6a *Aerial photograph showing the extent of the 2005 flood event. Green contour lines are extracted from a topographic map. Additional contour lines are shown in red. Height measurements coming from survey data are yellow dots.*

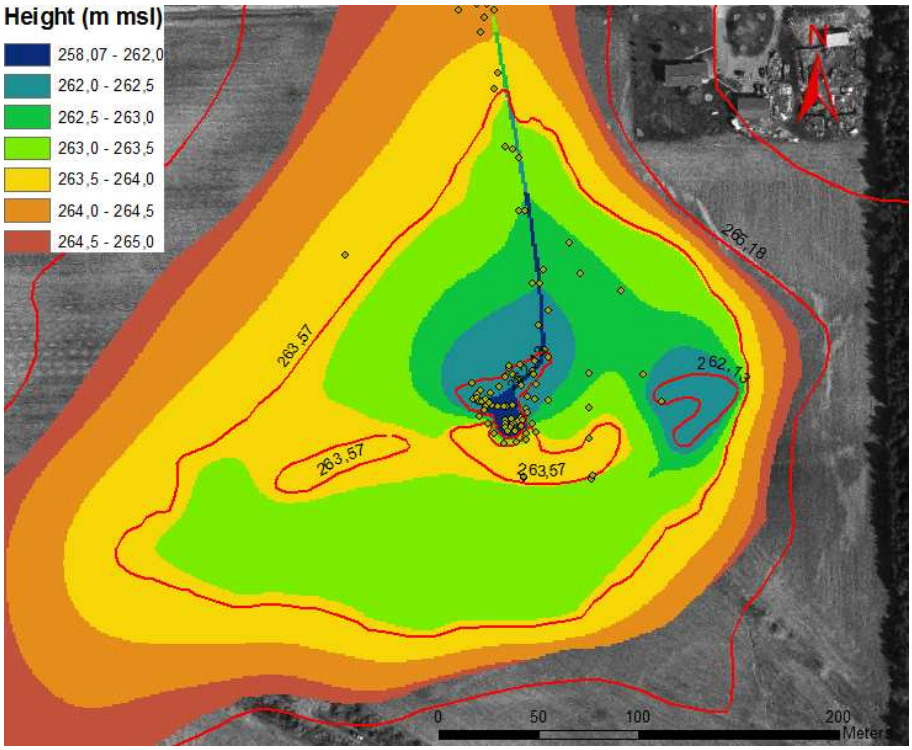

Figure 4.6b *DEM interpolated by combining information from height contours and survey data.*

4.3 Data sources of model parameters

Table 4.2 presents all model input parameters, the corresponding symbols and the origin of the data used to quantify the parameters. The data used for estimating these parameters are partly derived from values measured in the field and partly adopted from literature. In this section, choices and limitations with respect to the data are explained for each model component.

Table 4.2 *Model parameters and data sources.*

Model component	Parameter	Symbol	Data source
Rainfall interception	*Interception capacity*	IC_{max}	*Literature*
	Coverage	*Cov*	*Field*
Infiltration	*Saturated hydraulic conductivity*	*Ks*	*Field*
	Capillarity and saturation deficit parameter	*B*	*Field/stat. analysis*
	Volumetric rock content	*ROC*	*Field*
Depression storage	*Depression storage*	*Dst*	*Field*
	Slope	*x*	*DEM*
Routing	*Manning's n*	*n*	*Literature*
	Channel slope angle	*a*	*Field*
	Channel bottom width	*Bw*	*Field*

4.3.1 Rainfall interception

As explained in paragraph 3.1, two parameters have to be quantified in order to determine the volume of rainfall that is stored in the vegetation. These are the interception capacity of the vegetation (IC_{max}) and the percentage of vegetation cover. Values for IC_{max} are usually measured under laboratory conditions. For this study they are adopted from a literature review on the interception capacity of different plant species in temperate climates (Breuer *et al*., 2003). When values for a certain vegetation type are lacking, the maximum interception store of a similar plant is used. For values in land use classes that consist of multiple species, interception capacities of specific plant species are averaged. The input values are presented in Table 4.3.

The coverage parameter is estimated from field observations. Different layers of vegetation can be present in a field, for example understory in a forest and grasses in a scrubland area. In such cases, all layers of vegetation are taken into account to determine an overall coverage. The coverage values can be found on the land use map in appendix A.3.

Table 4.3 *Different types of land uses in the watersheds and their interception capacity (based on Breuer et al., 2003). For classes denoted with a '*', values for multiple species are averaged.*

Land use	IC_{max} (mm)	Land use	IC_{max} (mm)
soy	*2.2*	*winter wheat*	*2.1*
*forest**	*1.1*	*reed*	*2.4*
*shrubs & weeds**	*1.4*	*beans*	*2.2*
corn	*2.5*	*pine nursery*	*1.1*
*weeds**	*1.7*	*lawn*	*2.3*
*grass & herbs**	*1.7*	*alfalfa*	*3.6*
cucumber	*2.7*	*water*	*0*
urban	*0*		

4.3.2 Infiltration

Hydraulic conductivity measurements were conducted with the use of double-ring infiltrometers. Two different types of instruments were used, as pictured in the photographs of Figures 4.7a and 3.7b. Prior to a measurement, the soil was extensively wetted in order to approach saturated conditions. Once the measured conductivity values approach a constant, saturated conditions were assumed and the measurement was aborted. To determine the measurement locations, the watersheds were divided into combined classes of land use and soil texture. These factors are assumed to be of influence on the soil pore geometry, and are thus crucial in determining the saturated hydraulic conductivity of the soil. Based on the available time, equipment and the size of the watershed and classes, measurement sites were distributed randomly among the area. In this way, 120 conductivity measurements were carried out in the Britt Road watershed and 102 in the Quinlan Road watershed. Their locations are displayed in the land use map (appendix A.3). In order to gather information on the scale-dependency of *Ks*, measurements were conducted in couples, with individual measurements within a couple located at a distance of approximately 1.5 meter from each other.

Some parts of the watersheds may be frequently subject to swampy conditions, independent of the presence of surface water at the flood site. This was investigated through field observations and interviews with local residents. These sites were assumed saturated, thus impermeable, at the start of a model run. The land use classes *water*, *reed* and *urban* (including the abandoned railroad tracks) were assumed impermeable at the start of all simulations (see appendices A.11 and A.12). The bottom of the channels was assumed to be impermeable, so all water entering the channels eventually reaches the flood sites. No conductivity measurements were performed in these areas.

The capillarity and saturation deficit parameter *B* is based on physically related and measurable parameters, but restrictions in field equipment cause the estimation of *B* to be

Figure 4.7a *TurfTec double-ring infiltrometer.*

Figure 4.7b *Self-built double-ring infiltrometer.*

problematic. No device was available for measuring the soil moisture content before or after a *Ks* measurement is performed. The initial soil moisture content (ϑ_i) at the start of a rain event could be estimated using soil moisture models such as the Bridging Event And Continuous Hydrological (BEACH) model (Sheikh, *et al*. 2009), but this procedure demands detailed climate and land use data. Due to these difficulties, an empirical approach is chosen to determine the values for *B*. This method is explained in section 3.4.2.

A set of soil samples is taken from each of the watersheds to estimate the volumetric rock content of the soil (see appendix A.5 and A.6 for their locations). Because of restrictions in time and equipment, samples are limited in both size and number. The measured values are therefore compared to literature estimations (USDA, 1969), to improve the quality of the dataset. The sampling locations are distributed according to a classification based solely on soil type, similar to the reference data. The samples are evaluated by means of a 2 mm sieve, which is taken as the boundary between very coarse sand and rock fragment classes. Both the volumes of rock fragments and the residue are measured by putting the material in a known volume of water. By dividing the volume of rock fragments by the volume of finer material, the volumetric rock content ("stoniness") is calculated. The USDA soil survey provides a range of stoniness values for most of the soil types present in the study area (USDA, 1969). Measured values that lie out of the range valid for that soil are adjusted. For soil classes that remain unsampled (due to their surface area in the watersheds), values are taken from literature.

4.3.3 Depression storage

Microtopography storage was measured with the roughness clinometer, following the methodology of Richards *et al*. (2005). The concept of this device is pictured in Figure 4.8. A set of dowels is lowered to the ground surface, with their vertical displacement corresponding with the bumps in the surface. Since roughness is measured relative to a plane parallel to the slope, values have to be corrected for the spilling of water over the humps; in order words, the measured depression storage has to be converted to the effective depression storage (Figure 4.8). Since the slope angle is measured by the device as well, this can be done using trigonometry for each of the rods.

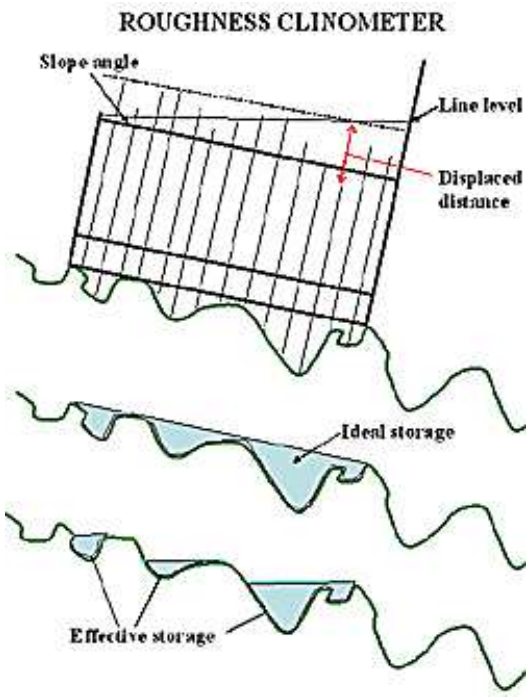

Figure 4.8 *The concept of measuring the effective microtopography storage with a roughness clinometer.*

Richards *et al*. (2008) studied the relation between microtopography storage and the slope of the ground surface in the vicinity of the study area. The roughness clinometer was used to measure depression storage in areas classified as successional oldfield, urban grassland and forest. Their measurement data were available for this study. They found a greater capacity for depression storage in areas with a high complexity and dense cover of vegetation. Furthermore, Richards *et al*.

(2008) stated that human management activities retard the development of microtopography. For these reasons, a classification based on land management was used in this study when determining the relation between depression storage and slope.

Depression storage for the cultivated land use class was determined through a dataset of values for different kinds of nearby crop fields (P.L. Richards, unpubl. data), in combination with a set of measurements randomly distributed in the agricultural fields of the Britt Road watershed. For the *urban* land use class, depression storage values were taken from literature (Walker, 2007). Values for all other classes were obtained by reclassifying and evaluating the Richards *et al*. (2008) dataset. Slope steepness for the two watersheds was derived from a Digital Elevation Model (DEM) of the study area (appendix A.1 and A.2).

Initial depression storage was assumed zero for all saturated areas in the *1b* and *2b* scenarios, including the Britt Road flood site. Microtopography is not measured by the semi-total station and was therefore not included in the flood volume. If full depression storage would be assumed at the start of an event, runoff at the flood site would be overestimated compared to the surveyed flood volume.

4.3.4 Routing

Based on the DEM of the study area (appendix A.1 and A.2), we constructed a map that describes the flow directions of surface water for each grid cell based on its ground slope. This map was checked in the field and corrected for errors, the presence of channels, culverts and obstacles preventing the water from flowing in the preferred direction. The railroad in the Britt Road watershed was surveyed with a semi-total station to investigate its impact on water flow. Also, aerial photographs were examined for geomorphological features associated with water flow. The resulting local drain direction (LDD) network is the basis for the delineation of the watersheds. It also determines where the concepts of sheet flow and channel flow are applied within the watershed. As described in paragraph 3.4, routing of channel flow requires information about the channel's dimensions. Top width, bottom width and channel depth (i.e. maximum water depth) were therefore measured in the field. These properties are used to calculate the slope angle of the trapezoid. Values for Manning's *n* were taken from literature (Chow, 1959 and Engman, 1986), and are presented per land use class in Table 4.4.

Land use	Manning's n	Land use	Manning's n
soy	0.06	*water*	0
forest	0.4	*beans*	0.06
shrubs and weeds	0.24	*reed*	0.24
corn	0.17	*pine nursery*	0.06
weeds	0.15	*urban*	0.011
grass and herbs	0.15	*lawn*	0.41
cucumber	0.06	*railroad*	0.2
winter wheat	0.06	*channels*	0.05
alfalfa	0.30		

Table 4.4 *Values for Manning's n per land use class (based on Chow, 1959 and Engman, 1986).*

4.4 Statistical preparation of model input

Infiltration and depression storage (*Dst*) data need to undergo statistical procedures to obtain the definitive model input values for *Ks*, *B* and *Dst*. This is explained per parameter in this section.

4.4.1 Infiltration: saturated hydraulic conductivity (Ks)

Figure 4.9a shows the typical shape of a hydraulic conductivity measurement, with an initial quick decline in infiltration rate and the approach of a constant value in the final stage of the measurement. We assumed that this constant value was eventually reached in all measurements. This constant value is equal to the saturated hydraulic conductivity (*Ks*) and was quantified by performing a linear regression between the cumulative amount of water that infiltrated and time since the start of the infiltration experiment (Figure 4.9b). In reverse order, measurement points were added to the regression and R^2 was evaluated. The gradient of the regression line with the best fit was assumed as *Ks*. Part of the measurement error of *Ks* is explained by the standard error of this fit. This error was computed for a randomly selected set of measurements, and expressed as a percentage of *Ks*. In case the averaged percentage was too large to be neglected (larger than 2%) it was subtracted from the variance of *Ks* in all of the procedures described in this paragraph.

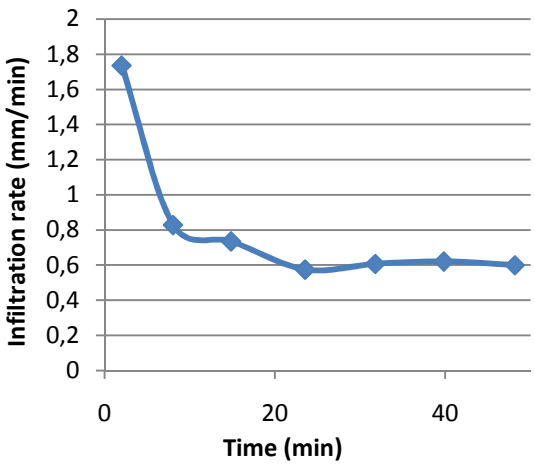

Figure 4.9a *Curve indicating the rate of infiltration in the course of a measurement (measurement 41B in the Britt Road catchment)*

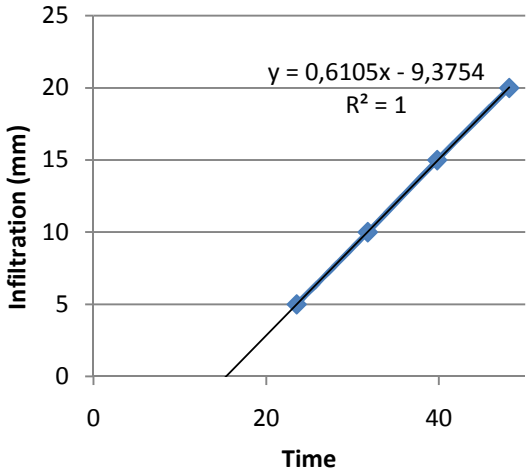

Figure 4.9b *Regression line based on the final four measurement points (measurement 41B in the Britt Road catchment).*

Normality of the *Ks* data was evaluated using the Kolmogorov-Smirnov test and if necessary, the data was transformed by taking the natural logarithm. At a 5% significance level, analysis of variance (ANOVA) was then performed on the *Ks* data to investigate whether the class distinction based on land use and soil texture was justified. Where possible, combining of the classes is desirable to increase the number of measurements within a class, and thus improve the reliability of the data during further statistical processing. F-tests were performed for all pairs of classes to test the equality of variance. If variances were accepted to be equal, equality of means was tested with the student's t-test. This procedure for testing the relevance of a classification is based on Bierkens (1994). If means or distributions were not significantly different for a certain pair of classes, merging

of these classes is considered. Apart from the outcome of the statistical analysis, field observations also played a role in the merging of classes. Some combinations were preferred above others because of similarities in vegetation type and the degree of cultivation

The measured *Ks* data served as the basis for the generation of saturated conductivity values for all grid cells within the watersheds. Sample variograms were constructed to test for the presence of a spatial correlation structure within the land use classes. This would enable the use of geostatistical simulation to assign *Ks* values to the watershed cells. If a semivariogram model could be fit through the sample variogram, conditional simulation would be applied. In case of the absence of a spatial structure, ln-transformed values would be randomly generated for each cell in a land use class from a normal distribution based on the class average and variance, both directly derived from the measured data. Simulated *Ks* values that have a value outside a range of four standard deviations around the class mean were omitted in the further analysis.

Assessing the scale-dependency of *Ks* is made possible by measuring on two scales, both within a grid cell (10 by 10 meter) and between different cells within a land use class. One might expect that *Ks* heterogeneity is smaller on the small scale compared to the larger scale. To be able to use the measured data in the model without applying an upscaling procedure, variation within a raster cell has to be assumed equal to larger-scale heterogeneity. The validity of this assumption was tested, for each land use, by comparing the averaged variances of the individual measurements within couples to the variances between the couples. If no difference in heterogeneity was found, all individual measurements would be used with equal weight when assigning *Ks* values to the raster cells in a certain land use class. If variances were significantly different, upscaling of the small-scale measurements would be necessary to successfully model the heterogeneity of the larger scale. This could be done using the upscaling method *g* developed by Karssenberg (2005).

4.4.2 Infiltration: capillarity and saturation deficit parameter (B)

Due to difficulties in measuring the individual components of the *B* parameter (see paragraph 4.3.2), an empirical approach was pursued to determine the values for *B*. For each hydraulic conductivity measurement, the solution of the Smith and Parlange infiltration model (equation 3.3) and the measured infiltration curve were plotted against time. The *B* parameter was varied until the optimal fit was achieved, according to the least square error principle (Figure 4.10). The derived values for *B* are only representative for the (near-)saturated conditions under which the infiltration measurements were performed. The saturation deficit (ϑ_s - ϑ_i) at the start of an infiltration measurement was derived by dividing fitted values for *B* by *G* values according to equation 3.4. The *G* values are based on soil texture and were taken from literature (Woolhiser, 1990). Unrealistic water deficit (ϑ_s - ϑ_i) values (larger than 0.5 or lower than 0.01) obtained by this method would indicate that tabulated data for *G* are not

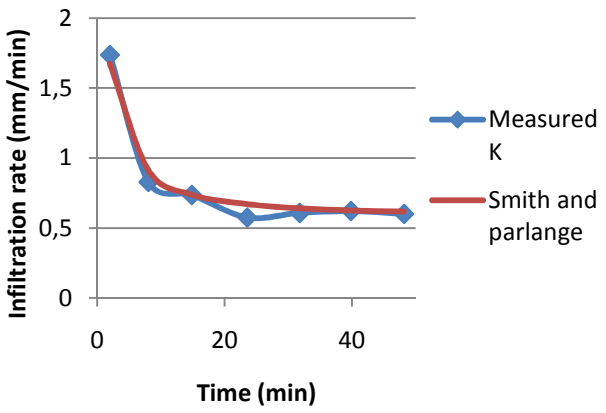

Figure 4.10 *Fitting the Smith and Parlange model to the measured hydraulic conductivity (measurement 41B in the Britt Road watershed).*

representative for soils found in the study area. This finding would support the use of empirically derived values for *B* instead of a soil moisture model in combination with *G* values from literature. The Smith and Parlange curve is fitted for all measurements, and the resulting *B* values were plotted against the corresponding *Ks* to evaluate the relation between the two parameters.

The error in the *B* parameter was estimated by adding and subtracting the measurement error in *Ks* to the Smith and Parlange curve for a set of conductivity measurements. Deviations between the resulting maximum and minimum B values and the original *B* were assessed. In case of an error larger than 2% of the actual parameter value, the error would be incorporated by subtracting it from the standard error.

4.4.3 Depression storage (Dst)

From the available depression storage datasets (see paragraph 4.3.3), the relation between depression storage and slope was evaluated for all land use classes except the urban class, which has its values taken from literature (Walker, 2007). Transformation of the data might be necessary to obtain a linear relation, which enables the use of equation 4.1.

4.5 Monte Carlo simulation

Realizations of Ks, B and Dst are simulated during the Monte Carlo simulation. As described in paragraph 4.4.1, *Ks* values for each raster cell in a certain land use class are generated from either conditional simulation or randomly picked from a normal distribution based on the measurements in that land use class. For each grid cell, values for *B* are randomly selected from a normal distribution with an average based on the relation between *Ks* and *B* and a standard deviation represented by the standard error in *B*. The following equation was used to quantify the standard error of the predicted value of *B*:

$$se_{\hat{B}} = \sqrt{{s_B}^2 \left(1 + \frac{1}{n} + \frac{(Ks_0 - \overline{Ks})^2}{\sum (Ks_i - \overline{Ks})^2} \right)} \qquad (4.1)$$

in which ${s_B}^2$ = the variance of the calculated *B* values from the measurements, *n* = the number of measurements, Ks_0 = the saturated hydraulic conductivity of the grid cell under consideration, $\overline{Ks}$ = the average saturated hydraulic conductivity observed and Ks_i is the observed saturated hydraulic conductivity of a certain measurement. Ks_i and $\overline{Ks}$ are the values on which the regression line is based. It should be noted that linearity of the relation between *B* and *Ks* is required to apply the procedure described above.

Similarly, depression storage values for a certain land use class are randomly selected from a normal distribution with an average based on the relation between slope, and *Dst* and a standard deviation represented by the standard error in *Dst*. If no *Dst* - slope relation can be found, values are picked from a normal distribution solely based on the measurement data.

Due to the randomness introduced to the model by *Ks, B* and *Dst*, every model run produces a different output. The most important model output is the cumulative volume of runoff arriving at the flood site at the final model timestep, since this is the actual volume of surface runoff that contributes to the flood. Monte Carlo simulation was performed to approach reality as closely as possible. The number of executed simulations depends on the output values produced by the model. Initially, a set of at least 100 Monte Carlo simulations was run for each flood scenario and the output

values and their distribution were evaluated. For scenarios producing runoff volumes distinctly different from the estimated total flood volume (i.e. negligibly small or much larger), no further simulations were run since the exact value was then of minor importance as the research question had been answered. If this was not the case, the following visual analysis was conducted, assuming a skewed distribution of the model output. The median cumulative runoff was plotted against the number of simulations used in calculating the median. The number of simulations was increased gradually and if the median eventually approached a constant value (a maximum change of $5m^3$ when adding 10 Monte Carlo simulations), the number of Monte Carlo simulations was assumed sufficient. If not, additional sets of simulations were executed until deviations around the median were assumed negligible. The same procedure would be carried out in case of a normal distribution, only then the mean would be used instead of the median.

4.6 Sensitivity analysis

Analysis of the sensitivity of the model to the different input parameters provides insight in how uncertainties and inaccuracies in input parameters propagate to the model output. A sensitivity analysis was performed to examine the influence of the input parameters on the cumulative volume of runoff arriving at the flood site at the final timestep. For one randomly selected model simulation, input values of IC_{max}, *Ks, B* and *Dst* are raised and lowered by 10% to evaluate their impact on the cumulative volume of runoff generated by the model. In this way, the analysis produces an overview of the relative importance of each parameter for the model output.

5. Results

5.1 Model input

This section presents the results of the procedures described in sections 4.3 and 4.4. For each model component, it provides an overview of the definitive input values to the model.

5.1.1 Infiltration

Of the planned 222 hydraulic conductivity measurements, 213 were carried out successfully. *Ks* values were determined through linear regression, and the standard error was evaluated for a randomly selected set of 10 measurements. This error was found to be negligibly small for the whole set, and is therefore neglected for all *Ks* measurements (appendix C.2). Appendix B.1 gives an overview of all *Ks* measurements.

Results of the Kolmogorov-Smirnov test show that the *Ks* dataset is not normally distributed. A normal distribution was obtained through ln-transformation of the values (appendix C.1). ANOVA of the transformed *Ks* showed that a classification based on soil texture is not statistically justified (Table 4.1). Therefore, a classification based on soil texture is abandoned in further data processing and data grouping is solely based on land use.

A table evaluating all possible class combinations can be found in appendix C.3. Some combinations were preferred above others because of similarities in vegetation type and the degree of cultivation. For example, a possible merging of the Quinlan Road weeds class with agricultural classes was declined for this reason. Except for the weeds classes, every class from the Britt Road watershed was merged with its Quinlan Road equivalent. Table 5.2 presents the resulting classification, and the corresponding averages and variances of ln(*Ks*).

Table 5.1 *ANOVA of ln-transformed Ks values classified according to texture. F is found to be smaller than Fcrit (SS = sum of squares, df, = degrees of freedom, MS = mean of squares, Fcrit = critical value for F (α = 0.05)).*

Groups	*Count*	*Sum*	*Average*	*Variance*
channery loam	4	-1.93614	-0.48403	3.543397
gravelly loam	10	-13.4499	-1.34499	2.428343
loam	42	-23.4589	-0.55855	2.01296
mucky silt loam	2	3.933302	1.966651	0.13605
silt loam	128	-66.6814	-0.52095	2.802032
very fine sandy loam	27	-13.5064	-0.50024	4.030862

ANOVA

Source of Variation	*SS*	*df*	*MS*	*F*	*P-value*	*F crit*
Between Groups	19.16284	5	3.832568	1.377776	0.23394	2.257695
Within Groups	575.8132	207	2.781706			
Total	594.976	212				

Table 5.2 *Merged classes and the corresponding distributions, used for generating ln(Ks) values in the model (B = Britt Road, Q = Quinlan Road, n = number of measurements, X = average value,* **σ** *= standard deviation).*

Original land use classes	Ks land use class	n	X	σ
corn (B+Q), alfalfa (B), cucumber (Q), soy (B+Q), beans (B+Q)	*cultivated*	*108*	-0.98	1.39
forest (B+Q)	*forest*	*19*	*1.34*	1.26
grass (B)	*grass*	*12*	*1.05*	0.55
grass and herbs, weeds (B)	*grass and herbs*	*22*	*-0.33*	1.48
lawn (B+Q)	*lawn*	*12*	*-0.65*	0.77
shrubs and weeds (B+Q)	*shrubs and weeds*	*18*	*1.33*	0.77
weeds (Q)	*weeds (Q)*	*8*	*-2.63*	1.78
winter wheat (B+Q)	*winter wheat*	*14*	*-2.26*	1.01
urban, reed, water	*impermeable*	*0*	-	-

Figure 5.1 shows the semivariogram of the natural logarithm of the *Ks* values for the *cultivated* land use class in the Britt Road watershed. This is the class with the highest number of measurement locations, and thus the one most likely to produce a reliable semivariogram. Figure 5.1 displays no relation between the semivariance and the distance between samples. Therefore, a semivariogram model cannot be fitted through the sample variogram. For the other classes, similar sample variograms were found, or the number of measurements is too small to construct a reliable semivariogram. Therefore, no spatial correlation structure of *Ks* was assumed for any land use class, and values were randomly generated per class according to the distribution described in Table 5.2.

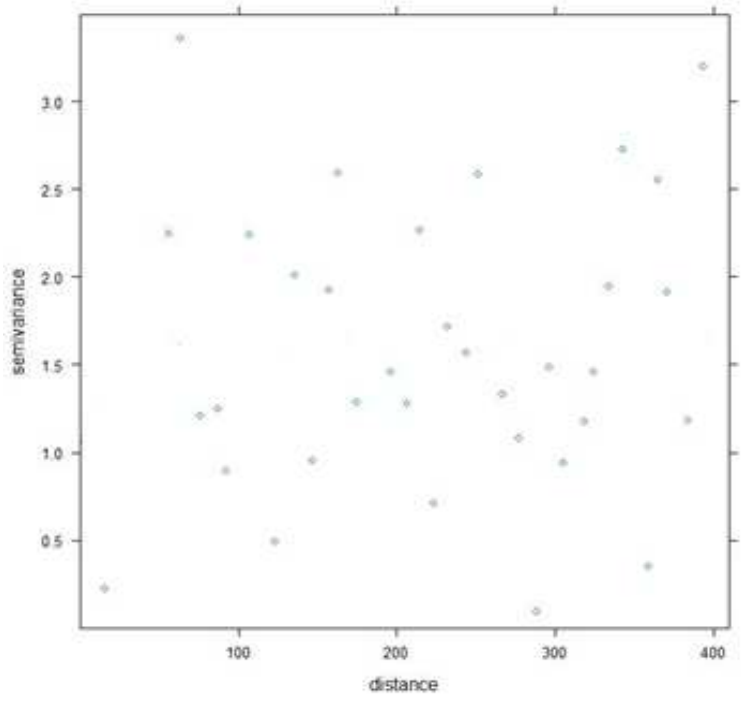

Figure 5.1 *Sample variogram of the* cultivated *land use class. Bin width is set to 15 m.*

Table 5.3 *Comparison of the variance of the ln(Ks) values within couples and the variance between couples.*

Averaged variance within couples		Variance between couples	
cultivated	1.185634928	cultivated	1.341689713
forest	1.548510279	forest	1.068397847
grass and herbs	0.467504494	grass and herbs	2.03589763
lawns	0.433860993	lawns	0.393956333
shrubs and weeds	0.398627729	shrubs and weeds	0.40508889
weeds (q)	0.693280387	weeds (q)	3.2474069
winter wheat	0.781699675	winter wheat	0.659004487

The heterogeneity of *Ks* at different scales is tested in Table 5.3. In three of the seven land use classes that were analyzed, variance between measurement couples is larger than the variance within the couples. Two classes display the opposite, and for the two other cases variances are almost equal. It was concluded from this analysis that there is no reason to assume a difference in heterogeneity between *Ks* values within a grid cell and values on a larger scale.

The following relation between *B* [m] and *ln(Ks)* [*Ks* in m/d] was found for the Britt Road and Quinlan Road watershed under saturated conditions:

$$B = e^{0.8574 * \ln(Ks) - 5.3325}$$

Based on this relation, and the standard error resulting from equation 4.1, *B* values were randomly assigned to the model grid cells. No error in *B* was included, since the error in *Ks* was found to be negligibly small. Details about the obtained relation between *B* and ln(*Ks*) can be found in appendix C.4.

A value for the water deficit (ϑ_s - ϑ_i) at the start of each infiltration measurement was derived by dividing *B* by the capillary drive (*G*) based on soil texture (Woolhiser, 1990). 37% of derived water deficit (ϑ_s - ϑ_i) values were unrealistic (larger than 0.5 or lower than 0.01)

The volumetric rock content measurements are summarized in Table 5.4, a complete overview of the measurements is given in appendix B.2. All measured values lie within the range provided by literature (USDA, 1969).

Table 5.4 *Volumetric rock content (ROC) values. For unsampled soil types, rock content values are taken from literature (USDA, 1969).*

Soil type	*n*	*ROC*
Ha	*0*	*0.25*
On	*21*	*0.04*
Ap	*5*	*0.03*
Ld	*9*	*0.015*
Lm	*17*	*0.05*
Gn	*1*	*0*
Lo	*2*	*0*
Ov	*0*	*0.125*
Ad	*0*	*0.05*
Kn	*11*	*0.025*

Soil type	*n*	*ROC*
Ca	*2*	*0*
Ng	*1*	*0*
Cl	*2*	*0.01*
Ar	*0*	*0*
Hl	*1*	*0*
Du	*0*	*0.025*
Ph	*1*	*0.21*
Ps	*3*	*0.07*
Be	*2*	*0.42*

5.1.2 Depression storage

Due to a lack of more specific data, the adjusted land use classification for *Ks* was used in determining values for depression storage. After reclassification and ln-transformation of the available data from Richards *et al*. (2008), the following relations were found between slope and microtopography storage:

Forest:

$$\ln(Dst) = -0.2422x - 4.5982$$

Shrubs and weeds / weeds / grass and herbs:

$$\ln(Dst) = -0.1809x - 4.9098$$

Lawns:

$$\ln(Dst) = -0.3121x - 5.7414$$

where *Dst*(m) = the effective depression storage and *x* is the slope (%). These relations are applicable for slopes under 8% for urban grassland and under 12% for the other classes (Richards *et al*., 2007). For steeper slopes, zero depression storage was assumed. More details on the above relations can be found in appendix C.5.

For the *cultivated* land use class, no relation between slope and depression storage was found (appendix C.5). Ln-transformed values for *Dst* in meters were taken from a distribution with an average of -5.01 and a standard deviation of 0.52. A storage value of 0.000635 m was assumed for the *urban* land use class (*impervious* in Walker, 2007). The different surface texture of the abandoned railroad is reflected in a value of 0.00506 m (*intermediate-textured streets* in Walker, 2007).

5.1.3 Routing

For the Britt Road watershed, the abandoned railroad is found to play an important role in the routing scheme of the watershed. Its morphology is described in detail by Figure 5.2. The railroad slopes from west to east. The railroad is lower than the surrounding land in the west of the watershed (eg. transect B), and higher in the east (as illustrated by transect D and the TIN). The transition zone lies just east of transect C. In the bushes adjacent to the railroad track, several small channels have formed, some of which persist along the entire length of the track. These channels are best developed south of the track, as illustrated by the transects. Water appears to have cut through the edge of the railroad system at several places (Figure 5.2). The two openings west of transect C indicate inlet points from the agricultural fields to the low-lying railroad, while the easternmost opening represents an outlet point from the railroad system, which here lies as a dike in the landscape. The outlet point can be followed as a small depression into the flood site. A larger depression in the railroad track, marked in Figure 5.2, is surveyed to determine its volume (appendix A.10). It is found that this depression can contain a volume of 46.1 m^3.

Figures 5.3a and 5.3b display the preferred flowpaths of surface water in the Britt Road and Quinlan Road watershed respectively, and indicate which channels are visible in the field. For these channels, the concept of channel flow was applied. The railroad acts as both a dam (where it is higher than the adjacent land) and a channel, with inlet and outlet points determined according to

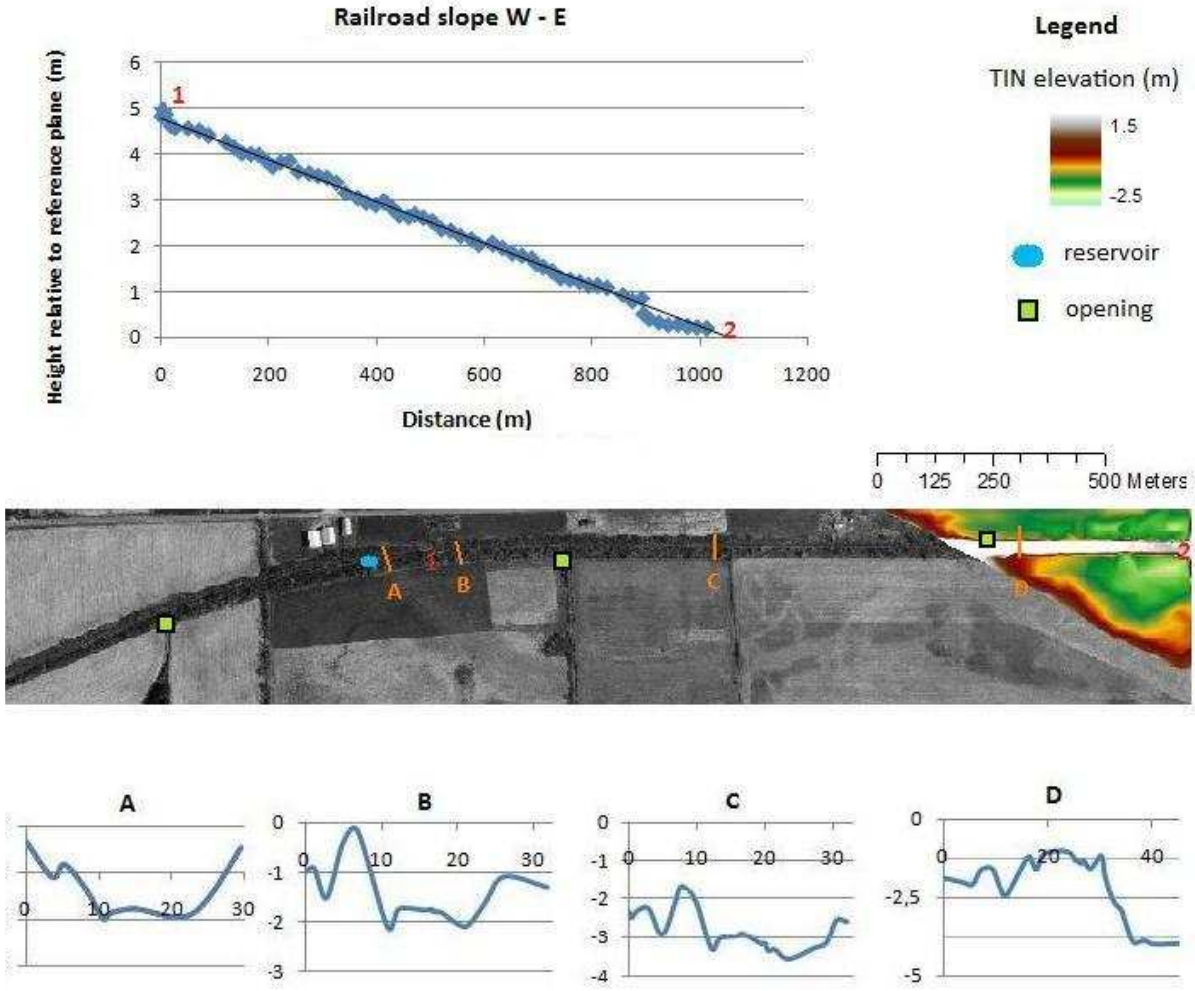

Figure 5.2 *Morphological characteristics of the abandoned railroad in the Britt Road watershed. Its slope is surveyed from point 1 to point 2 on the map. A, B, C, and D indicate the location of surveyed transects. All transects are plotted from south to north. All distances and heights are in m.*

the openings marked in Figure 5.2. The bottom width and slope angle of the railroad channel were derived from the surveyed cross-sections (Figure 5.2), with the collection of smaller channels being treated as one large channel. The depression in the track is treated as a reservoir which needs to fill up before the runoff can continue its way along the railroad. Therefore, it is included in the depression storage component of the model.

For the Quinlan Road watershed (Figure 5.3b), no well-defined channel is present around point C and to the west of the Keeney Road lake, although the flow accumulation map suggests otherwise. Surface water does accumulate in these areas, but this results in a swampy area as observed during the field study. The 'wetness' of these areas was taken into account by assuming saturation of the soil in the area near the lake, which implies that we assumed impermeability of the *reed* land use class.

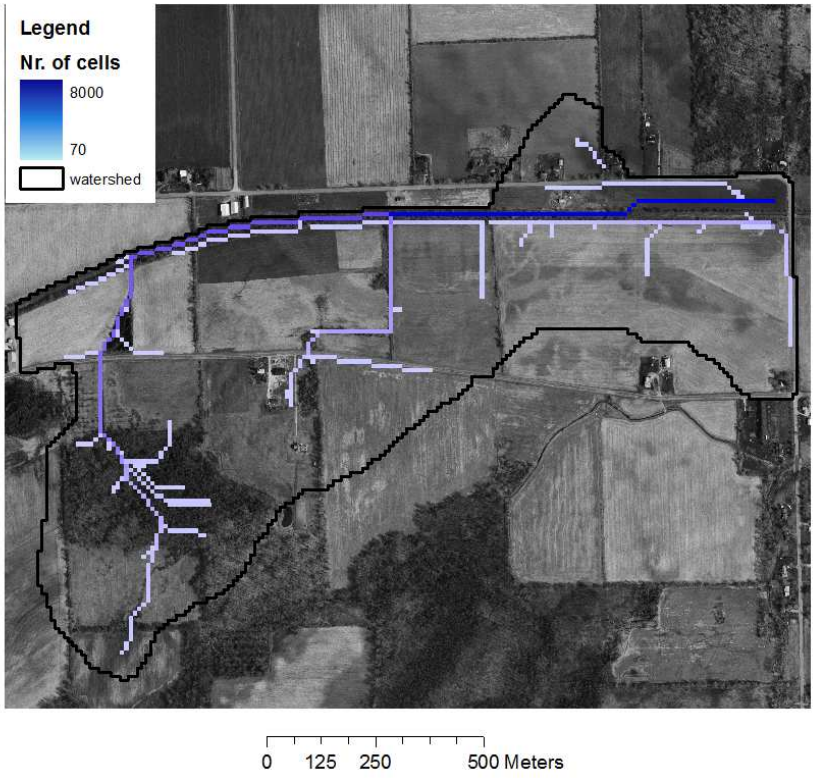

Figure 5.3a *Flow accumulation map of the Britt Road watershed. Values indicate the number of cells discharging on a certain cell.*

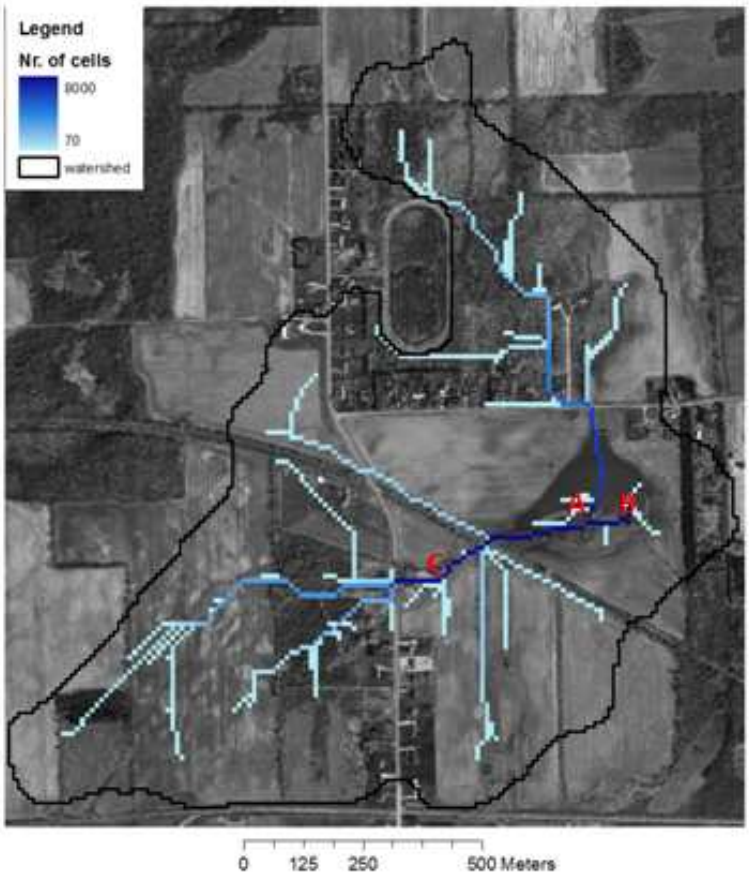

Figure 5.3b *Flow accumulation map of the Quinlan Road watershed. A and B indicate sinkhole locations.*

5.2 Model output

The behavior of the different parameters through time is expressed in Figure 5.4. The graph shows that the infiltration flux closely follows precipitation. The depression storage curve has an early peak before the runoff flux starts increasing, since it has to be satisfied first. At a certain point in time, the depression storage flux becomes negative while the runoff flux is still positive. This means that, on average for the whole watershed, water disappears from micro-depressions while there still is an increase of surface runoff. This phenomenon is due to the influence of the impermeable areas, where the depression storage remains satisfied (a zero flux) and runoff is still generated (positive flux). At the same time, in other areas, the fluxes for both parameters are negative due to infiltration. The interception flux is very small compared to the other parameters.

Table 5.5 presents an overview of the model results for the Britt Road and Quinlan Road watersheds. Cumulative runoff volumes reaching the flood site are given per scenario. For the *1a* and *2a* scenarios in the Britt Road watershed, the portion of the total flood volume coming from surface runoff is very small. For the *1b* scenario in Quinlan Road, the total flood volume is explained by surface runoff generation in the watershed. For the other scenarios, part of the total flood volume is explained by surface runoff. A cumulative frequency distribution of the model output for all model scenarios can be found in appendix E.

The runoff coefficient for all scenarios is presented in Table 5.6. Values are extremely small for the 1aB and 2aB scenarios, possibly indicating an error in the assumptions regarding saturation. For the other scenarios, values have a similar order of magnitude as literature values for forests, lawns, and cultivated land in areas with low slopes (Chin, 2000; Corbitt, 1999). This implies that the *1b* and *2b* scenarios are more realistic than the *1a* and *2a* scenarios.

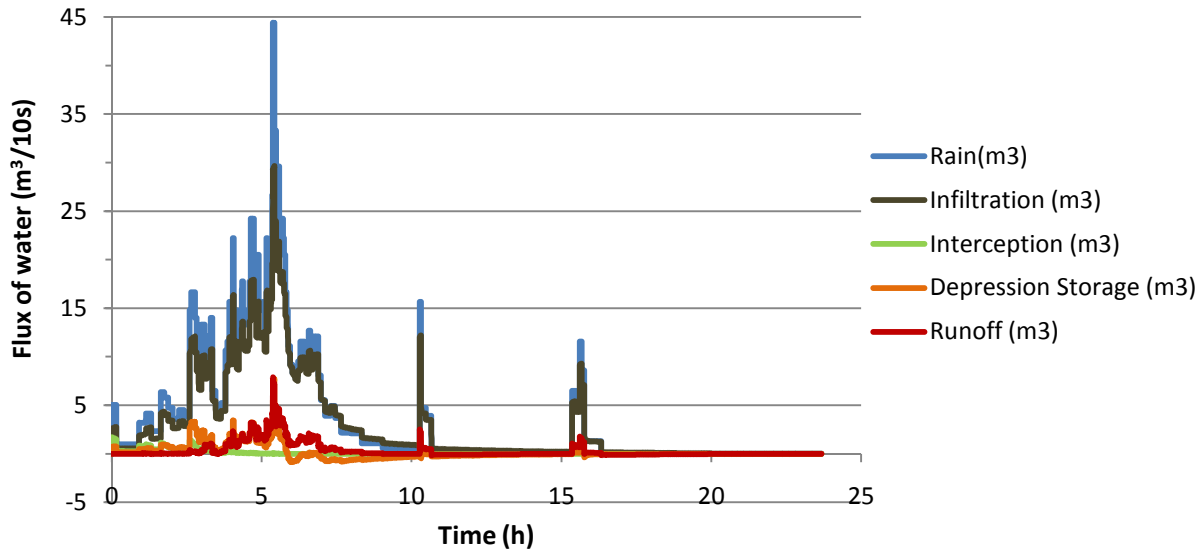

Figure 5.4 *Graph of the fluxes belonging to the different model parameters for event 1 in the Britt Road catchment.*

Table 5.5 *The cumulative volume of runoff reaching the flood site at the final timestep, compared to the total flood volume (1,2 = flood events, a = all infiltration according to measured Ks, b = additional impermeable areas, B = Britt Road, Q = Quinlan Road, n = number of Monte Carlo simulations, perc. = percentile,).*

Cumulative volume of runoff (m^3)					% of flood volume explained			
scenario	**n**	**10^{th} perc.**	**median**	**90^{th} perc.**	**flood volume (m^3)**	**10^{th} perc.**	**median**	**90^{th} perc.**
1aB	400	20.5	88.8	133.4	?	-	-	-
1bB	400	2306.3	2581.3	2760.0	?	-	-	-
1aQ	300	930.6	954.3	986.1	1352.5	68.8	70.6	72.9
1bQ	400	1654.9	1682.9	1714.4	1352.5	122.4	124.4	126.8
2aB	400	193.6	287.0	456.3	14454.3	1.3	2.0	3.2
2bB	800	6088.5	7068.3	7437.8	14454.3	42.1	48.9	51.5
2aQ	400	2119.5	2170.6	2221.1	8674.6	24.4	25.0	25.6
2bQ	400	3944.8	3999.2	4055.1	8674.6	45.5	46.1	46.7

Table 5.6 *Runoff coefficients for all model scenarios (1,2 = flood events, a = all infiltration according to measured Ks, b = additional impermeable areas, B = Britt Road, Q = Quinlan Road).*

Scenario	Precipitation (mm)	Watershed area (m^2)	Volume of precipitation (m^3)	Cumulative volume of runoff (m^3)	Runoff coefficient
1aB	*28.194*	*1240100*	*34963.379*	*85.5*	*0.00244542*
1bB	*28.194*	*1240100*	*34963.379*	*2166.4*	*0.06196197*
1aQ	*28.194*	*1053300*	*29696.74*	*954.3*	*0.03213484*
1bQ	*28.194*	*1053300*	*29696.74*	*1682.9*	*0.05666952*
2aB	*58.166*	*1240100*	*72131.657*	*276.8*	*0.00383743*
2bB	*58.166*	*1240100*	*72131.657*	*6653.4*	*0.09223967*
2aQ	*58.166*	*1053300*	*61266.248*	*2170.6*	*0.03542897*
2bQ	*58.166*	*1053300*	*61266.248*	*3999.2*	*0.06527575*

4.3 Sensitivity analysis

The model run producing the median cumulative runoff amount for the 1B scenario in the Britt Road watershed is selected for evaluation in a sensitivity analysis, since this is the event producing the largest amounts of runoff (see Table 5.5). The Quinlan Road watershed is less suitable to investigate in a sensitivity analysis, since the spreading of the runoff values produced by the model was found to be quite small.

In Table 5.7, the original cumulative runoff volume is compared to the values resulting from a 10% increase of different model input parameters. It was found that deviations from the original value are small, with the model being most sensitive to adjustments in depression storage and Ks, and least sensitive to changes in IC_{max} and *B.* The influence of changes in *Ks* and *B* could be diminished by the majority of the runoff coming from saturated areas, where *Ks* was assumed to be zero for both the original and the adjusted model run.

Table 5.7 *Final cumulative runoff volume reaching the flood site (m^3) for adjusted parameter values.*

	original	10% increase	Difference (%)
IC_{max}		6648.36	0.089
Ks	6654.29	6549.66	1.572
B		6653.87	0.006
Dst		6517.2	2.060

6. Discussion

Rainfall runoff modeling commonly requires calibration data to compare model results with field measurements. By calibrating the runoff model, discharge simulated by the model will more accurately describe the quick flow component of a hydrograph measured in the field. In this study it is hypothesized that groundwater contributes to the flood. This implies that a portion of the surface water originates from groundwater and that there is a strong interaction between these two components. This makes simple hydrograph separation problematic, and therefore the model was not calibrated. Most of its important input parameters are represented by a large dataset of field measurements and are therefore accurate representations of reality. The accuracy of the model is evaluated with the simulation of the rainfall event of October 20, 2006 for the Quinlan Road watershed. Transducer data of several years indicate that groundwater levels in early autumn are low and a major groundwater contribution during the event of October 20, 2006 is not likely (appendix B.3). Therefore surface runoff contribution to the flooding for this event is expected to be around 100% of the total flood volume. This is consistent with the model results, about 70.6% (median of scenario 1aQ) to 124.4% (median of scenario 1bQ) of the flood volume is explained by the runoff model, depending on the inclusion of saturated areas or not.

Event based runoff modeling is sensitive to the initial soil moisture content at the start of a rainfall event (Sheikh, *et al*. 2009). A dry soil exerts a larger suction force than a wet soil at the start of a rainfall event which enlarges the infiltration capacity and reduces runoff generation. In this study the integral capillary and saturation deficit parameter *B* determines the suction force of the soil at the start of a rainfall event, and is derived by fitting the infiltration model of Smith and Parlange (equation 3.3) to the infiltration measurements. The resulting values for *B* are only representative for (near-)saturated conditions under which the measurements were performed, as the soil was wetted prior to an infiltration measurement. These near-saturated conditions are expected to be valid for both simulated events, because these events are preceded by a period of numerous rainfall events (appendix B3). Furthermore the event of November 30, 2006 has a slow build-up towards a sharp peak of high rainfall intensity (figure 4.2) which reduces the importance of the initial soil moisture content, as the soil is wetted during the first part of the event when hardly any runoff is generated. To extract a value for the water deficit (ϑ_s - ϑ_i) at the start of an infiltration measurement, derived values for *B* were divided by the capillary drive (G) based on soil texture (Woolhiser, 1990). 37% of derived water deficit (ϑ_s - ϑ_i) values were unrealistic (larger than 0.5 or lower than 0.01) which indicate that tabulated data for *G* are not representative for soils found in the study area. This finding supports the use of empirically derived values for *B* instead of a soil moisture model in combination with *G* values from literature.

From the sensitivity analysis it is clear that depression storage has a larger influence on the cumulative amount of runoff reaching the flood zone than infiltration or interception parameters. The long-lasting, low-intensity rain event simulated in the sensitivity analysis of the Britt Road watershed reduces the importance of infiltration parameters, as most of the time rain intensities are below the potential infiltration capacity. Consequently impervious surfaces in the area are the main contributors to surface runoff. Changing the depression storage of impervious surfaces directly changes the amount of surface runoff generated in the watershed, resulting in high model sensitivity to depression storage. In contrast to depression storage, interception by vegetation has no importance in the model which is mainly caused by the low vegetation coverage during the model simulation. If a vegetation type has a high interception store, it is frequently found in combination

with a high potential infiltration. Changing interception values in areas with high infiltration capacity doesn't lead to a change in runoff generation. The model sensitivity to different input parameters is mainly dependent on the combination of the parameter of interest and the potential infiltration capacity. Furthermore it is dependent on seasonal variations. Model input values presented in this study are only representative for events occurring in autumn and model sensitivity will change during other annual seasons.

Urban structures in both watersheds have a major influence on runoff generation. Houses, driveways, roads, and railroad tracks reduce infiltration and divert the flow of surface water. Especially the surface water drainage system of the Britt Road watershed is artificial. The abandoned railroad track in the Britt Road watershed determines the shape of the watershed and discharges all the water flowing to the north towards the flood zone. Ditches from farm fields discharge onto the railroad track at two locations. Besides drainage water from agricultural fields, groundwater from basement flooding during extreme events is discharged by a local resident onto the railroad track. All the water that enters the railroad in the Britt road watershed ultimately reaches the flood zone. The Quinlan Road watershed has a more natural drainage system with two streams discharging the surface water from the watershed into two sinkholes. The Keeney Road Lake is connected by a stream with the eastern sinkhole and therefore precipitation falling in the Keeney road lake contributes without loss of water to the flood volume. The presence of more surface water in the Quinlan Road watershed enlarges the potential of flooding in the Quinlan Road watershed independent on vegetation and soil conditions. This is in contrast with the Britt road watershed where runoff generation is dependent on particularly the sate of agricultural fields.

From model simulations of the event of November 30, 2006 for the Quinlan Road watershed it appears that the total volume of flood water cannot be generated by surface runoff alone. About 46% of the flood water originates from surface runoff during the event of November 30, 2006, assuming saturated conditions for the swampy forest and Keeney Road lake area. The other 54% is generated by other sources of water which are not included in the model. These sources are represented by drainage water from tile drains, subsurface quick flow in the unsaturated zone through voids and cracks and groundwater mounding. The volume of water coming from tile drains is expected to be small, because not all agricultural fields are equipped with tile drains and a large area of the Quinlan Road watershed is covered with forest and scrubland. Subsurface quick flow through the unsaturated zone is also assumed to be small as the unsaturated zone is shallow. This would mean that a major part of the unexplained 54% of flood water originates from groundwater mounding.

The flood events in the Britt Road watershed are expected to be less groundwater driven than events occurring in the Quinlan Road watershed. About 49% of the flood water originates from surface runoff during the event of November 30, 2006, assuming saturated conditions for the flood zone and swampy forest. The other 51% is generated by other sources of water which are not included in the model. The amount of water originating from tile drains is expected to be substantial as agricultural fields in the watershed are all equipped with tile drains. Furthermore the Britt Road watershed has an additional source of water by pumping of groundwater out of a flooded basement during extreme events by a local resident. These sources are not included in the model and make up part of the unexplained 51% of flood water. The remaining part should come from a groundwater phenomenon, but how large this percentage is remains unknown. It is likely that the groundwater level is close to the surface during the flooding, otherwise all the surface water entering the flood

zone would infiltrate. This is indicated by the simulation of scenario 2aB, which explained 2% of flood water by runoff generation.

For both watersheds flood events only occur during autumn, winter and early spring. Major rainfall events during the summer time (appendix B.3) do not coincide with flood events. Interception by vegetation is larger at the end of the growing season, which for most agricultural species in the region is during the summer period. Also, soil moisture content is smaller during the hot summer time, which enlarges the suction force of the soil. This is represented by the B parameter of the Smith and Parlange infiltration model. These conditions decrease the amount of runoff generation in the area and, in combination with low groundwater tables, reduce the risk of flooding during summer. The height of the water table is however the most influential factor in causing the floods. Floods do not occur without high groundwater levels in both watersheds. Even the event of October 20, 2006, which is entirely explained by overland flow for the Quinlan Road watershed, occurs only under the assumption that the sinkholes have no drainage capacity due to groundwater seepage.

7. Conclusions and recommendations

- Depression storage is an important parameter in runoff modeling and in case of modeling low-intensity precipitation events in autumn in gently sloping areas, the runoff model is more sensitive to depression storage than infiltration or interception parameters.
- Runoff generation in the Britt Road watershed is more dependent on vegetation and soil conditions than runoff generation in the Quinlan Road watershed, because more surface water is present in the Quinlan Road watershed leading to direct increase of surface water discharge during heavy rainfall events.
- The surface runoff contribution to the flood event of November 30, 2006 in the Britt road watershed, assuming saturated conditions for the flood zone, is about 49%. If the flood zone is not saturated, so without high groundwater tables, all the surface water reaching the flood zone will infiltrate into the soil and no flood will occur.
- For the Quinlan Road watershed the surface runoff contribution during the flood event of November 30, 2006 was lower than in the Britt Road watershed. About 46% of the flood volume originates from surface runoff. Groundwater mounding is probably occurring at the sinkholes as other sources of water contributing to the flood are of minor importance. The rainfall event of October 20, 2006 led to a flooding which is fully explained by runoff generation. Early in the season it is expected that flood events are driven less by groundwater.
- This study is primarily focused on quantifying the contribution of surface runoff to karst-related flooding without taking other quickflow components into account. Using this method the importance of a groundwater component can be evaluated, but quantifying the contribution of groundwater to the flooding is difficult. To estimate the actual groundwater contribution a tracer study can be performed during the time of flooding.
- Whether the floodings between Le Roy and Caledonia are caused by a regional groundwater phenomenon cannot be concluded from this study. A better documentation of the timing of the flood events, increased groundwater monitoring during the floodings and local tracer studies are required to investigate the hypothesis of a regional groundwater phenomenon.

References

Bierkens, M.F.P. (1994) *Complex confining layers: a stochastic analysis of hydraulic properties at various scales*, Netherlands Geographical Studies 184, Utrecht University, 263 pp.

Bonacci, O., Ljubenkov, I. and Roje-Bonacci, T. (2006) *Karst flash floods: an example from the Dinaric karst (Croatia)*, Natural Hazards Earth System Science 6, pp. 195–203

Breuer, L. , Eckhardt, E. and Frede, H-G. (2003) *Plant parameter values for models in temperate climates,* Ecological Modelling 169 (2-3), pp. 237-293

Chin, D.A. (2000) *Water-Resources Engineering.* Prentice-Hall, New Jersey.

Chow, V. T. (1959) *Open-channel hydraulics,* Mc-Graw-Hill, New York.

Corbitt, R.A. (1999) *Standard Handbook of Environmental Engineering (2nd ed.),* McGraw-Hill, New York

Darboux, F. and Huang, C. (2005) *Does soil surface roughness increase or decrease particle transfers?* Soil Science Society of America Journal 69, pp. 748-756

Dunn Geo. Eng. (1992) *Task 2, Phase :A Report State Superfund Standby Program Lehigh Valley Railroad Derailment Site RI/FS, Town of Leroy County of Genesee, New York,* Dunn Geoscience Engineering Co., P.C. Albany, NY 12205 80pp.

Engman, E.T. (1986) *Roughness coefficients for routing surface runoff,* Journal of Irrigation and Drainage Engineering 112, pp. 39–53.

Fairchild, H.L. (1909) *Glacial Waters in Central New York*, Bulletin 127 of the New York State Museum, Albany NY

Federal Research Division (FRD) of the US Library of Congress (1988-1998), *Country studies*

Fronk, A.M. (1991) *Lehigh Valley Railroad Spill: A Study of a Contaminated Carbonate Aquifer*, Undergraduate Thesis, Hobart William Smith Colleges, Geneva, NY 44pp.

Karssenberg, D. (2005) *Upscaling of saturated conductivity for Hortonian runoff modelling,* Advances in Water Resources, 29-5, pp. 735-759

Maréchal, J.C., Ladouche, B., Dörfliger, N. & Lachassagne, P. (2008) *Karst flash flooding in a Mediterranean karst, the example of Fontaine de Nîmes*, Engineering Geology 99(3), pp. 138-146

Merriam, R.A. (1973) *Fog drip from artificial leaves in a fog wind tunnel*, Water Resources Research 9, pp. 1591-1598

Miller, J.E. (1984) *Basic concepts of kinematic- wave models* US Geological Survey Professional Paper (1302) 29 p.

Mishra, S.K., Tyagi, J.V. and Singh, V.P. (2003) *Comparison of infiltration models,* Hydrological processes 17, pp. 2629-2652

Morgan, R.P.C., Quinton, J.N., Smith, R.E., Govers, G., Poesen, J.W.A., Auerswald, K., Chisci, G., Torri, D., Styczen, M.E. (1995) *The European soil erosion model EUROSEM: a dynamic approach for predicting sediment transport from fields and small catchments* Earth Surface Processes and Landforms 23 (6), pp. 527-544

Onstad, C.A., Wolfe, M.L., Larson, C.L. and Slack, D.C. (1984) *Tilled soil subsidence during repeated wetting*, Transactions of the ASAE (27), pp. 733-736

PCRaster (2008), info at: http://pcraster.geo.uu.nl/

Peel M.C., Finlayson B.L. and McMahon T.A. (2007) *Updated world map of the Köppen*-Geiger *climate classification*, Hydrology and Earth System Sciences 11, pp. 1633-1644

Potter, K.N. (1990*) Soil Properties Effect on Random Roughness Decay by Rainfall,* Transactions of the ASAE (33), pp. 1889-1892.

Rhinehart, S. (2005) *Origin of Anomalous Flooding in the Quinlan Rd Sinkhole, Leroy, New York,* Undergraduate Thesis, SUNY College at Brockport.

Richards, P.L., Grimm, R. and Cannon, D. (2005) *Depression storage in landuses common to the Finger Lakes, 1st Annual Conference*, Finger Lakes Institute, Hobart and William Smith Colleges, Geneva NY.

Richards, P.L. (2007) *Karst-related flooding between Le Roy and Caledonia*, oral abstract, 3rd annual Finger Lakes research conference, Geneva NY.

Richards, P.L., Norris, M.D. and Lin, B.B. (2008), *The hydrologic implications of ecologic succession: Depression storage and leaf litter,* 93rd ESA annual meeting, Miwaukee, Wisconsin.

Sheikh, V., Visser, S., Stroosnijder, L. (2009*) A simple model to predict soil moisture: Bridging Event and Continuous Hydological (BEACH) modelling*, Environmental Modelling & Software (24) pp. 542-556

Smith, R.E. and Parlange, J,-Y. (1978) *A parameter-efficient hydrologic infiltration model*, Water Resources Research 14(3), pp. 533-538

United States Department of Agriculture (USDA) Soil Conservation Service (1969), *Soil survey Genesee County, New York,* 177 pp., U.S. Government Printing Office, Washington DC

Van Deursen, W.P.A. (1995), *Geographical Information Systems and Dynamic Models.* Utrecht: Koninklijk Nederlands Aardrijkskundig Genootschap/Faculteit Ruimtelijke Wetenschappen, Universiteit Utrecht.

Walker, W. W. (2007), *P8 Model Coefficients for SLAMM Impervious Area Categories*, prepared for Minnesota PCA.

Wesseling, C.G., D. Karssenberg, W.P.A. van Deursen & P.A. Burrough (1996*), Integrating dynamic environmental models in GIS: the development of a Dynamic Modelling language.* Transactions in GIS 1, pp. 40-48.

Woolhiser, D.A., Smith R.E. and Goodrich, D.C. (1990) *KINEROS, a kinematic runoff and erosion model: documentation and user manual.*

Zhou, W. (2006) *Drainage and flooding in karst terranes,* Environmental Geology 51, pp. 963-973

Appendices

A. Maps

A.1)

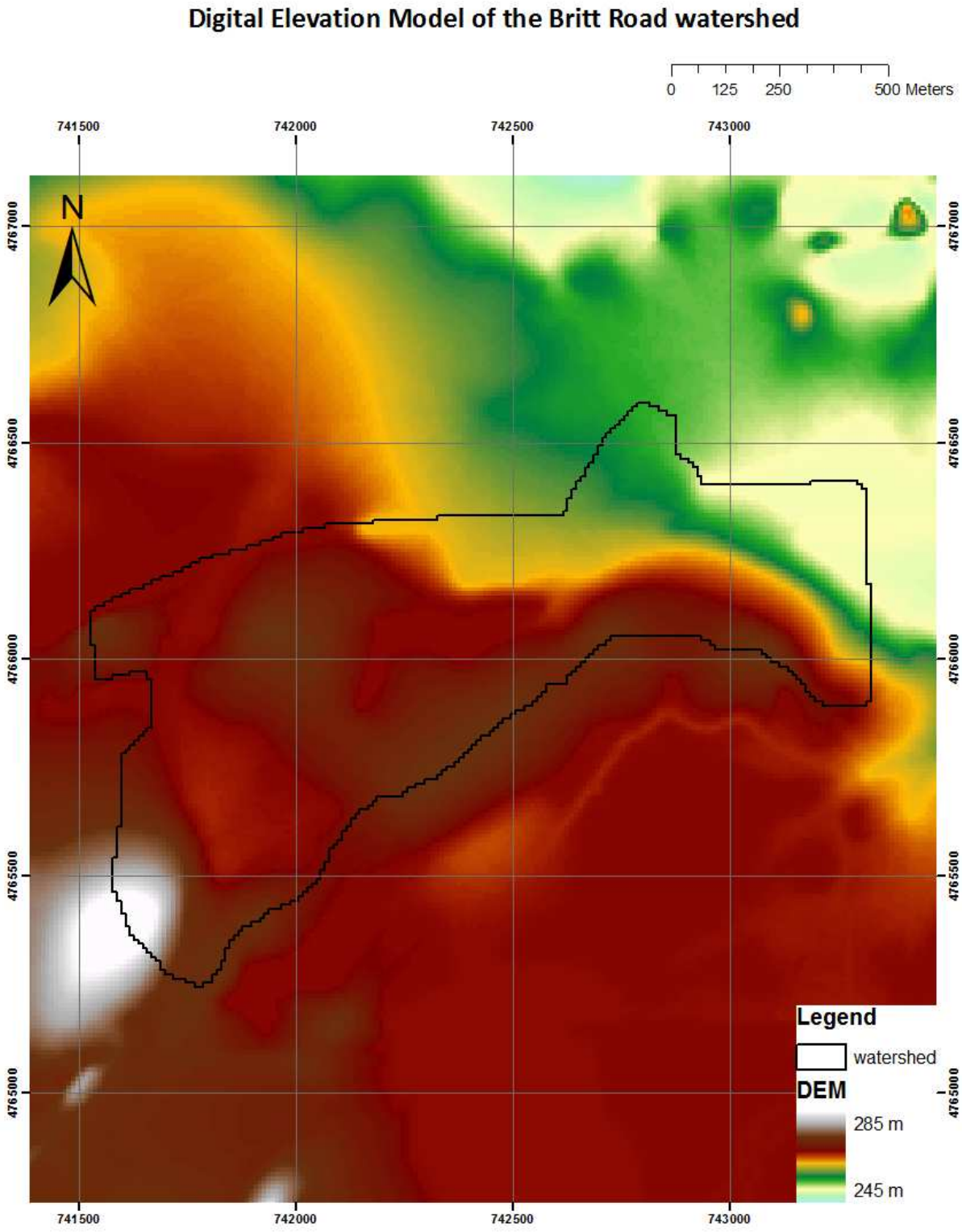

A.2)

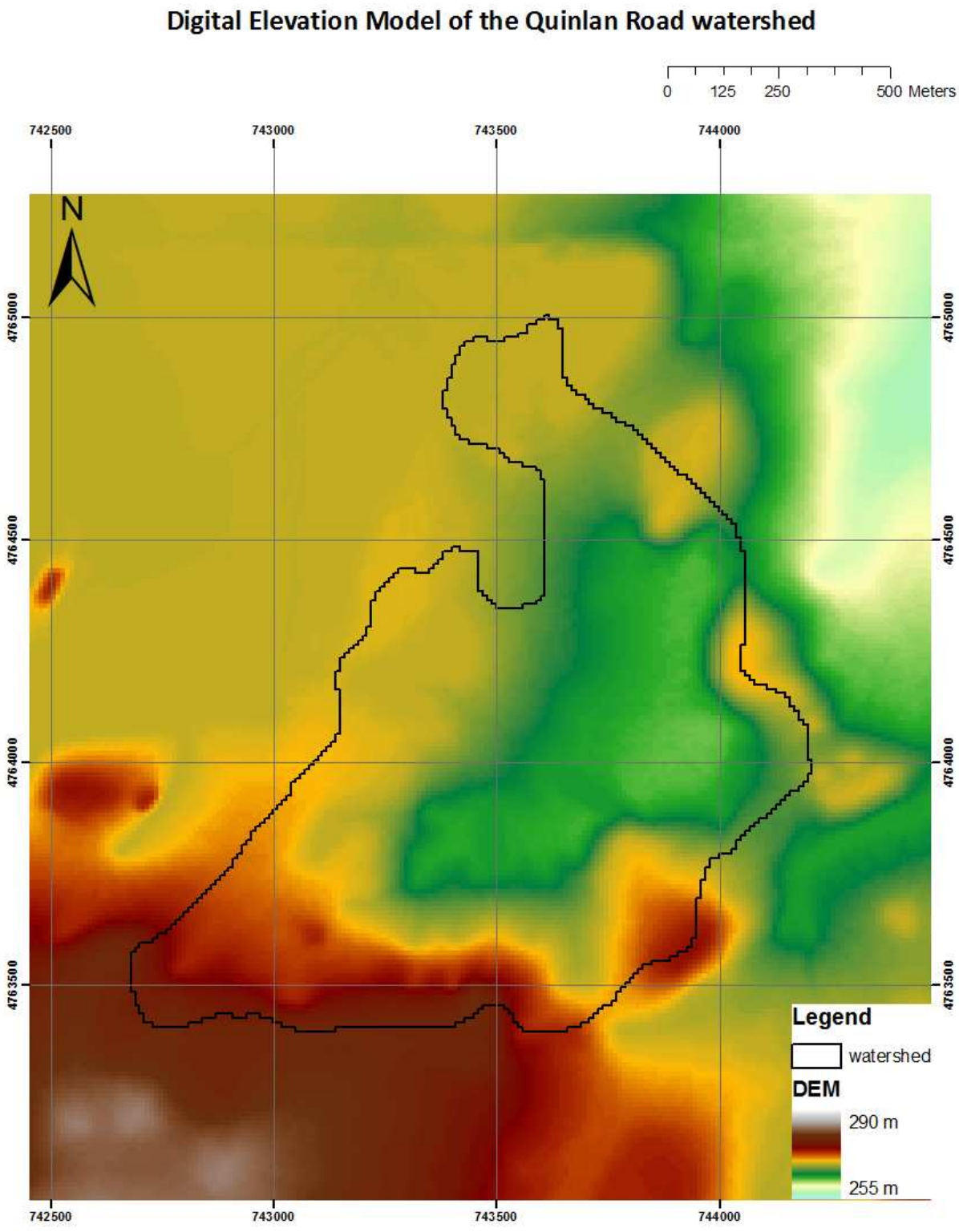
Digital Elevation Model of the Quinlan Road watershed
0
125
250
500 Meters
742500
743000
743500
744000
N
4765000
4764500
4764000
4763500
Legend
watershed
DEM
290 m
255 m

A.3)

Land cover map with Ks measurement locations (Britt Road)

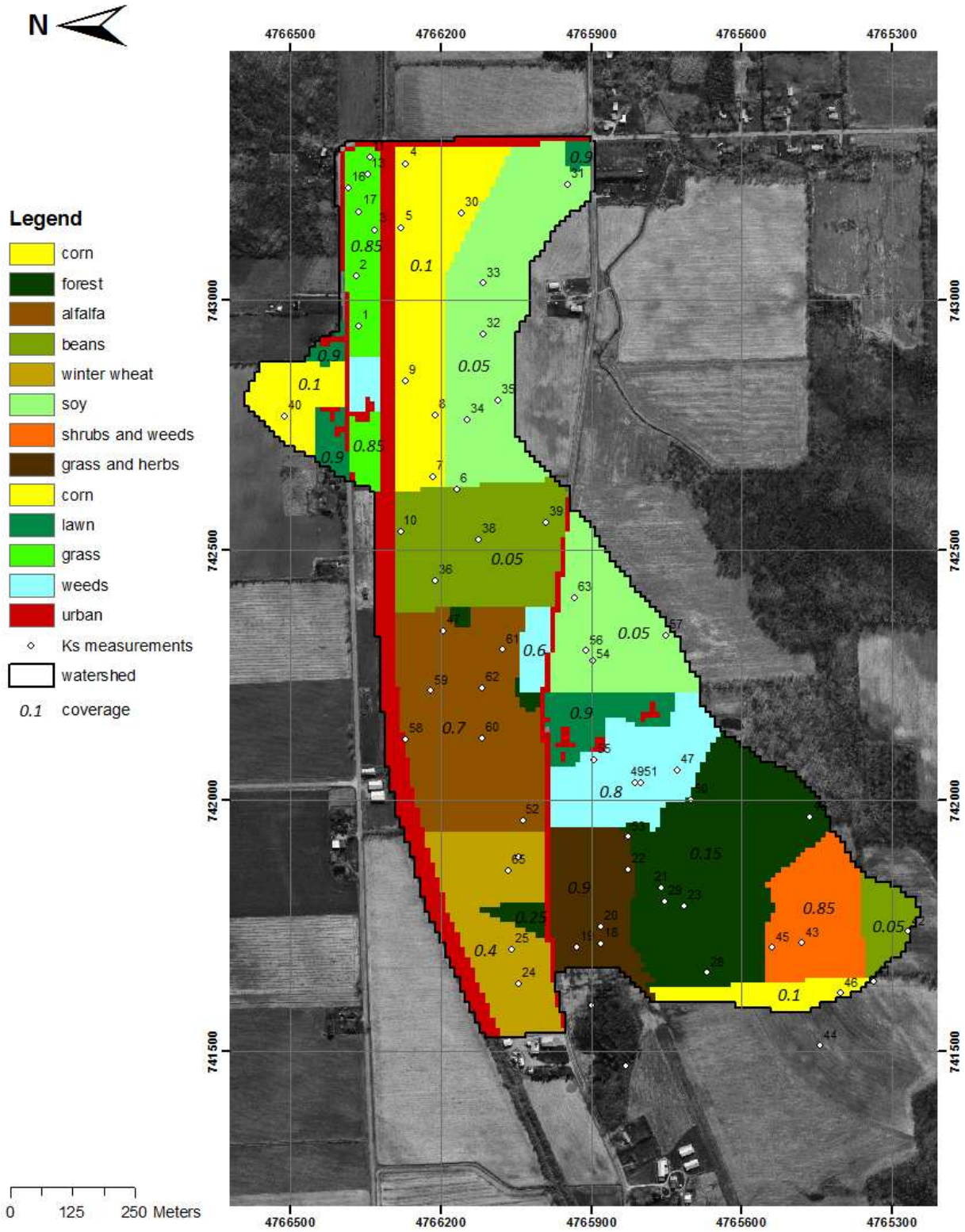

A.4)

Land cover map with Ks measurement locations (Quinlan Road)

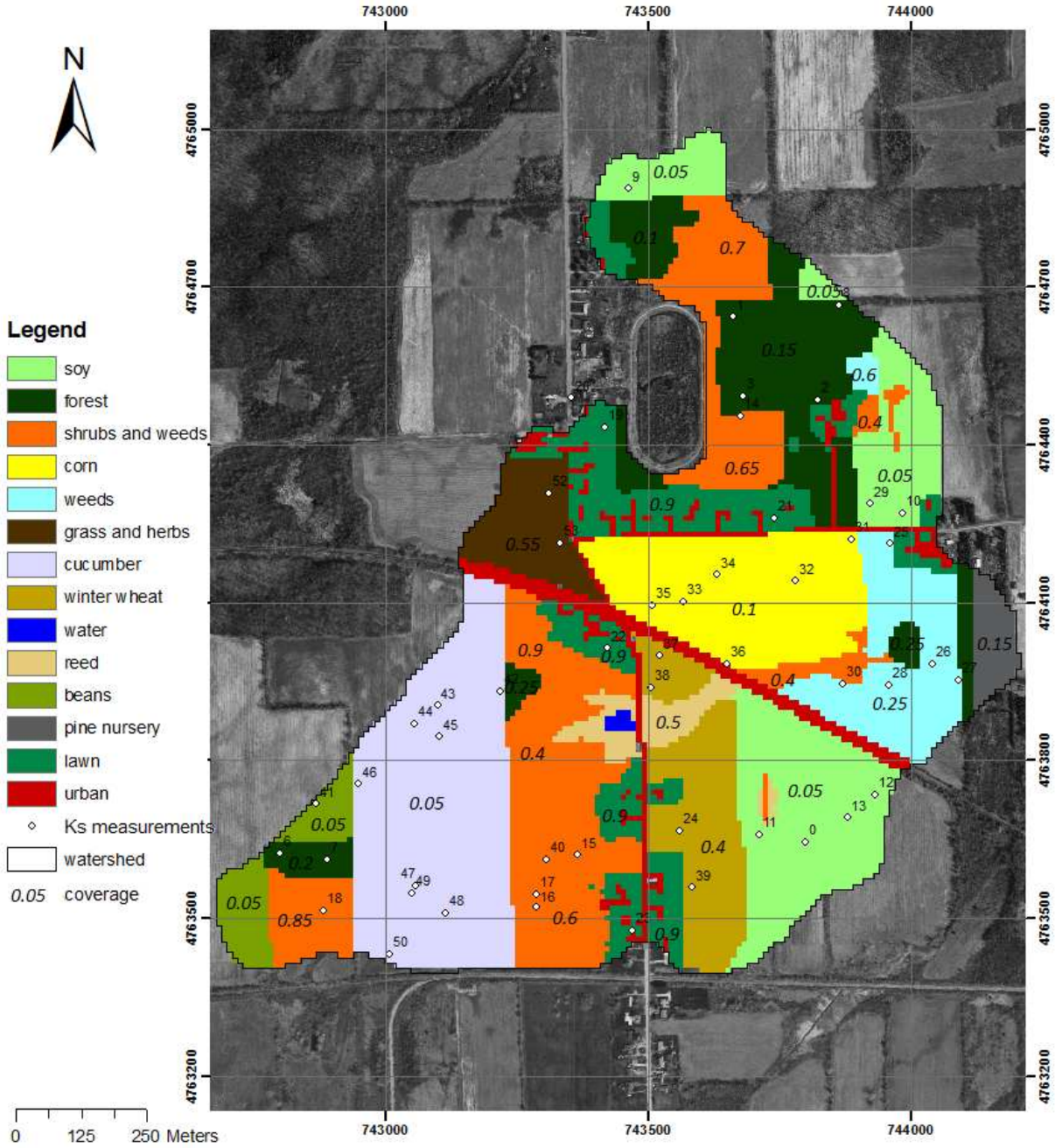

A.5)

Soil map with rock content measurement locations (Britt Road)

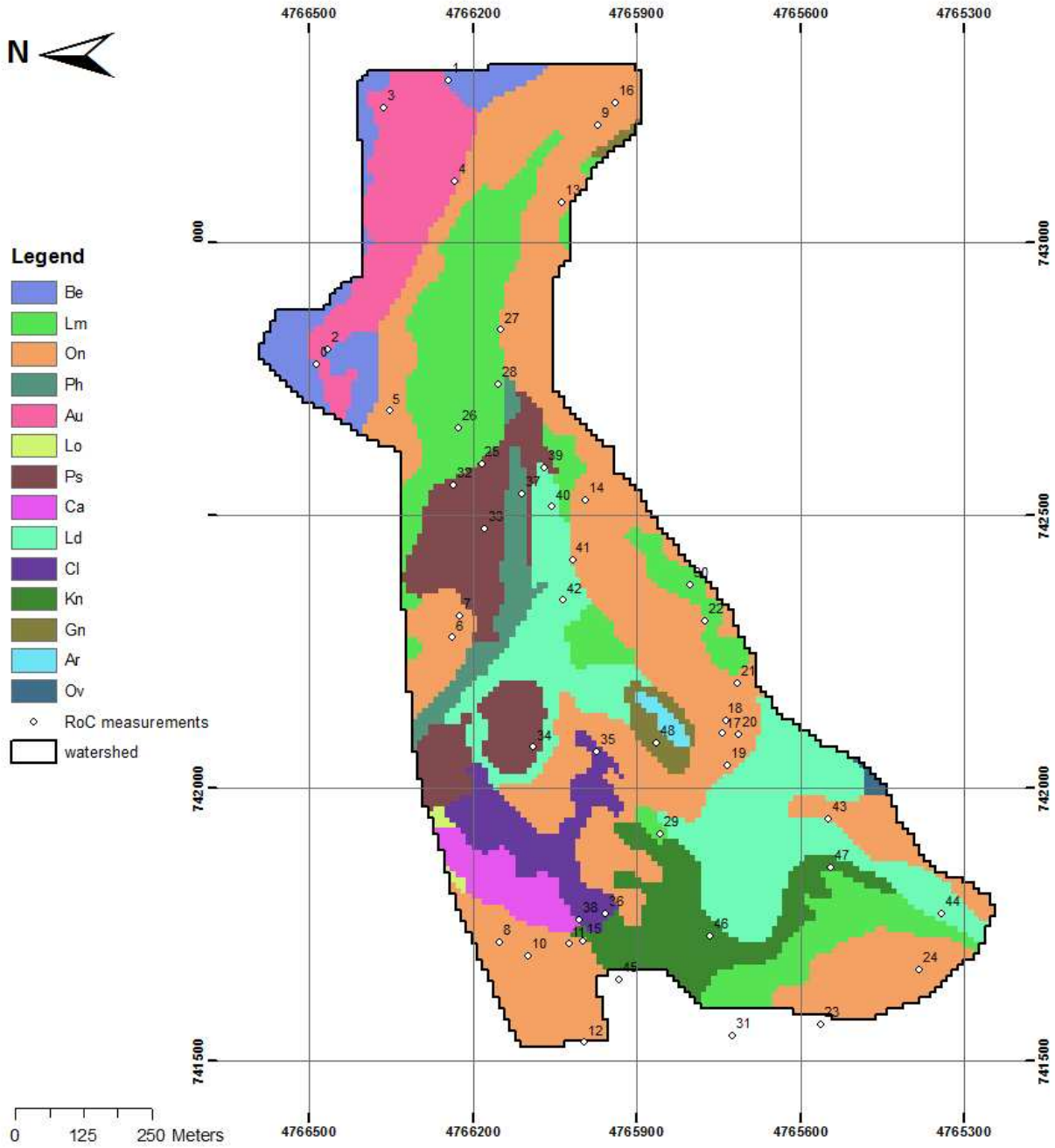

Be	*Benson silt loam*	*Ps*	*Phelps gravelly loam*
Lm	*Lima silt loam*	*Ca*	*Canadaigua silt loam*
On	*Ontario loam*	*Ld*	*Lamson very fine sandy loam*
Ph	*Phelps gravelly silt loam*	*Cl*	*Collamer silt loam*
Au	*Au Gres and Wareham loamy sand*	*Kn*	*Kendaia silt loam*
Lo	*Lyons-Appleton silt loam*	*Gn*	*Galen very fine sandy loam*
Ar	*Arcport very fine sandy loam*	*Ov*	*Ovid silt loam*

A.6)

Soil map with rock content measurement locations (Quinlan Road)

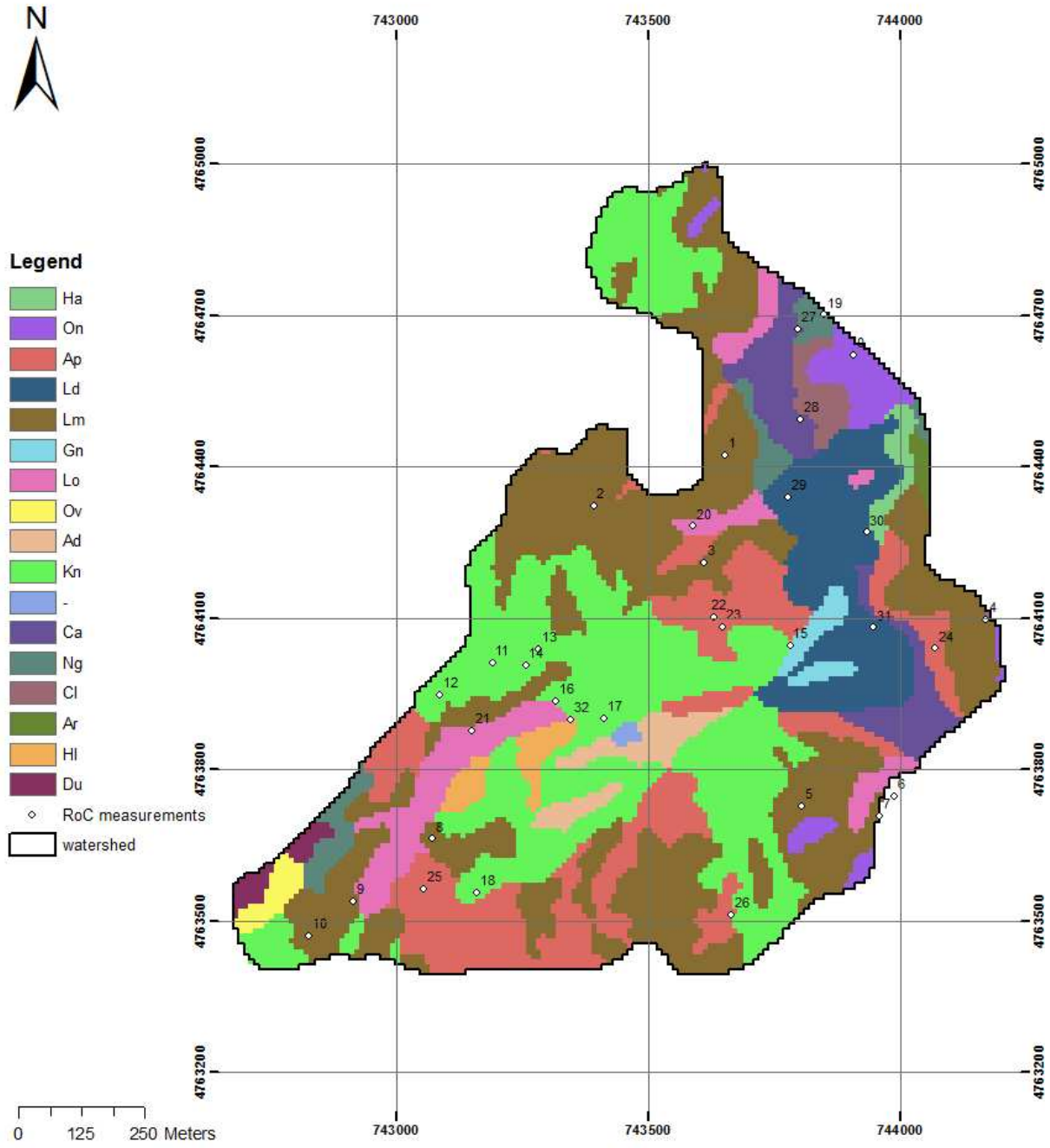

Ha	*Halsey silt loam*	*Ad*	*Alden mucky silt loam*
On	*Ontario loam*	*Kn*	*Kendaia silt loam*
Ap	*Appleton silt loam*	*Ca*	*Canandaigua silt loam*
Ld	*Lamson very fine sandy loam*	*Cl*	*Collamer silt loam*
Lm	*Lima silt loam*	*Ar*	*Arkport very fine sandy loam*
Gn	*Galen very fine sandy loam*	*Hl*	*Hilton loam*
Lo	*Lyons-Appleton silt loam*	*Du*	*Dunkirk silt loam*
Ov	*Ovid silt loam*		

A.7)

Texture map of the Britt Road and Quinlan Road catchments

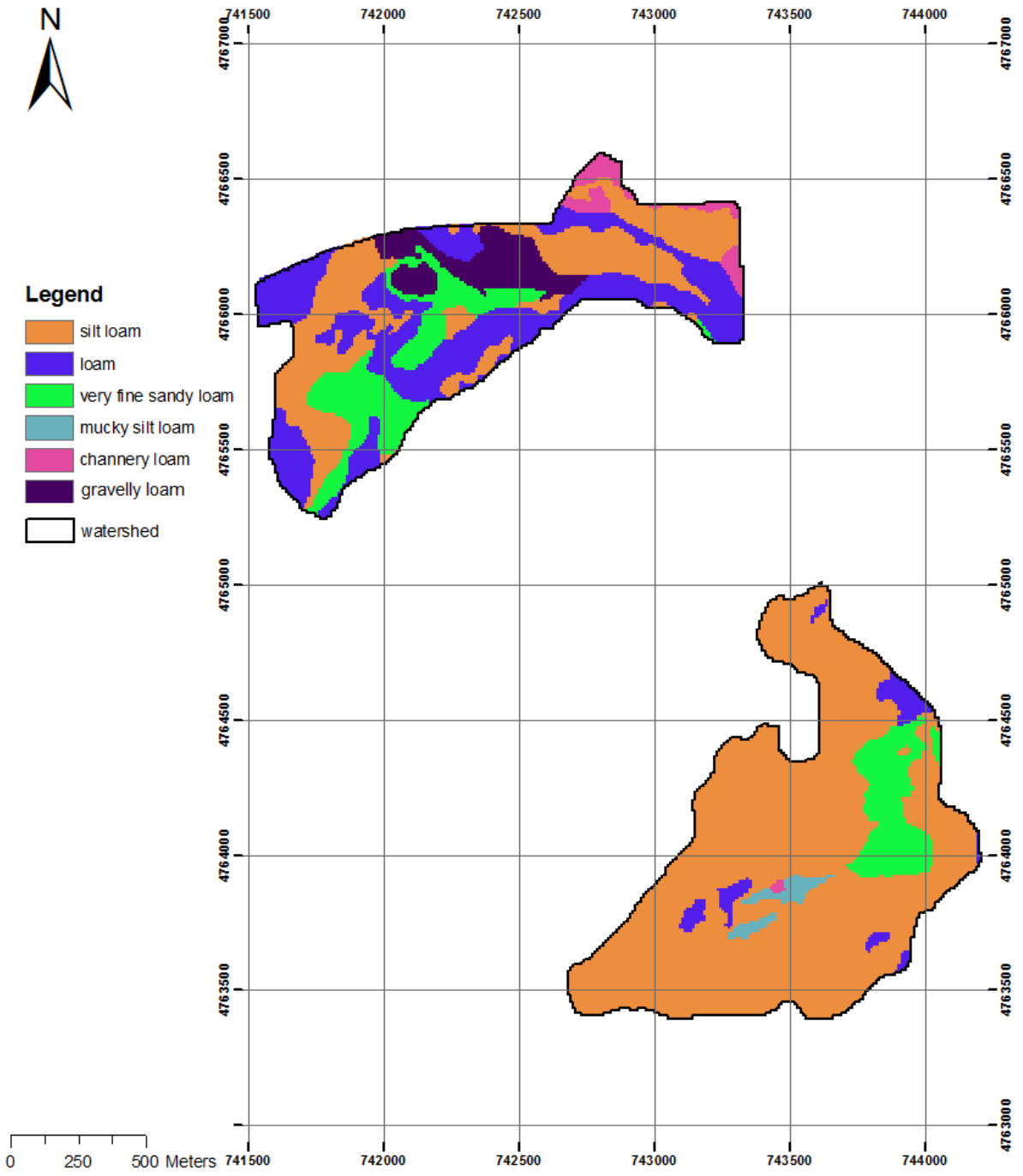

A.8)

Local drain direction network of the Britt Road catchment

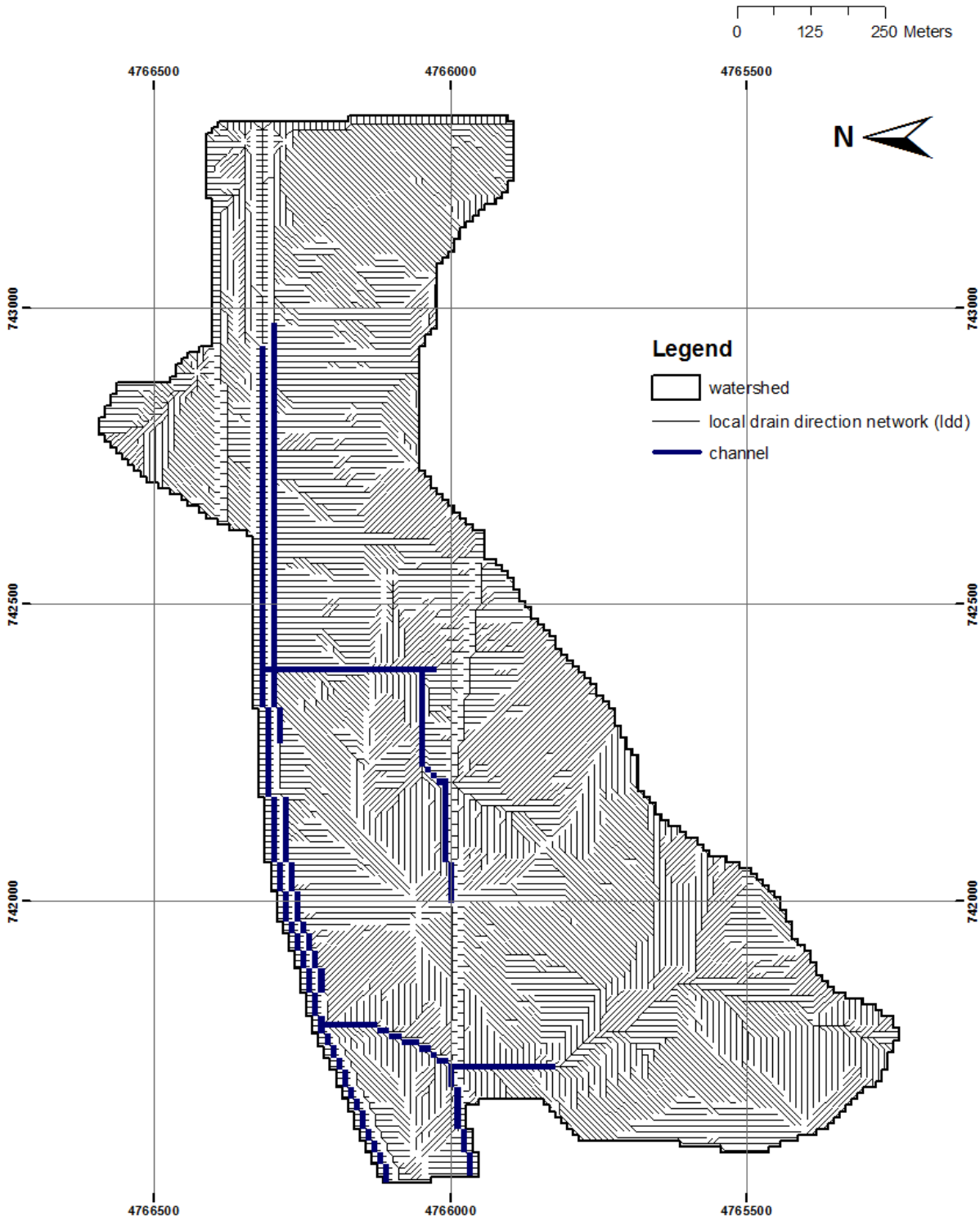

A.9)

Local drain direction network of the Quinlan Road catchment

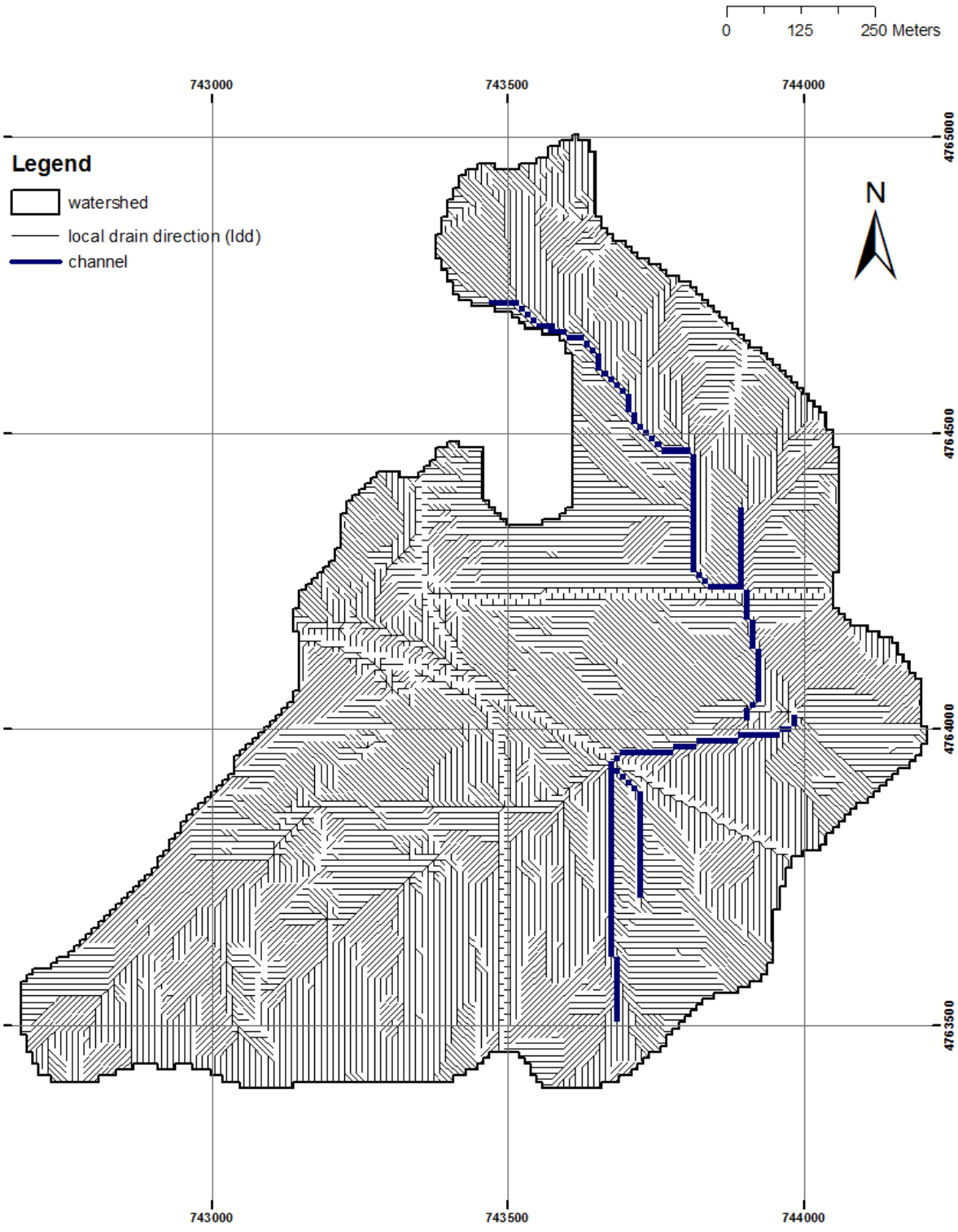

A.10)

Reservoir in the Britt Road railroad

The pictures below display the reservoir in the Britt Road railroad. The photograph (courtesy of Microsoft Windows Live Maps) is taken at a time when the depression was partly filled up with water. The DEM was constructed according to the survey of the depression, and is the basis for the computation of the reservoir volume (which is found to be 46.1 m^3).

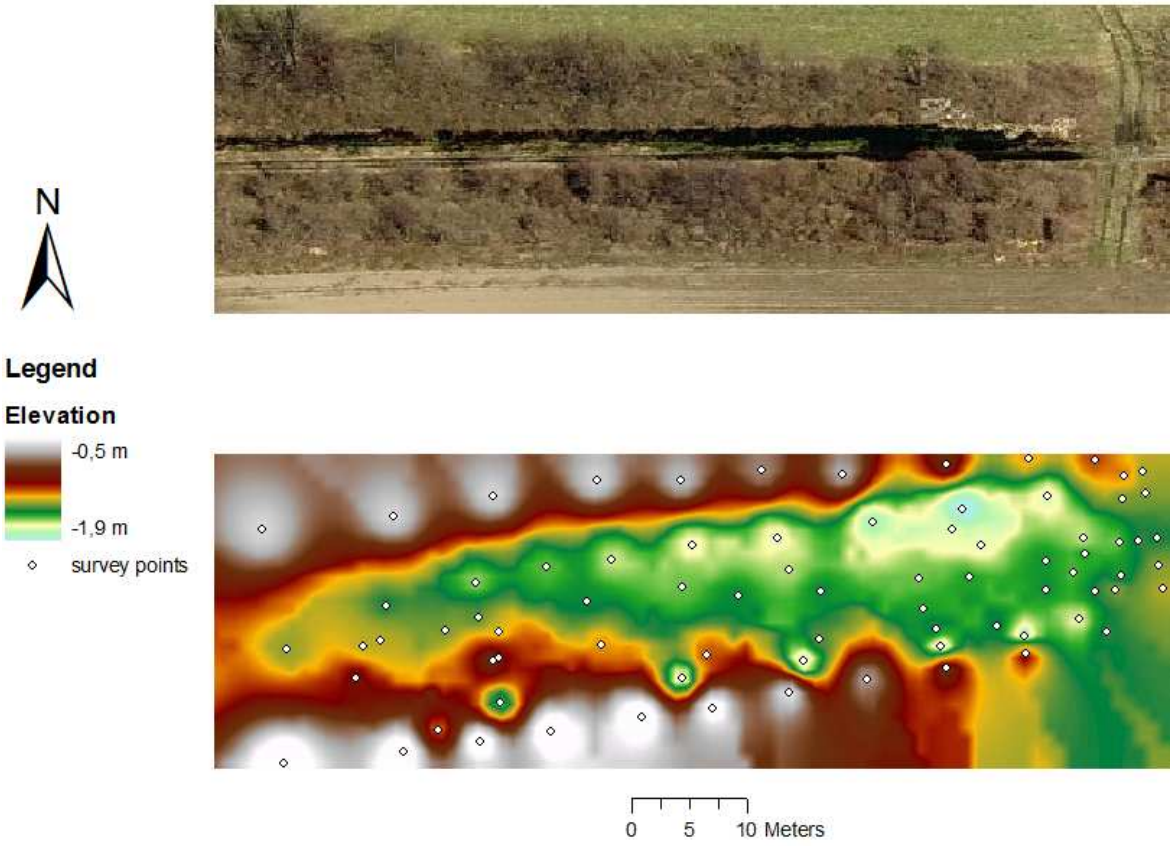

A.11)

Impermeable areas in the Britt Road catchment

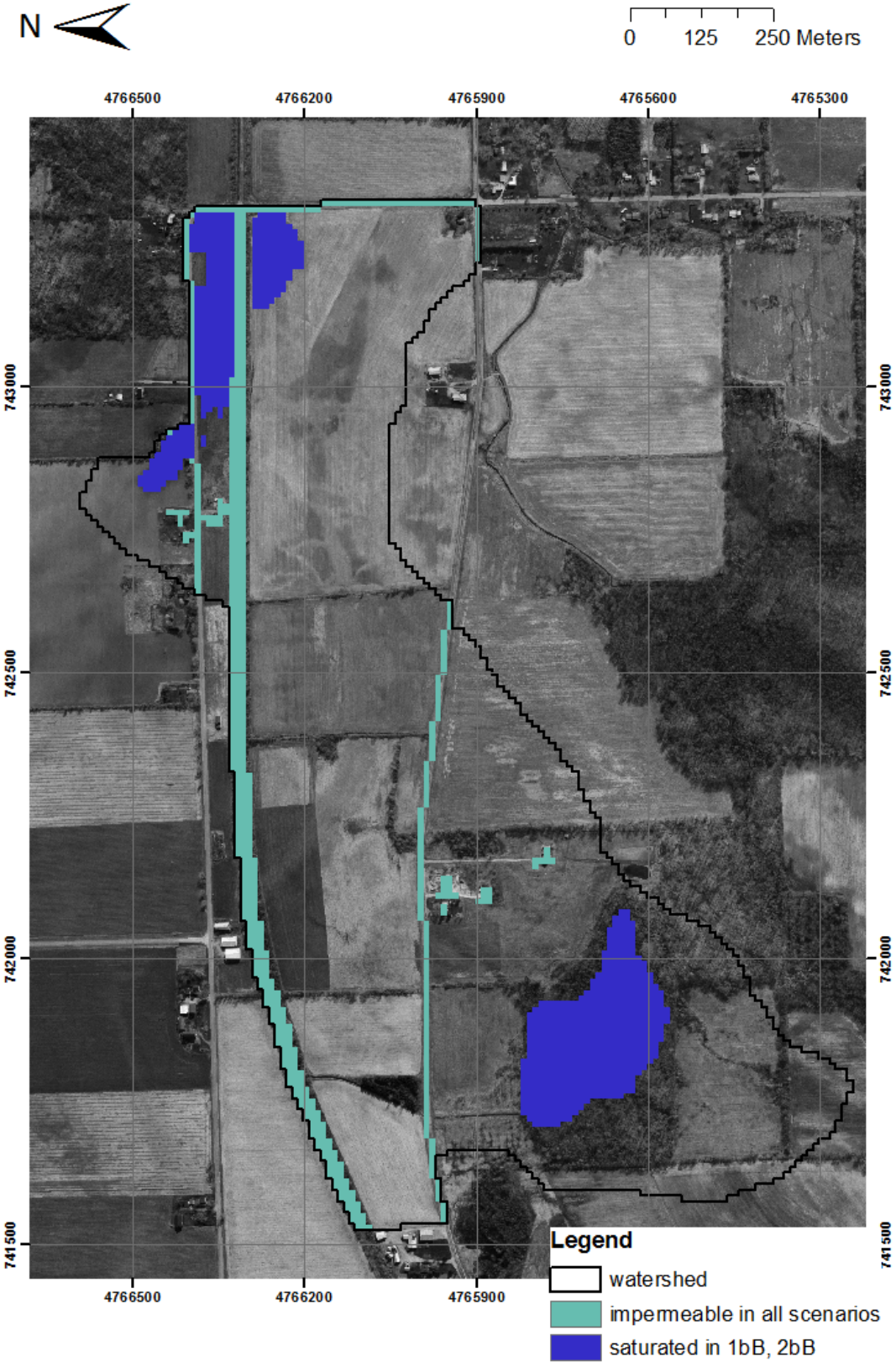

A.12)

Impermeable areas in the Quinlan Road catchment

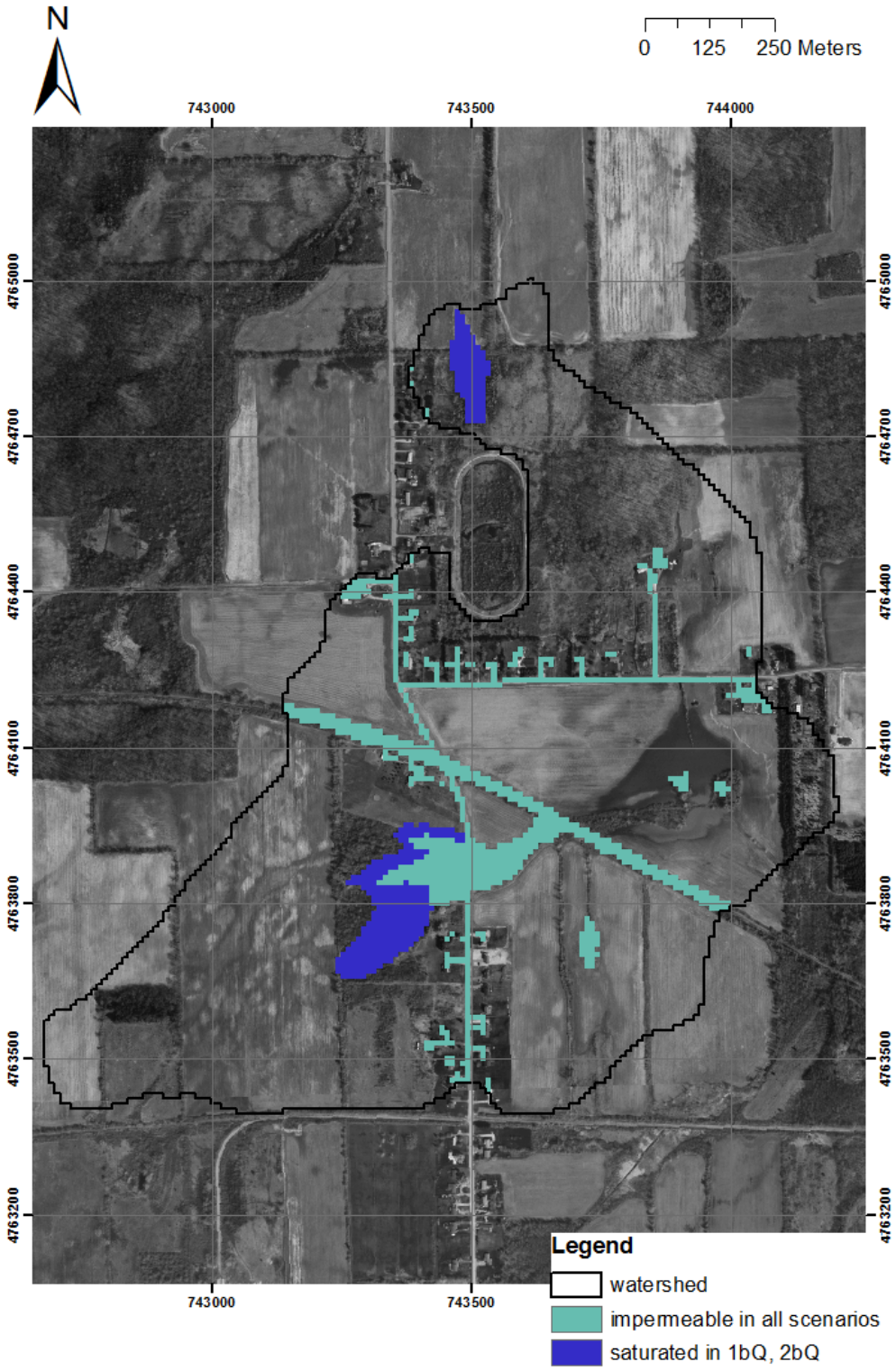

B. Measured values

B.1)

Saturated hydraulic conductivity (Ks)

Britt Road catchment:

id#	x-coordinate	y-coordinate	land cover	texture	K_s(mm/min)
1a	742947	4766365	grass	silt loam	3.3697
1b	742947	4766365	grass	silt loam	0.7878
2a	743047	4766369	grass	silt loam	2.3773
2b	743047	4766369	grass	silt loam	3.4187
3	743139	4766332	grass	silt loam	2.6833
4	743270	4766271	corn	silt loam	0.75
5	743143	4766279	corn	silt loam	1.0814
6a	742621	4766168	beans	silt loam	1.1521
6b	742621	4766168	beans	silt loam	0.0193
7a	742646	4766215	corn	silt loam	0.4008
7b	742646	4766215	corn	silt loam	0.0304
8a	742769	4766210	corn	silt loam	0.835
8b	742769	4766210	corn	silt loam	0.0483
9a	742837	4766272	corn	silt loam	0.0838
9b	742837	4766272	corn	silt loam	0.592
10a	742537	4766281	beans	silt loam	0.0446
10b	742537	4766281	beans	silt loam	0.0398
11a	743283	4766342	grass	silt loam	2.8871
11b	743283	4766342	grass	silt loam	0.9555
13a	743249	4766345	grass	silt loam	2.7886
13b	743249	4766345	grass	silt loam	1.8868
16a	743223	4766384	grass	channery loam	2.7139
16b	743223	4766384	grass	channery loam	1.148
17	743174	4766364	grass	silt loam	0.927
18a	741713	4765881	grass and herbs	silt loam	2.7495
18b	741713	4765881	grass and herbs	silt loam	1.964
19a	741707	4765928	grass and herbs	silt loam	2.1434
19b	741707	4765928	grass and herbs	silt loam	3.1957
20a	741748	4765881	grass and herbs	silt loam	0.6045
20b	741748	4765881	grass and herbs	silt loam	0.595
21a	741825	4765759	swamp forest	very fine sandy loam	3.1017
21b	741825	4765759	swamp forest	very fine sandy loam	5.7251
22a	741862	4765826	grass and herbs	silt loam	2.7357
22b	741862	4765826	grass and herbs	silt loam	1.4506

23a	741789	4765714	swamp forest	very fine sandy loam	4.0657
23b	741789	4765714	swamp forest	very fine silt loam	0.069
24a	741633	4766046	winter wheat	loam	0.9348
24b	741633	4766046	winter wheat	loam	0.0936
25a	741701	4766059	winter wheat	loam	0.0687
25b	741701	4766059	winter wheat	loam	0.0358
28a	741655	4765669	forest	silt loam	1.1803
28b	741655	4765669	forest	silt loam	4.0540
29b	741798	4765753	swamp forest	very fine silty loam	5.9227
30a	743173	4766159	corn	loam	0.1233
30b	743173	4766159	corn	loam	0.5174
31a	743230	4765946	soy	loam	1.0712
31b	743230	4765946	soy	loam	0.1945
32a	742931	4766115	soy	loam	0.0688
32b	742931	4766115	soy	loam	0.1128
33a	743032	4766116	soy	silt loam	2.8318
33b	743032	4766116	soy	silt loam	1.2609
34a	742759	4766147	soy	silt loam	0.1049
34b	742759	4766147	soy	silt loam	0.0656
35a	742798	4766086	soy	loam	2.4574
35b	742798	4766086	soy	loam	3.3858
36a	742438	4766212	beans	gravelly loam	0.0561
36b	742438	4766212	beans	gravelly loam	0.0079
37a	742337	4766196	hay	gravelly loam	0.0478
37b	742337	4766196	hay	gravelly loam	0.117
38a	742521	4766125	beans	gravelly loam	0.561
38b	742521	4766125	beans	gravelly loam	1.3722
39a	742555	4765991	beans	loam	3.3706
39b	742555	4765991	beans	loam	1.0094
40a	742766	4766512	corn	channery loam	0.0361
40b	742766	4766512	corn	channery loam	0.2983
41a	741637	4765335	corn	loam	0.091
41b	741637	4765335	corn	loam	0.6105
42a	741737	4765267	beans	very fine sandy loam	0.652
42b	741737	4765267	beans	very fine sandy loam	0.7624
43a	741714	4765480	shrubs and wheeds	loam	2.9533
43b	741714	4765480	shrubs and wheeds	loam	2.0633
44a	741509	4765443	corn	loam	0.1387
44b	741509	4765443	corn	loam	0.5175
45a	741705	4765538	shrubs and wheeds	silt loam	2.4695
45b	741705	4765538	shrubs and wheeds	silt loam	0.8602
46a	741614	4765401	corn	loam	0.5061
46b	741614	4765401	corn	loam	0.1334

47a	742059	4765729	weeds	loam	0.7731
47b	742059	4765729	weeds	loam	2.7906
48a	741967	4765464	forest	loam	1.4963
48b	741967	4765464	forest	loam	0.1522
49a	742034	4765813	weeds	very fine sandy loam	0.5946
49b	742034	4765813	weeds	very fine sandy loam	1.3483
50a	742000	4765701	swamp forest	very fine sandy loam	6.9878
50b	742000	4765701	swamp forest	very fine sandy loam	7.843
51a	742034	4765801	wheeds	loam	0.0718
51b	742034	4765801	wheeds	loam	0.0846
52a	741959	4766037	hay	loam	0.0605
52b	741959	4766037	hay	loam	0.2856
53a	741926	4765826	grass and herbs	very fine sandy loam	0.0465
53b	741926	4765826	grass and herbs	very fine sandy loam	0.0391
54a	742279	4765897	soy	loam	2.3818
54b	742279	4765897	soy	loam	2.6636
55a	742081	4765895	wheeds	loam	0.0603
55b	742081	4765895	wheeds	loam	0.277
56a	742298	4765911	soy	loam	3.3594
56b	742298	4765911	soy	loam	1.3574
57a	742328	4765751	soy	silt loam	0.2468
57b	742328	4765751	soy	silt loam	0.1102
58a	742122	4766271	hay	gravelly loam	0.3975
58b	742122	4766271	hay	gravelly loam	0.3205
59a	742218	4766221	hay	loam	0.8185
59b	742218	4766221	hay	loam	0.4003
60a	742123	4766117	hay	gravelly loam	0.8507
60b	742123	4766117	hay	gravelly loam	0.1815
61a	742300	4766077	hay	very fine sandy loam	0.0208
61b	742300	4766077	hay	very fine sandy loam	0.0644
62a	742223	4766118	hay	very fine sandy loam	0.4454
62b	742223	4766118	hay	very fine sandy loam	0.0778
63a	742404	4765933	soy	loam	0.6046
63b	742404	4765933	soy	loam	0.0646
64a	741886	4766044	winter wheat	silt loam	0.0423
64b	741886	4766044	winter wheat	silt loam	0.1867
65a	741859	4766065	winter wheat	silt loam	0.0232
65b	741859	4766065	winter wheat	silt loam	0.0572

Quinlan Road catchment:

id#	x	y	landcover	texture	K_s (mm/min)
0a	743799	4763644	soy	loam	0.4388
0b	743799	4763644	soy	loam	0.1002
2a	743823	4764485	forest	silt loam	2.9243
3a	743680	4764493	forest	silt loam	2.0107
3b	743680	4764493	forest	silt loam	4.8583
6a	742800	4763623	forest	silt loam	2.6056
6b	742800	4763623	forest	silt loam	4.2465
7a	742889	4763612	forest	silt loam	5.6603
7b	742889	4763612	forest	silt loam	6.1983
8b	743863	4764665	forest	silt loam	5.7111
9a	743462	4764887	soy	silt loam	0.6424
9b	743462	4764887	soy	silt loam	0.2056
10a	743983	4764270	soy	silt loam	0.0698
10b	743983	4764270	soy	silt loam	0.0185
11a	743712	4763658	soy	silt loam	0.3814
11b	743712	4763658	soy	silt loam	1.4572
12a	743931	4763735	soy	silt loam	0.112
12b	743931	4763735	soy	silt loam	0.675
13a	743879	4763691	soy	silt loam	0.0585
13b	743879	4763691	soy	silt loam	0.0569
14a	743676	4764440	weeds and shrubs	silt loam	3.5294
14b	743676	4764440	weeds and shrubs	silt loam	3.2487
15a	743366	4763620	weeds and shrubs	silt loam	4.7981
15b	743366	4763620	weeds and shrubs	silt loam	0.5716
16a	743288	4763522	weeds and shrubs	silt loam	9.0744
16b	743288	4763522	weeds and shrubs	silt loam	7.8947
17a	743288	4763546	weeds and shrubs	silt loam	3.4108
17b	743288	4763546	weeds and shrubs	silt loam	1.5346
18a	742882	4763514	weeds and shrubs	silt loam	0.9652
18b	742882	4763514	weeds and shrubs	silt loam	1.196
19a	743418	4764434	lawns	silt loam	0.7688
19b	743418	4764434	lawns	silt loam	0.4654
20a	743354	4764489	lawns	silt loam	0.3699
20b	743354	4764489	lawns	silt loam	0.157398
21a	743739	4764261	lawns	silt loam	0.6837
21b	743739	4764261	lawns	silt loam	0.2268
22a	743422	4764013	lawns	silt loam	0.0718
22b	743422	4764013	lawns	silt loam	0.22
23a	743469	4763477	lawns	silt loam	0.9677
23b	743469	4763477	lawns	silt loam	0.449
24a	743559	4763666	lawns	silt loam	0.8065

24b	743559	4763666	lawns	silt loam	0.2741
25a	743959	4764212	weeds	silt loam	2.2304
25b	743959	4764212	weeds	silt loam	0.2348
26a	744040	4763983	weeds	silt loam	0.0111
26b	744040	4763983	weeds	silt loam	0.0184
27a	744090	4763952	weeds	silt loam	0.0247
27b	744090	4763952	weeds	silt loam	0.0305
28a	743957	4763943	weeds	very fine sandy loam	0.027195
28b	743957	4763943	weeds	very fine sandy loam	0.017778
29a	743923	4764288	soy	very fine sandy loam	0.2637
29b	743923	4764288	soy	very fine sandy loam	1.1962
30a	743869	4763946	weeds and shrubs	very fine sandy loam	4.2055
30b	743869	4763946	weeds and shrubs	very fine sandy loam	2.189781
31a	743887	4764221	corn	very fine sandy loam	0.6059
31b	743887	4764221	corn	very fine sandy loam	0.050884
32a	743780	4764141	corn	very fine sandy loam	0.383834
32b	743780	4764141	corn	very fine sandy loam	0.07954
33a	743567	4764102	corn	silt loam	0.9263
33b	743567	4764102	corn	silt loam	1.1751
34a	743631	4764153	corn	silt loam	0.7941
34b	743631	4764153	corn	silt loam	0.260531
35a	743507	4764095	corn	silt loam	0.049311
35b	743507	4764095	corn	silt loam	0.051756
36a	743649	4763994	corn	silt loam	0.043025
36b	743649	4763994	corn	silt loam	0.034451
37a	743521	4763999	winter wheat	silt loam	0.045766
37b	743521	4763999	winter wheat	silt loam	0.183527
38a	743506	4763939	winter wheat	silt loam	0.019362
38b	743506	4763939	winter wheat	silt loam	0.031377
39a	743584	4763558	winter wheat	silt loam	0.110912
39b	743584	4763558	winter wheat	silt loam	0.089343
40a	743306	4763611	weeds and shrubs	very fine sandy loam	3.8236
40b	743306	4763611	weeds and shrubs	very fine sandy loam	6.4419
41a	742867	4763717	beans	silt loam	0.051213
41b	742867	4763717	beans	silt loam	1.2119
42a	743219	4763931	cucumber	silt loam	1.5909
42b	743219	4763931	cucumber	silt loam	0.2425
43a	743099	4763904	cucumber	silt loam	1.5635
43b	743099	4763904	cucumber	silt loam	1.3048
44a	743055	4763869	cucumber	silt loam	0.046844
44b	743055	4763869	cucumber	silt loam	1.2453
45a	743103	4763845	cucumber	silt loam	0.2839
45b	743103	4763845	cucumber	silt loam	0.179809

46a	742949	4763755	cucumber	silt loam	0.073804
46b	742949	4763755	cucumber	silt loam	0.205692
47a	743057	4763562	cucumber	silt loam	0.380469
47b	743057	4763562	cucumber	silt loam	0.254023
48a	743114	4763510	cucumber	silt loam	0.083311
48b	743114	4763510	cucumber	silt loam	0.163443
49a	743051	4763548	cucumber	silt loam	0.6687
49b	743051	4763548	cucumber	silt loam	0.497275
50a	743008	4763431	cucumber	silt loam	0.5648
50b	743008	4763431	cucumber	silt loam	0.2465
52a	743311	4764308	grass and herbs	silt loam	0.265896
52b	743311	4764308	grass and herbs	silt loam	0.7545
53a	743333	4764214	grass and herbs	silt loam	0.095335
53b	743333	4764214	grass and herbs	silt loam	0.6735

B.2)

Volumetric rock content (ROC)

Values for both catchments are combined and averaged to obtain the definitive ROC input values (Table 5.4).

Britt road catchment:

Soil	Sample ID	Average measured RoC value	Literature value (2mm sieve)	RoC value (-)
Ha			0.25	0.25
On	0	0.0884		0.0884
Ap	22-26	0.0322		0.0322
Ld	29-31	0.0263		0.0263
Lm	1-10	0.0229		0.0229
Gn			0	0
Lo	20,21	0		0
Ov				0.125
Ad			0.05	0.05
Kn	11-18	0.0337		0.0337
Ca	27,28	0.0175		0.0175
Ng	19	0		0
Cl				0.075
Ar			0	0
Hl	32	0		0
Du			0.025	0.025

Quinlan Road catchment:

Soil	Sample ID	Average measured RoC value	Literature value (2mm sieve)	RoC value
On	5-24	0.0385		0.0385
Lm	25-31	0.0942		0.0942
Ld	39-44	0.0110		0.0110
Kn	45-34	0		0
Ph	37	0.2088		0.2088
Ps	32-34	0.0719		0.0719
Be	0,1	0.4217		0.4217
Au	2-4	0.1829		0.1829
Ca	38	0		0
Cl	35,36	0.0107		0.0107
Gn	48	0		0
Lo			0	0
Ar			0	0
Ov			0.125	0.125

B.3) Sinkhole water level and climate data

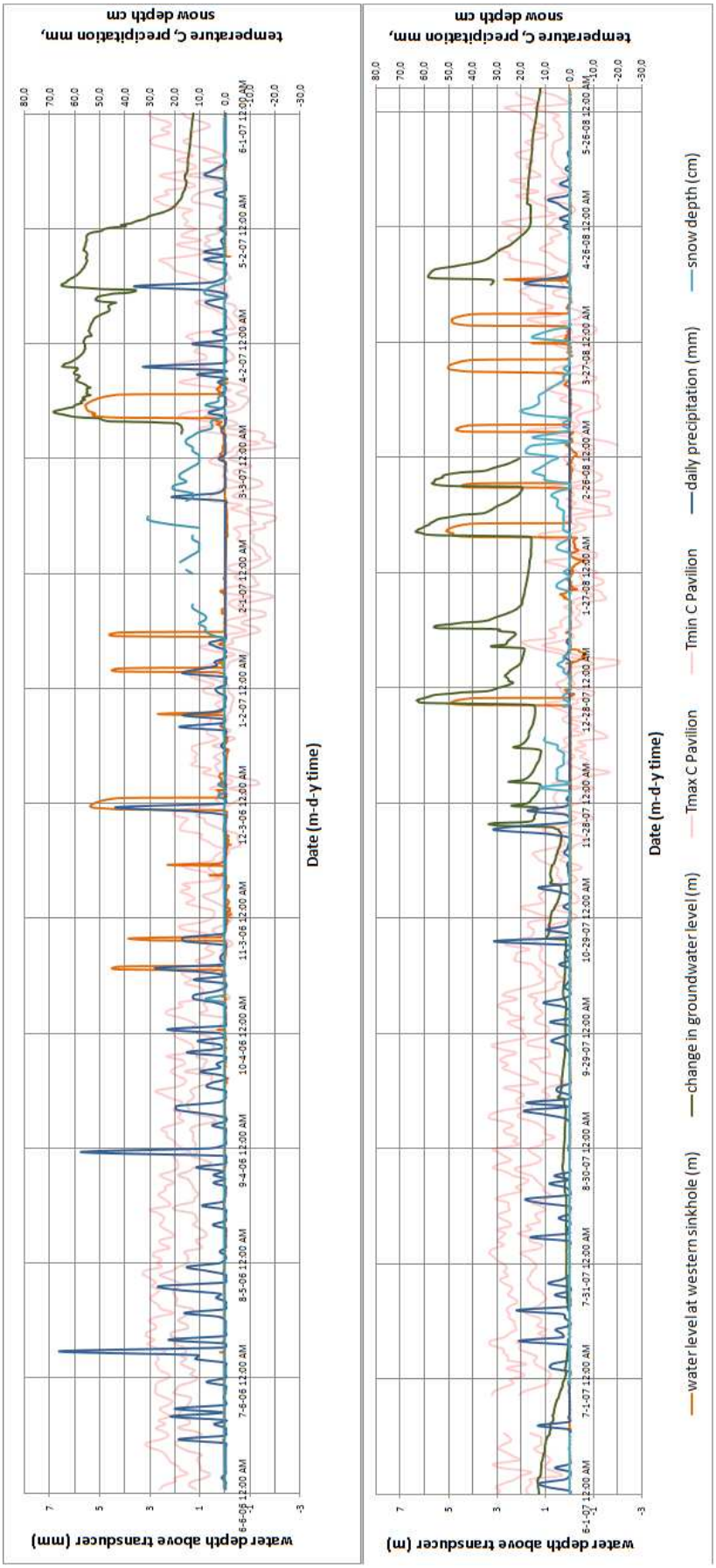

C. Statistics

C.1)

Normality check Ks

The Kolmogorov-Smirnov test was performed on the untransformed K_s data, to test whether the data fits a normal distribution. The resulting D-statistic was compared to a tabulated critical value.

Sample size	213				
D-statistic	0,23864				
P-value	4,0800E-11				
α	0,2	*0,1*	*0,05*	*0,02*	*0,01*
Critical value	0,07352	0,0838	0,09305	0,10401	0,11162
Reject?	Yes	Yes	Yes	Yes	Yes

The hypothesis that the data fits a normal distribution was rejected for all signifance levels. After ln-transformation, the following results were obtained:

Sample size	213				
D-statistic	0,07368				
P-value	0,18825				
α	**0,2**	***0,1***	***0,05***	***0,02***	***0,01***
Critical value	0,07352	0,0838	0,09305	0,10401	0,11162
Reject?	**Yes**	**No**	**No**	**No**	**No**

Thus, the ln-transformed data was used in favour of the untransformed data. The following graph visualizes the fit of the transformed Ks data to a normal distribution with σ = 1,6753 and μ = -0,54037.

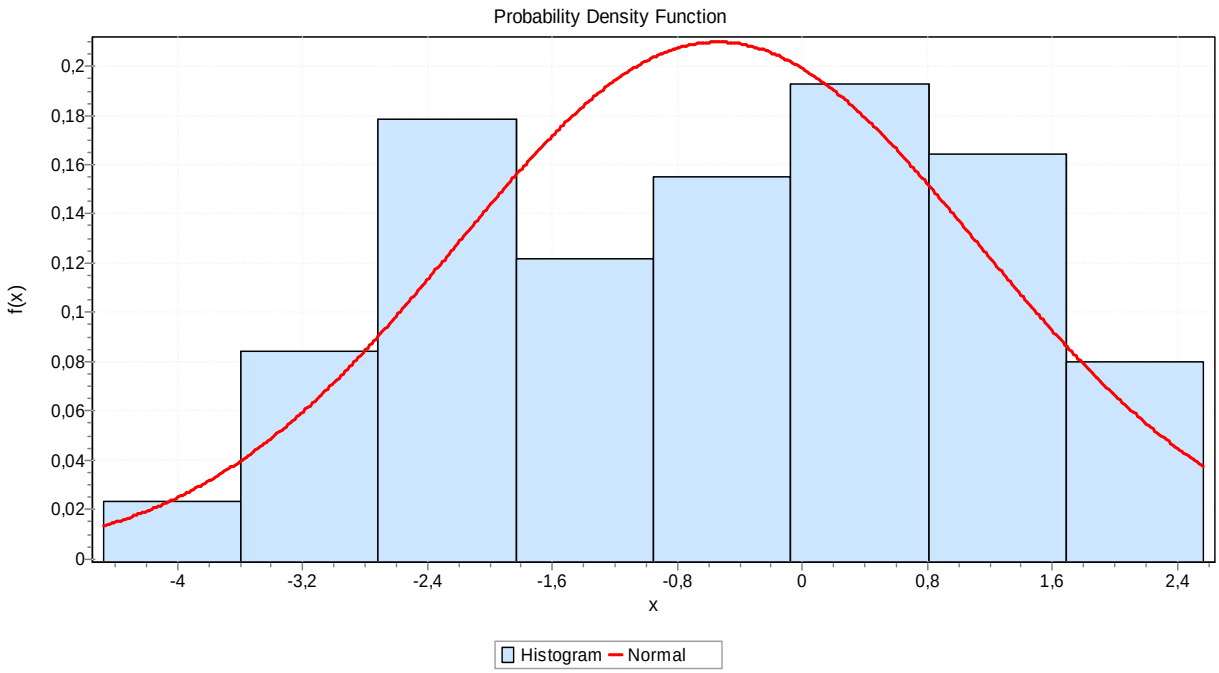

C.2)

Measurement error in K_s

The following table is a list of 10 conductivity measurements randomly selected from the two catchments, and the standard error of fit (e) found through the linear regression procedure explained in paragraph 4.4.1. The error was evaluated as a percentage of the K_s value. On average it was found to be negligibly small.

Britt Road			
id	**K_s (mm/min)**	**e (mm/min)**	**% e/Ks**
25A	0.0687	0.0031	4.512373
49B	1.3483	0.0052	0.385671
6A	1.1521	0.0144	1.249892
9B	0.592	0.0034	0.574324
39B	1.0094	0.0034	0.336834

Quinlan Road			
id	**K_s (mm/min)**	**e (mm/min)**	**% e/Ks**
23A	0.9677	0.0058	0.599359
11B	1.4572	0.039	2.676366
41B	1.2119	0.0089	0.734384
21B	0.2268	0.0064	2.821869
46B	0.2028	0.0033	1.627219
		average	1.551829

C.3)

Reclassification of land cover for Ks

The first step in checking the validity of the initial land use classification was the evaluation of combinations of the classes present in both catchments. Equality of variances was tested with the F-test and the t-test is used to test the equality of means. The table below summarizes the results for all possible class combinations. Acceptance or rejection of the test hypothesis is indicated with a *Y* or *N* respectively. Green boxes indicate the class combinations that were accepted, red boxes indicate the rejection of a combination. In the end, all classes except the *weeds* class were merged.

Q → / B ↓	***beans*** n = 2 X = -1.025 s = 2.237	***corn*** n = 12 X = -1.323 s = 1.333	***forest*** n = 8 X = 1.477 s = 1.400	***grass and herbs*** n = 4 X = -0.723 s = 0.963	***soy*** n = 16 X = -0.763 s = 1.685	***weeds*** n = 8 X = -2.631 s = 1.783	***shrubs and weeds*** n = 12 X = 1.316 s = 0.916	***winter wheat*** n = 6 X = -2.321 s = 0.690
beans n = 12 X = -1.1017 s = 1.994	F: Y t: Y							
corn n = 18 X = -1.0983 s = 1.1476		F: Y t: Y						
forest n = 11 X = 1.588 s = 1.044			F: Y t: Y					
grass and herbs n = 10 X = 0.1306 s = 1.648				F: Y t: Y				
soy n = 18 X = -0.4087 s = 1.4879					F: Y t: Y			
weeds n = 8 X = -0.7164 s = 1.4493						F: N		
shrubs and weeds n = 4 X = 1.0048 s = 0.5471							F: Y t: Y	
winter wheat n = 8 X = -2.1237 s = 1.1643								F: Y t: Y

Combinations of the remaining classes was evaluated, according to the same procedure, in the following tables. The definitive classification, based on both test results and field observations, can be found in Table 5.2 and the following boxplots.

	beans n = 14 X = -1.091 s = 1.937	*corn* n = 30 X = -1.211 s = 1.229	*forest* n = 19 X = 1.541 s = 1.264	*grass and herbs* n = 14 X = -0.113 s = 1.501	*soy* n = 32 X = -0.677 s = 1.497	*shrubs and weeds* n = 18 X = 1.337 s = 0.770
beans n = 14 X = -1.091 s = 1.937		F: N	F: Y t: N	F: Y t: Y	F: Y t: Y	F: N
corn n = 30 X = -1.211 s = 1.229			F: Y t: N	F: Y t: N	F: Y t: Y	F: N
forest n = 19 X = 1.541 s = 1.264				F: Y t: N	F: Y t: N	F: N
grass and herbs n = 14 X = -0.113 s = 1.501					F: Y t: Y	F: N
soy n = 32 X = -0.677 s = 1.497						F: N
shrubs and weeds n = 18 X = 1.337 s = 0.770						

	winter wheat n = 14 X = -2.257 s = 1.015	*cucumber (Q)* n = 18 X = -0.744 s = 1.052	*alfalfa (B)* n = 14 X = -1.369 s = 1.139	*lawn* n = 12 X = -0.654 s = 0.771	*weeds (B)* n = 8 X = -0.716 s = 1.449	*weeds (Q)* n = 8 X = -2.631 s = 1.783	*grass (B)* n = 12 X = 1.014 s = 0.548
beans n = 14 X = -1.091 s = 1.937	F: N	F: N	F: Y t: Y	F: N	F: Y t: Y	F: Y t: Y	F: N
corn n = 30 X = -1.211 s = 1.229	F: Y t: N	F: Y t: Y	F: Y t: Y	F: Y t: Y	F: Y t: Y	F: Y t: N	F: N
forest n = 19 X = 1.541 s = 1.264	F: Y t: N	F: Y t: N	F: Y t: N	F: Y t: N	F: Y t: N	F: Y t: N	F: N
grass and herbs n = 14 X = -0.113 s = 1.501	F: Y t: N	F: Y t: Y	F: Y t: N	F: N	F: Y t: Y	F: Y t: N	F: N
soy n = 32 X = -0.677 s = 1.497	F: Y t: N	F: Y t: Y	F: Y t: Y	F: N	F: Y t: Y	F: Y t: N	F: N
shrubs and weeds n = 18 X = 1.337 s = 0.770	F: Y t: N	F: Y t: N	F: Y t: N	F: Y t: N	F: Y t: N	F: Y t: N	F: Y t: Y

	winter wheat n = 14 X = -2.257 s = 1.015	***cucumber (Q)*** n = 18 X = -0.744 s = 1.052	***alfalfa (B)*** n = 14 X = -1.369 s = 1.139	***lawn*** n = 12 X = -0.654 s = 0.771	***weeds (B)*** n = 8 X = -0.716 s = 1.449	***weeds (Q)*** n = 8 X = -2.631 s = 1.783	***grass (B)*** n = 12 X = 1.014 s = 0.548
winter wheat n = 14 X = -2.257 s = 1.015		**F: Y** **t: N**	**F: Y** **t: N**	**F: Y** **t: N**	**F: Y** **t: N**	**F: Y** **t: Y**	**F: N**
cucumber(Q) n = 18 X = -0.744 s = 1.052			**F: Y** **t: Y**	**F: Y** **t: Y**	**F: Y** **t: Y**	**F: Y** **t: N**	**F: N**
alfalfa (B) n = 14 X = -1.369 s = 1.139				**F: Y** **t: Y**	**F: Y** **t: Y**	**F: Y** **t: Y**	**F: N**
lawn n = 12 X = -0.654 s = 0.771					**F: Y** **t: Y**	**F: Y** **t: N**	**F: Y** **t: N**
weeds (B) n = 8 X = -0.716 s = 1.449						**F: Y** **t: N**	**F: N**
weeds (Q) n = 8 X = -2.631 s = 1.783							**F: N**
grass (B) n = 12 X = 1.014 s = 0.548							

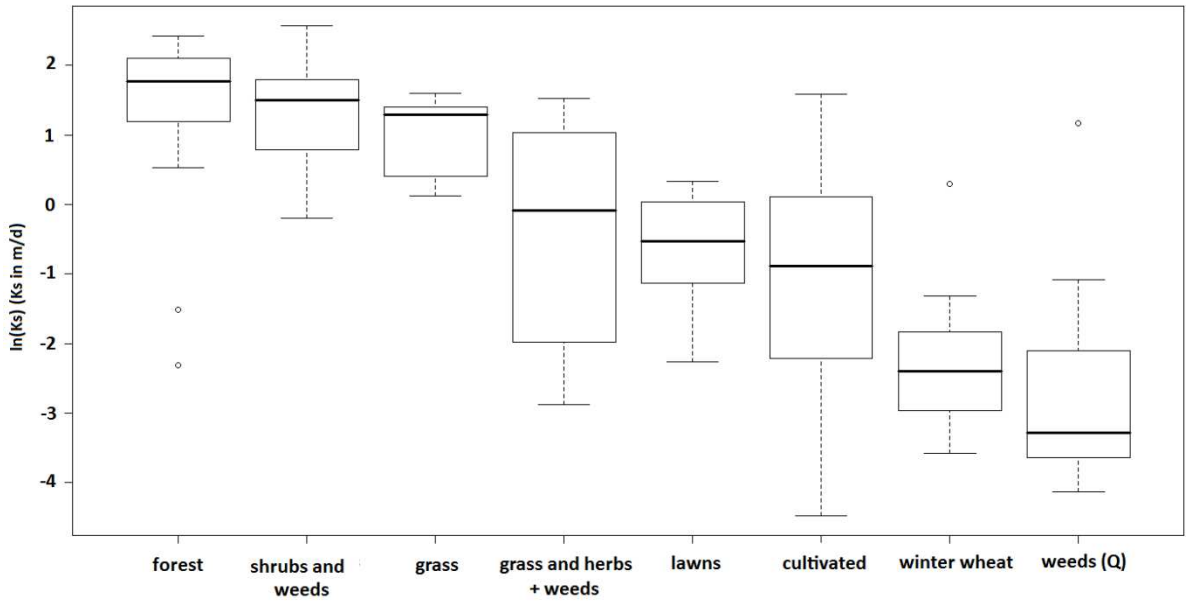

C.4)

The relation between ln(Ks) and ln(B)

The following graph displays the regression line, with confidence interval, on which the generating of *B* values is based.

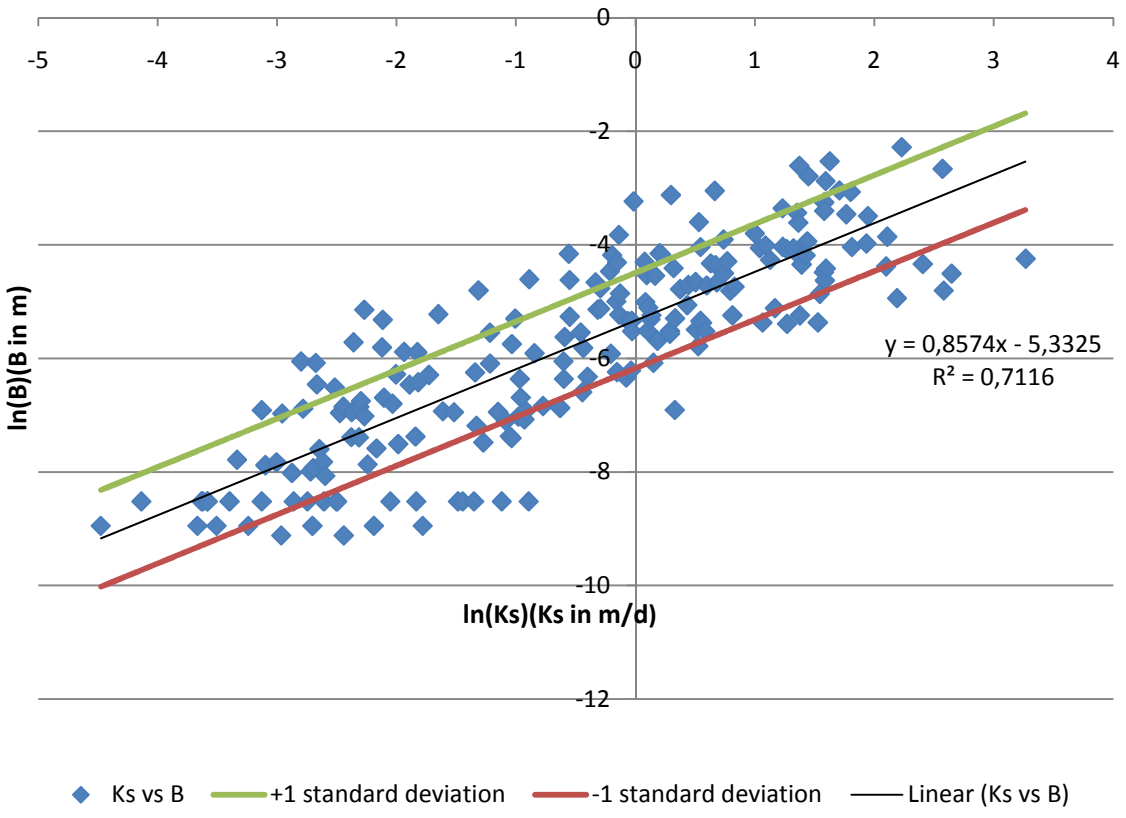

C.5)

The relation between slope and depression storage

The following graphs display the relation between slope and the natural logarithm of the effective depression storage. Presented confidence intervals for the regression lines were obtained from equation 4.1.

For the *forest* class:

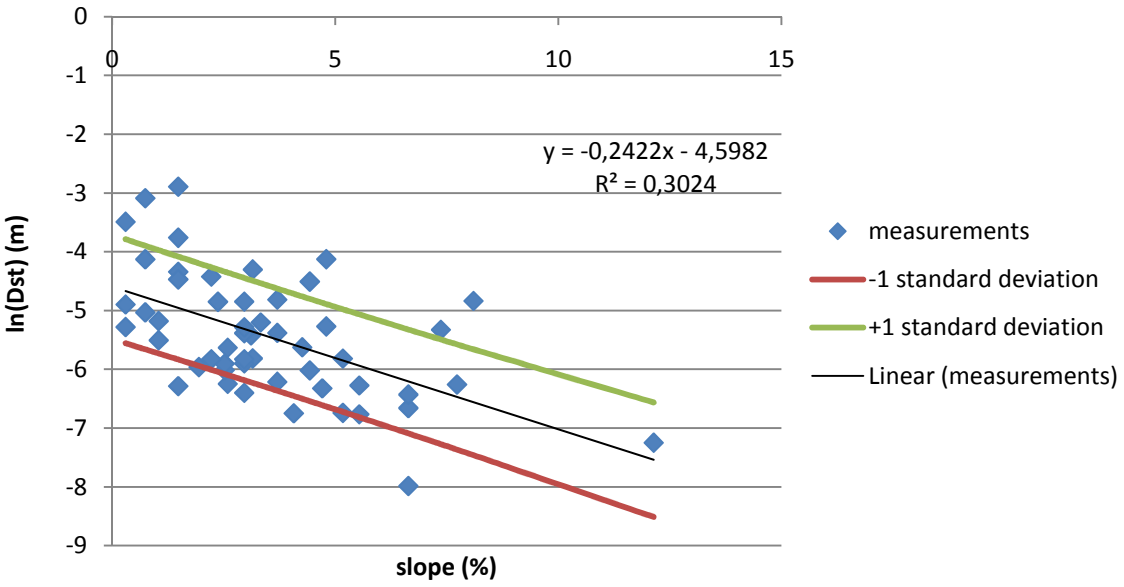

Shrubs and weeds / weeds / grass and herbs:

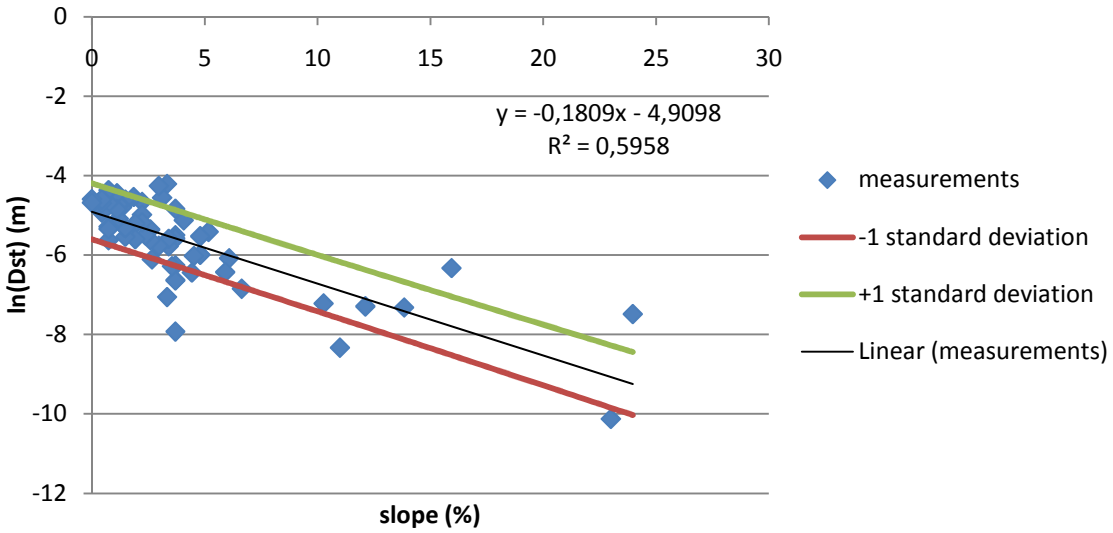

Lawns:

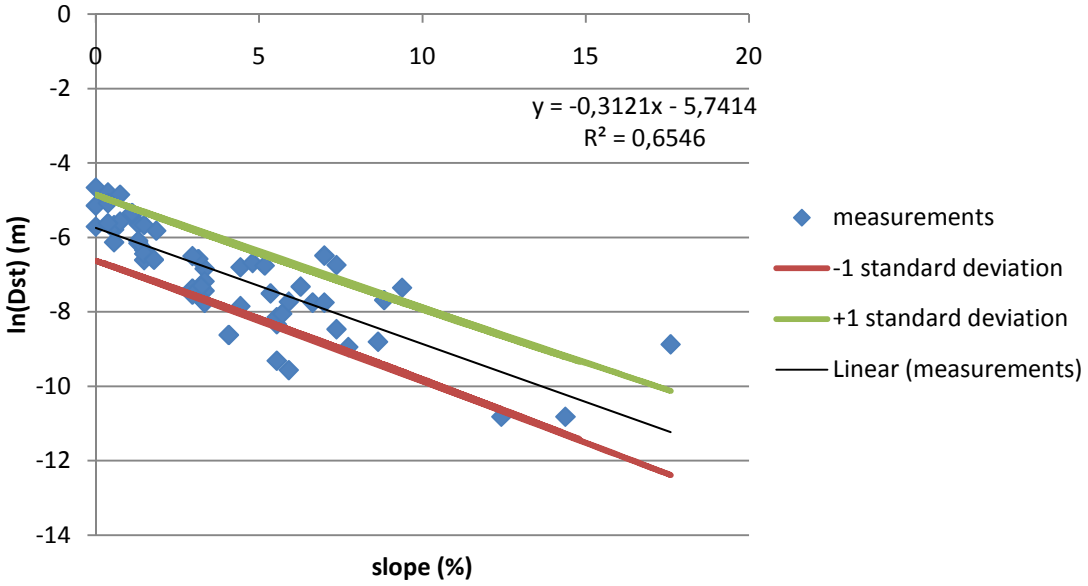

For the *cultivated* land use class no relation was found between slope and depression storage, as shown below. The average of the ln-transformed depression storage (m) is found to be -5.01, with the dataset having a standard deviation of 0.52. Dst values were randomly generated according to this distribution.

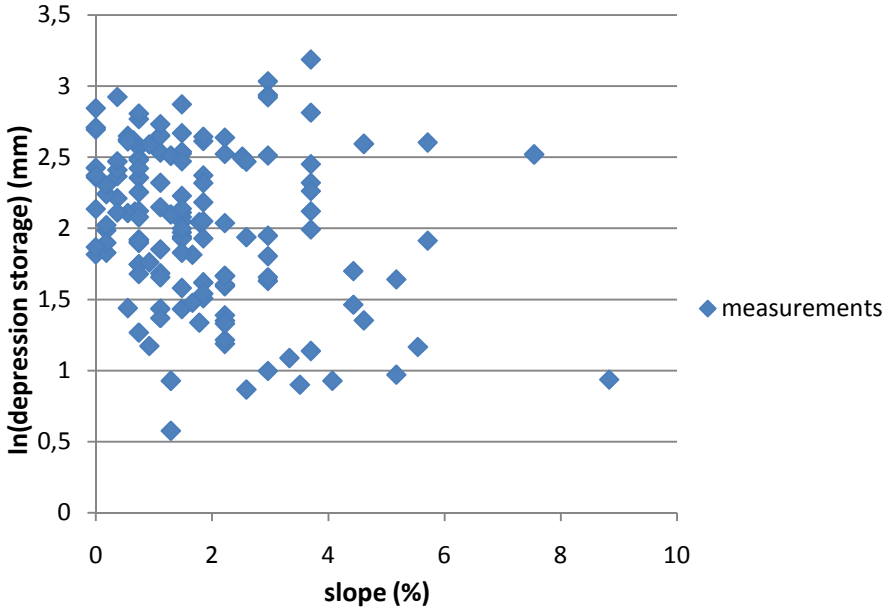

D. Model script

Included below is the PCRaster model script used for the modelling of runoff in the Quinlan Road catchment.

```
#Surface Runoff model Quinlan Road (Le Roy, New York State, USA)
#G.W.H Simons and B.R. Voortman
#Utrecht University March 2009
#Simulation of the precipitation event of November 30, 2006, 11820 timesteps of 10 seconds
#Assuming saturated conditions for the area around the lake and the swamp forest (scenario code 2bQ)
#Light version of the runoff model used for Monte Carlo simulations

binding
##RAIN-##INTERCEPTION
T=scalar(10);                              #duration of a timestep(seconds)
Clone=WatershedBoolean.map;                #mask showing the catchment(boolean)
PrecipitationTSS=ymd061130_11820Raw.tss;   #timeseries with rainfall per timestep (m/timestep)
COV=COV.map;                               #map with the vegetation coverage (m2/m2)
IntStM=InStM.map;                          #map with the maximum interception store (m)

##INFILTRATION
KsAve=KsAve.map;                  #map with the average ln(Ks)(Ks in m/d)
KsStdev=KsStdev.map;              #map with the standard deviation of ln(Ks)
Saturated=Saturated.map;          #map with the areas that are possibly saturated
ROC=ROC.map;                      #map with the volumetric rock content per soil(m3/m3)
KsT=$1\Ks.map;                    #reported map with saturated conductivity (m/timestep)
lnKs=$1\Ksln.map;                 #reported map with ln of the saturated conductivity (m/timestep)
B=$1\B.map;                       #reported map with the integral capillary and saturation deficit parameter B(m)

##DEPRESSION STORAGE
LandUseKs=LandUseKs.map;          #map representing units with different infiltration capacity
Dem=dem.map;                      #elevation model (m+msl)
Slope=Slope.map;                  #map with the slope
DepressionStore=$1\depstore.map;  #reported map with potential depression storage (m)

##ROUTING
Ldd=ldd.map;                      #local drain direction map
Bw=Bw.map;                        #map with the bottom width of streams (m)
Ang=Ang.map;                       #map with the angle of channel borders (deg)
ManningLandUse=Manning.map;       #map representing units with different values for manning's n
N=N.map;                          #map with Manning's n (-)
CL=CL.map;                        #map with the cell length
CA=CA.map;                         #map with the cell area
DCL=DCL.map;                      #map with the downstream distance
Beta=Beta.map;                    #map with the Beta routing parameter for every cell 0.6

#output
Sinkholes11=Sinkholes11mv.map;    #map with the location of the sinkholes used as outflow points/pits
Sinkholes12=Sinkholes12mv.map;    #map with the location of the sinkholes eastern sinkhole(1) western sinkholes(2)
RunoffPerPit=$1\RunPSink.tss;     #reported timeseries showing the amount of runoff per pit (m3/timestep)
SumRunoff=$1\SumRun.tss;          #reported timeseries showing the sum of runoff of the three pits (m3/timestep)
CumRunoff=$1\CumRun.tss;          #reported timeseries showing the cumulative total runoff (m3)
```

```
areamap
 Clone;

timer
 1 11820 1;

initial
##RAIN##INTERCEPTION
#initial cumulative rain (m)
RainCum=scalar(0);
#set the interception store to initial content(m)
IntSt=scalar(0);

##INFILTRATION
#Random number from a normal distribution with mean 0 and stdev 1
RandomStdev1=normal(Clone);
#include saturated areas in KsAve and KsStdev
KsAve=if(Saturated==1, scalar(-200), KsAve);
KsStdev=if(Saturated==1, scalar(0), KsStdev);
#ln of Saturated conductivity (Ks in m/d)
report lnKs=KsAve+RandomStdev1*KsStdev;
#Saturated conductivity m/timestep
report KsT=exp(lnKs)/(24*60*60)*T;
#B determined by the emperical relation Ks vs B (m)
report B=max(exp(0.8574*lnKs-scalar(5.3325)+normal(Clone)*sqrt(0.840339*(1+1/207+((scalar(lnKs)--
0.55274)**2)/580.9931))),0.00000000001);
#water deficit parameter including rocks (m)
BRock=B*(1-ROC);
#initial ponded water (m)
Pond=scalar(0);
#Initial actual infiltration (m/timestep)
FcA=scalar(0.000000000001);
#initial cumulative infiltration (m)
FCum=if(Clone,scalar(0));

##DEPRESSION STORAGE
#empirical relations for effective depression storage for different land use types as a function of slope
Forest=exp((-0.2422*scalar(Slope)-4.5982)+normal(Clone)*sqrt(0.739307*(1+1/52+((scalar(Slope)-
3.4875)**2)/278.5654)));
Oldfield=exp((-0.1809*scalar(Slope)-4.9098)+normal(Clone)*sqrt(0.484172*(1+1/67+((scalar(Slope)-
3.895224)**2)/1439.281)));
Lawn=exp((-0.3121*scalar(Slope)-5.7414)+normal(Clone)*sqrt(0.688026*(1+1/57+((scalar(Slope)-
4.120351)**2)/749.5192)));
Cultivated=exp(-5.0103723+normal(Clone)*0.52015551);
#calculates the depression storage (m) per land use type
report DepressionStore=if(LandUseKs==2,Forest, if(LandUseKs==14,Lawn, if(LandUseKs==3 or LandUseKs==5 or
LandUseKs==6,Oldfield, if(LandUseKs==9 or LandUseKs==11, scalar(0), if(ManningLandUse==50, scalar(0.00506),
if(ManningLandUse==15, scalar(0.000635), Cultivated))))));
#initial depression storage
Dst=scalar(0.00000000001);

##ROUTING
#term for alpha
AlphaTerm=(N/sqrt(Slope))**Beta;
#power for Alpha
```

```
AlpPow=(2/3)*Beta;
#initial water height (m)
H=scalar(0.00000000001);
#initial approximation for alpha
P=if(ManningLandUse==100,Bw+2*(H/cos(Ang)),Bw);
Alpha=if(Clone,AlphaTerm*(P**AlpPow));
#initial stream flow (m3/s)
Q=if(Clone,scalar(0.00000000000000001));
#initial volume of runoff water (m3)
Q_V=scalar(0.00000000000000001);

##Output
#initial cumulative runoff
CumRunoff=scalar(0);

dynamic
##RAIN-##INTERCEPTION
#rain m/timestep
Rain=timeinputscalar(PrecipitationTSS,Clone);
#cumulative rain (m)
RainCum=RainCum+Rain;
#intercepted water, spreaded over grid cell(m)
Int=Rain*COV;
#interception store for area covered, previous timestep (m)
IntStOld=IntSt;
#interception store for area covered (m)
IntSt=IntStM*(1-exp(-RainCum/IntStM));
#flux to interception store for area covered (m/timestep)
ToIntSt=IntSt-IntStOld;
#flux to interception store for whole cell (m/timestep)
ToIntStC=ToIntSt*COV;
#throughfall(m)
TF=Int-ToIntStC;
#total net rain per timestep for whole cell (m)
RainNet=Rain-Int+TF;

##INFILTRATION
#water on surface as runoff of the previous timestep m
Qsurf=Q_V/CA;
#water on surface available for infiltration (m);
SurfW=if(ManningLandUse==100, RainNet+Dst, RainNet+Dst+Qsurf);
#cumulative infiltration (m);
FCum=FCum+FcA;
#exponent of Smith and Parlange
ExpFB=exp(min(FCum/BRock,30));
#potential infiltration (m/timestep)
Fc=KsT*(ExpFB/max((ExpFB-1),0.00000000001));
#actual infiltration(m/timestep)
FcA=if(SurfW gt Fc,Fc,SurfW);
#water on surface after infiltration (m);
Pond=max(SurfW-FcA,0);

##DEPRESSION STORAGE
#Amount of water in surface storage (m) and (%) respectively
Dst=if(Pond gt DepressionStore, DepressionStore, Pond);
```

```
#Flux of excess water (m/timestep) going in or out the Routing model
#(could be negative for cells where part of Qsurf has infiltrated or filled the Dst)
ExcessW=if(ManningLandUse==100, max(Pond-Dst,0), max(Pond-Dst,0)-Qsurf);

##ROUTING
#Excess water multiplied by cell area and timestep to convert to (m3/s)
QIn=ExcessW*CA/T;
#lateral inflow per distance along stream ((m3/s)/m)
q=QIn/DCL;
#discharge (m3/s)
Q=kinematic(Ldd,Q,q,Alpha,Beta,1,T,DCL);
#water depth (m)
H=(Alpha*(Q**Beta))/Bw;
#wetted perimeter
P=if(ManningLandUse==100,Bw+2*(H/cos(Ang)),Bw);
#Alpha
Alpha=AlphaTerm*(P**AlpPow);
#flow velocity (m/s)
V=Q/(H*Bw+H*H*tan(Ang));
#volume of runoff water in raster cell (m3)
Q_V=Q*(DCL/V);

##OUTPUT
RunoffAtPits=if(Sinkholes11, Q*T);
# runoff that reached the three pits(depressions/outflowpoints)(m3/timestep)
report RunoffPerPit=timeoutput(Sinkholes12, RunoffAtPits);
# the sum of the runoff that reached the three pits (m3/timestep)
report SumRunoff=maptotal(RunoffAtPits);
# cumulative total runoff (m3)
report CumRunoff=CumRunoff+SumRunoff;
```

E. Model output

The following graphs display the cumulative frequency distribution of the simulated values for the cumulative volume of runoff reaching the flood site at the final model timestep, for each of the scenarios.

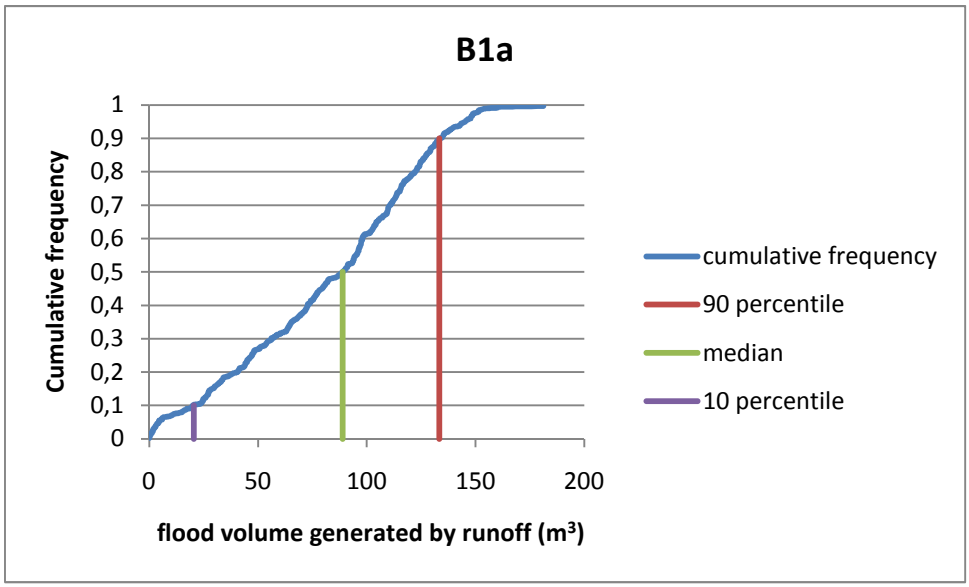

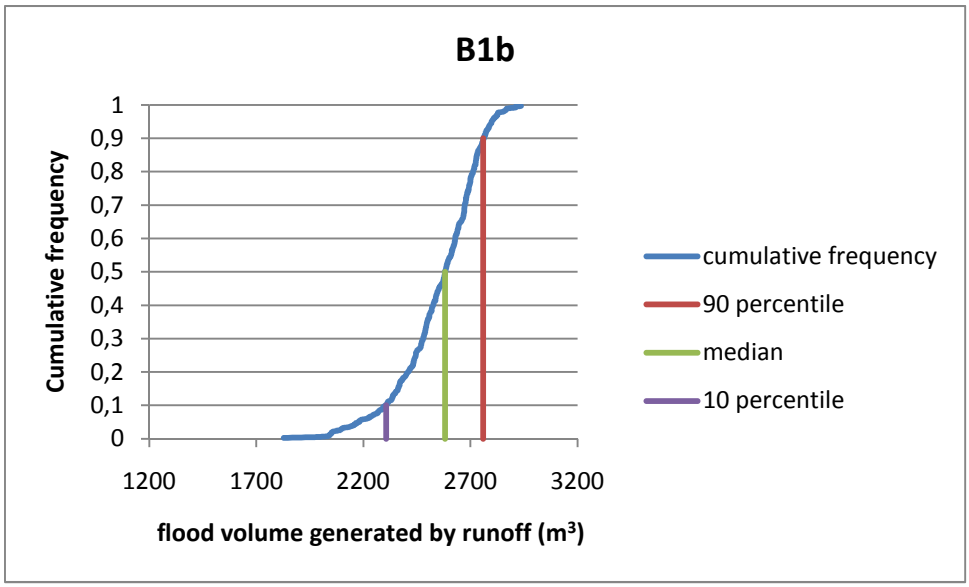

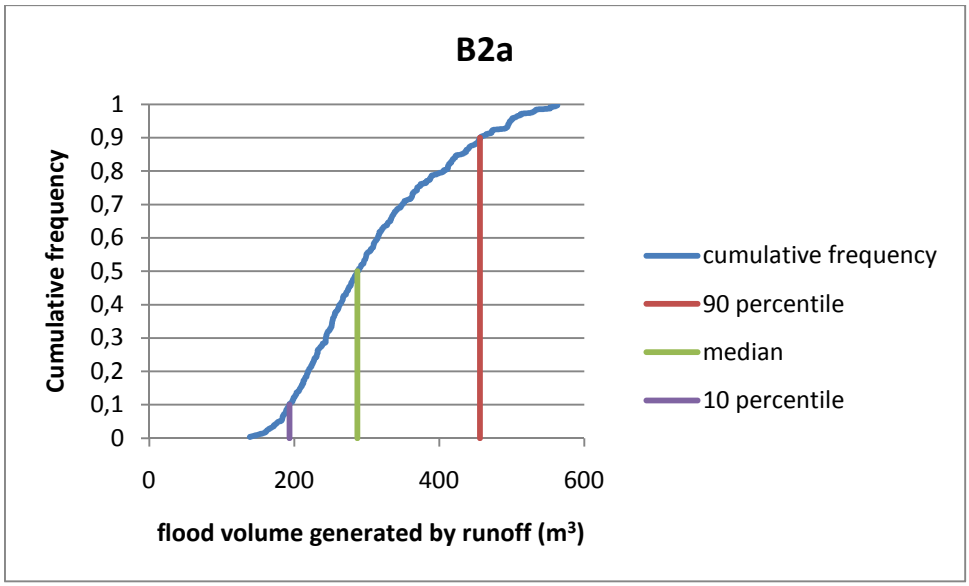
B2a
Cumulative frequency
1
0,9
0,8
0,7
0,6
0,5
0,4
0,3
0,2
0,1
0
0
200
400
600
flood volume generated by runoff (m³)
cumulative frequency
90 percentile
median
10 percentile

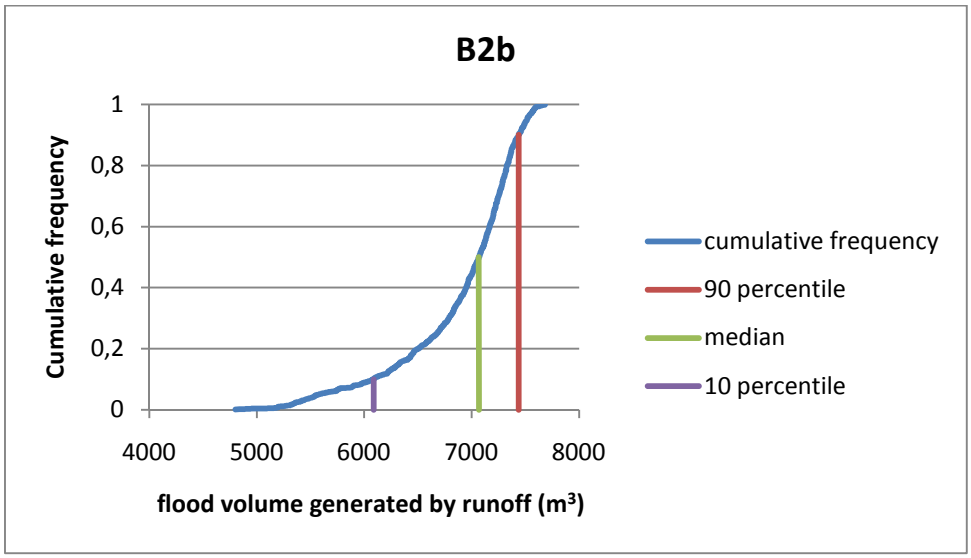
B2b
Cumulative frequency
1
0,8
0,6
0,4
0,2
0
4000
5000
6000
7000
8000
flood volume generated by runoff (m³)
cumulative frequency
90 percentile
median
10 percentile

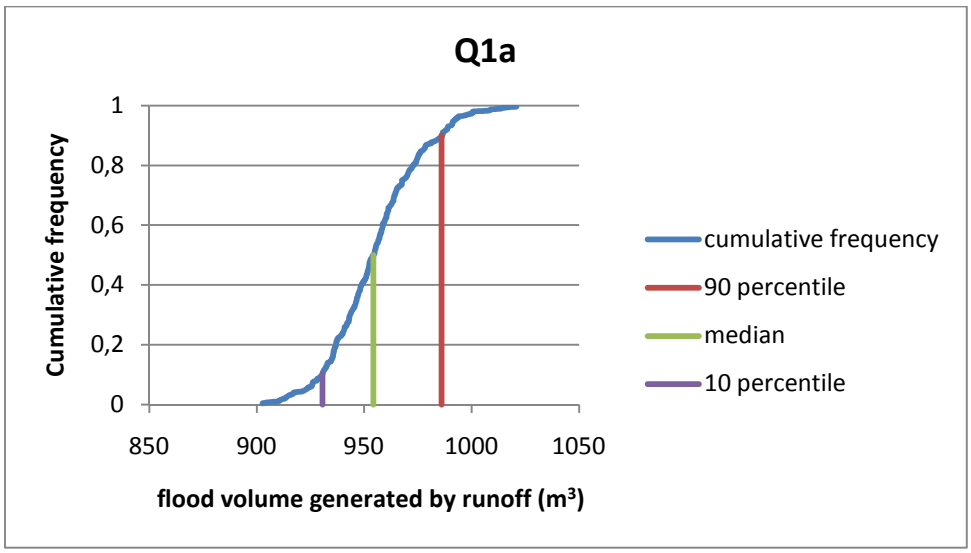
Q1a
Cumulative frequency
1
0,8
0,6
0,4
0,2
0
850
900
950
1000
1050
flood volume generated by runoff (m³)
cumulative frequency
90 percentile
median
10 percentile

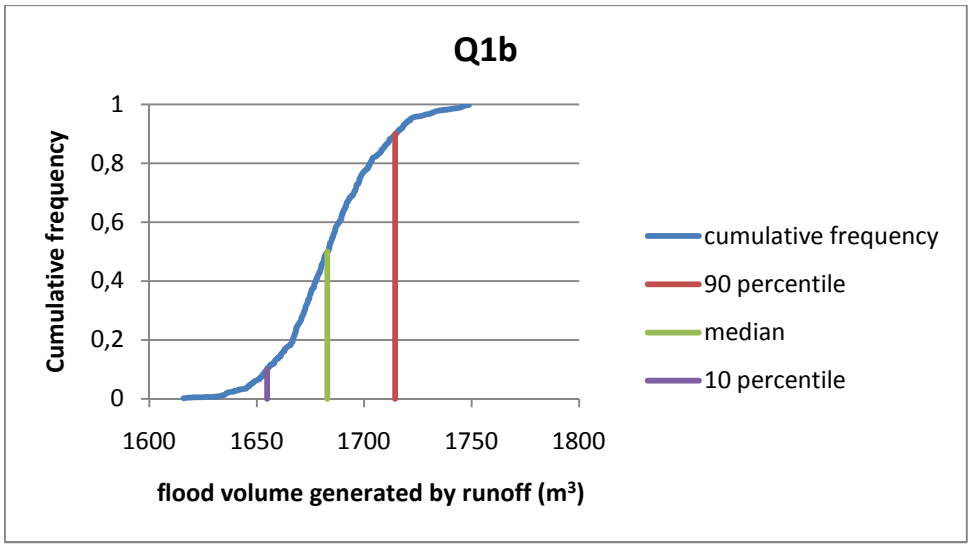
Q1b
Cumulative frequency
1
0,8
0,6
0,4
0,2
0
1600
1650
1700
1750
1800
flood volume generated by runoff (m³)
cumulative frequency
90 percentile
median
10 percentile

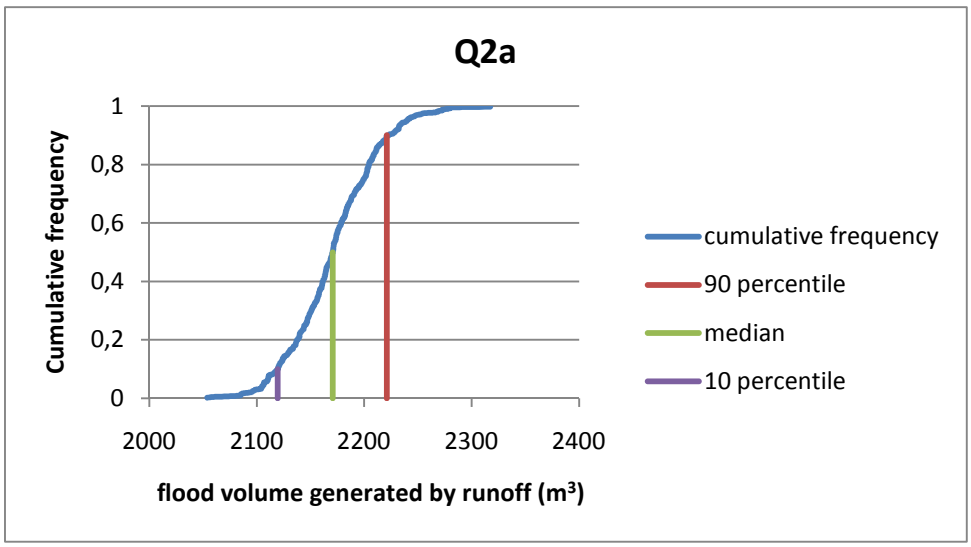
Q2a
Cumulative frequency
1
0,8
0,6
0,4
0,2
0
2000
2100
2200
2300
2400
flood volume generated by runoff (m³)
cumulative frequency
90 percentile
median
10 percentile

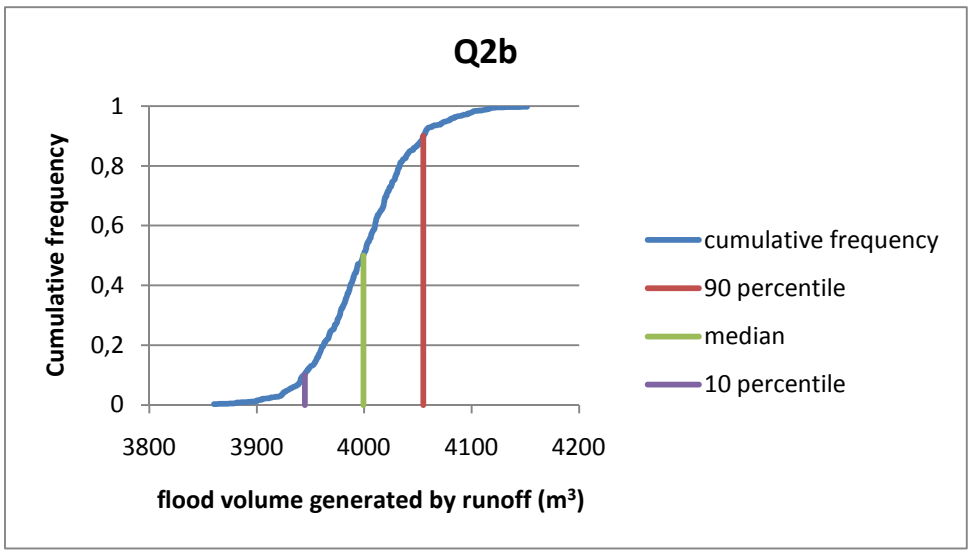
Q2b
Cumulative frequency
1
0,8
0,6
0,4
0,2
0
3800
3900
4000
4100
4200
flood volume generated by runoff (m³)
cumulative frequency
90 percentile
median
10 percentile